December 2022 ISSN 1650-3414 Volume 33 Number 4

eJIFCC

Communications and Publications Division (CPD) of the IFCC

Editor-in-chief: Prof. János Kappelmayer, MD, PhD
Faculty of Medicine, University of Debrecen, Hungary
e-mail: ejifcc@ifcc.org

The Journal of the International Federation of Clinical Chemistry and Laboratory Medicine

In this issue

The Journal of the International Federation of Clinical Chemistry and Laboratory Medicine

eJIFCC

On the introduction of the Editorial Manager system for eJIFCC manuscript handling

János Kappelmayer, Harjit Pal Bhattoa

In the past years, the eJIFCC has become increasingly visible among laboratory specialists worldwide. This, on the one hand resulted in the increase of the number of downloads of papers published since the eJIFCC is a platinum open access forum and on the other hand, it resulted in a considerable increase in the number of submissions. We detailed the progress in the advancement of the scientometric parameters of the journal in a review in the eJIFCC in Issue 4 of 2021. In order to cope with the increase in submissions we decided to advance our manuscript handling process, and recently subscribed for the Editorial Manager (EM) manuscript handling system. As most people are aware, Editorial Manager is a long-established and one of the best-known editorial submission and manuscript processing program that belongs to the Aries systems and was founded in 1986 and is headquartered in North Andover, MA. It is a very popular manuscript handling system that manages all kind of scientific journals, which is more than 1000, for details see: https://www.ariessys.com/journals-list/.

The introduction of the Editorial Manager system will have profound effects in at least two areas. As a trial period, from January 1 to February 28, 2023, we request all contributing authors to submit their manuscripts both via the traditional email submission system as well as by uploading their submission on the Editorial Manager system as detailed below. Starting March 1, 2023, only submissions via the Editorial Manager system will be allowed.

INFORMATION FOR CONTRIBUTING AUTHORS

Each author has to register for the program. For the registration there are two possible ways: with an ORCID ID, or with an email address.

To finalize the registration, a few questions will be asked that will be necessary for later communication and work-flow handling. The following questions can be expected during the end of the registration: workplace, contact details (email address, phone number), professional qualifications and availability lists.

You will receive a system message about the successful registration.

If you encounter any problems, or registration fails, log in to the site or if you would like to initiate the deletion of your account, you will be able to communicate it to us on the following e-mail address: ejifcc.editorialoffice@ifcc.org.

INFORMATION FOR EDITORIAL BOARD MEMBERS

Each Editorial Board member also has to register for the program. For the registration there will be two possibilities: with an ORCID ID, or with an e-mail address. To finalize the registration, a few questions that will be asked that will be necessary for further communication and work. The following questions can be expected during the end of the registration: workplace, contact details (e-mail address, phone number), professional qualifications and availability lists.

Everyone will receive a system message about the successful registration.

If you have any problems with the registration, with the log in or if you would like to initiate the deletion of your account, you will be able to communicate it to us on the following e-mail address: ejifcc.editorialoffice@ifcc.org.

After a plagiarism check (with the iThenticate software) and a general technical check by the Editoral Office, manuscripts will be forwarded for evaluation to Reviewers. An email message will inform you that an article has been added to your account for a review. After logging into the program, you will be able to download it and do the evaluation.

After logging into the EM, you can start under the Main page item via the following steps:

1. On the main menu, click on the Submissions with required Reviewers complete menu
2. Click on the Submit Editors's decisions and comments
3. In the upper part of the page, you can see the participants and the status of the review of the manuscript or if any previous decisions were made previously (major or minor revision).
4. By scrolling down, you will see two boxes: confidential comments to the Editor appear and Comments to Author in which you can enter your opinion about the manuscript as a Reviewer. In this part you can also see the other's comments below.
5. The manuscript must be scored in the next menu item.
6. Choose from the Editor decision phrases menu.

After completing each menu item, you will see a summary section based on the completed evaluation. There will be an option to still edit here. If you find it appropriate, please press the proceed button.

7. In the last menu, you can modify the letter you want to send to the Editor-in-Chief about your decision and add an attachment if you want to.

We sincerely hope that both the Authors as well as our Reviewers will benefit from this advancement, and are looking forward to receive any comments.

János Kappelmayer
Editor-in-Chief, eJIFCC

and

Harjit Pal Bhattoa
Assistant Editor, eJIFCC

The Journal of the International Federation of Clinical Chemistry and Laboratory Medicine

eJIFCC

Methods of low-density lipoprotein-cholesterol measurement: analytical and clinical applications

S.M. Touhidul Islam[1], Bremansu Osa-Andrews[1], Patricia Mary Jones[1,2], Alagar R. Muthukumar[1], Ibrahim Hashim[1], Jing Cao[1,2]

[1] *University of Texas Southwestern Medical Center, Dallas, TX, USA*

[2] *Children's Medical Center, Dallas, TX, USA*

ARTICLE INFO

Corresponding authors:
S.M. Touhidul Islam
Department of Pathology
University of Texas Southwestern
Medical Center (UTSW)
5161 Harry Hines Blvd
Dallas, TX 75390-9072
USA
E-mail: smtouhidul.islam@utsouthwestern.edu

Jing Cao
Department of Pathology
University of Texas Southwestern
Medical Center (UTSW)
5323 Harry Hines Blvd.
Dallas, TX 75390-9072
USA
E-mail: jing.cao2@utsouthwestern.edu

Key words:
low-density lipoprotein-cholesterol, cardiovascular diseases, analytical and automated methods, calculation methods

ABSTRACT

Among the five major classes of lipoprotein particles, low-density lipoprotein-cholesterol (LDL-C) is the primary lipoprotein risk factor for the development of cardiovascular diseases (CVD) through the promotion of atherosclerotic pathogenesis. Therefore, it is of paramount importance to accurately measure the plasma concentration of LDL-C using an appropriate method to examine the risk of CVD and determine the efficacy of therapeutic interventions to reduce the cholesterol level and examine the risk assessment strategy. At present, there is a wide variety of methods available for LDL-C measurement. In this review, we have outlined the commonly used methods of LDL-C measurement. These methods have been classified into non-automated analytical methods, calculation methods, and automated direct measurement of LDL-C. We have also described some recently proposed promising calculation methods which are being considered for clinical adoption. This current

review could assist the clinicians to have a better understanding regarding the measurement techniques and comparative utilities of different methods of LDL-C measurement and guide them to select an appropriate method based on accuracy, turnaround time, and cost of test.

❖❖❖❖❖

INTRODUCTION

Lipids are essential for tissue structure and different aspects of function, including energy storage, cellular membrane formation, insulation of nerve conduction and heat dissipation, and hormone production (1). Lipids are either synthesized or absorbed from the diet and then transported to different tissues to meet their metabolic needs. Because of a relatively insoluble nature of lipids, they are transported in blood to different tissues through packaging into lipoproteins which are heterogeneous particles composed of proteins and lipids. Solubility of lipoprotein is determined by the location of proteins and polar lipids (e.g., phospholipids, sphingolipids, fatty acids (FAs) and cholesterol) at the outer surface of the particles. On the other hand, nonpolar triglycerides and cholesterol esters are retained at the core of particles (2). Based on their hydrated density and electrophoretic pattern, lipoproteins are divided into five major fractions including chylomicron, very low-density lipoprotein [VLDL], intermediate-density lipoprotein [IDL], low-density lipoprotein [LDL], high-density lipoprotein (HDL), and lipoprotein (a) [Lp (a)]. Triglycerides and cholesteryl esters-containing chylomicrons and VLDL are generated by the intestines and liver, respectively. Endothelial lipoprotein lipase activity in the capillaries of peripheral tissues converts triglycerides in lipoproteins into free FAs which is taken up by the tissues with a high demand for lipids. After losing some triglycerides, chylomicron and VLDL are converted into smaller and denser remnant lipoproteins and IDL, respectively, which are taken up and recycled by the liver. The taking up of remnant lipoproteins and IDL by the liver is mediated by the interaction between apolipoprotein E (apoE) on remnant lipoproteins/IDL and hepatic low-density lipoprotein receptor (LDLR) or LDLR-related protein. However, if remnant lipoproteins/IDL loses nearly all of their triglycerides through the lipoprotein lipase-mediated conversion of triglycerides into free FAs while they are still in circulation, they become too small to carry apoE which results in an inappropriate clearance of remnant lipoproteins/IDL from circulation by the liver. These smaller and denser lipoproteins are called LDL which is rich in cholesteryl ester/cholesterol (2).

In the clinical context, the term ‘lipids’ is kind of synonymously used for cholesterol due to the long-studied association between cholesterol and cardiovascular disease (CVD). Although a remarkable progress has been made in its treatment and prevention, CVD remains the single most common cause of death in the United States. Plasma cholesterol has an essential biological function as a structural component of cellular membranes and a precursor of many essential compounds including vitamin D, bile salts, and hormones. However, plasma cholesterol can accumulate on arterial wall leading to plaque formation which can eventually result in myocardial infarction upon rupture (3). Because LDL is the principle carrier of cholesterol in blood, low-density lipoprotein-cholesterol (LDL-C) level is used as a major risk factor for future CVD development (4). Due to the strong and positive association between LDL-C and CVD, the 2018 American Heart Association/American College of Cardiology (AHA/ACC) guideline on managing blood cholesterol emphasizes target level of LDL-C as a benchmark on directing prevention and management strategies of the Atherosclerotic CVD (5). Therefore,

a precise and accurate measurement of the concentration of circulating LDL-C using an appropriate method has become the cornerstone of cardiovascular risk assessment for the past decades. As per the recommendations of the National Cholesterol Education Program (NCEP) Working Group on Lipoprotein Measurement, methods used to measure the plasma level of LDL-C should give results equivalent to those used to establish the epidemiologic database that was used to develop the recommendations for risk evaluation (6). Currently, a variety of methods of LDL-C measurement are clinically available. In the present review, we have delineated widely used methods of LDL-C measurement which are classified into non-automated analytical methods, LDL-C calculation, and automated direct measurements including their merits and limitations.

NON-AUTOMATED ANALYTICAL METHODS

The analytical methods of LDL-C measurement are usually considered as reference methods. Commonly studied analytical methods are Beta-quantification, vertical spin density gradient ultracentrifugation-based vertical auto-profile, gradient gel electrophoresis, high-performance liquid chromatography, proton nuclear magnetic resonance spectroscopy (^{1}H-NMR), and ion mobility (Table 1). Due to their long turnaround time, non-suitability for automation, and requirement of expert technologists for operation, these non-direct methods are not used in a regular clinical laboratory setting. Rather, they are used as reference for the validation of other clinically suitable methods of LDL-C measurements using method comparison.

Beta-quantification

Beta-quantification is the precursor to the contemporary reference method adopted by NCEP in 1995. The name of the assay is originated from the location of LDL in the beta region upon electrophoretic migration of lipoprotein particles in early studies. This is the gold standard method for LDL-C measurement adopted from the National Institute Health (NIH) laboratory (6-8). An aliquot of plasma at native density of 1.006 g/mL is ultracentrifuged which separates VLDL and chylomicrons on the floating layer (d < 1.006 g/mL) over the infranatant containing IDL, LDL, Lp (a), and HDL (d > 1.006 g/mL). Concentration of cholesterol in the bottom layer fraction is measured by treating with heparin and manganese (II) chloride solution to precipitate the apoB containing particles (IDL, LDL, Lp (a)) and the precipitate is removed by centrifugation. After centrifugation, HDL is the only particle that remains in the solution. Then the concentration of HDL cholesterol is measured, and the concentration of LDL cholesterol is determined by subtracting the HDL concentration from the cholesterol concentration measured in the bottom fraction containing IDL, LDL, Lp (a), and HDL [d > 1006 g/mL cholesterol] (equation I). Concentration of VLDL-C in the discarded ultra-centrifugal supernatant fraction is measured by subtracting the cholesterol concentration measured in the bottom fraction [d > 1006 g/mL cholesterol] from the total concentration of cholesterol measured in the initial aliquot of plasma before ultracentrifugation (equation II) (9). It is preferred to calculate VLDL-C than direct measurement in the ultra-centrifugal supernatant as it is difficult to recover cholesterol in this fraction, especially at a high concentration of triglyceride.

[LDL-C] = [d > 1006 g/mL cholesterol] – [HDL-C] (I)

[VLDL-C] = [Total cholesterol] - [d > 1006 g/mL cholesterol] (II)

Because beta-quantification of LDL-C ignores the amount of IDL and Lp (a) in the precipitate, the term non-HDL-C is widely used, which reflects the cholesterol contents of all atherogenic

lipoproteins (non-HDL = TC-HDL-C) in several guidelines. One important shortcoming of beta-quantification is the heterogeneity and lack of molecular specificity as it cannot distinguish the concertation of LDL-C from the concentration of IDL-C and LP (a)-C. Both IDL and Lp (a) particles contribute to the total cholesterol measurement in the precipitated fraction. Thus, the measured concentration of LDL-C is always higher than the actual concentration, particularly in the cases of patients with CVD and the individuals who are at risk of developing CVD because of dyslipidemias. However, the elevated concentration of LDL-C measured by beta-quantification due to the inclusion of IDL-C and Lp (a)-C is considered beneficial to the clinical performance as both of IDL-C and Lp (a)-C are atherogenic in nature (9, 10). Furthermore, the NCEP Working Group

Table 1 Merits and limitations of different analytical methods of low-density lipoprotein cholesterol measurement

Analytical methods	Merits	Limitations
Beta-quantification	Highly standardized and high resolution	Cannot distinguish LDL-C from IDL-C and LP (a)-C Tedious and requires large amount of sample
Vertical spin density gradient ultracentrifugation-based vertical auto-profile	Separate LDL-C from IDL-C and LP (a)-C Directly measures cholesterol in different fractions of lipoproteins	Tedious and requires large amount of sample
Gradient gel electrophoresis	Can determine both particle concentration and diameter	Tedious, time consuming, and resource intensive
High-performance liquid chromatography	Can determine both particle concentration and diameter	Resource intensive and requires expertise
Proton nuclear magnetic resonance spectroscopy	High throughput quantification of particle size/concentration No preanalytical sample preparation is required	Cholesterol concentration cannot be not directly measured Requirement of costly equipment and expertise
Ion mobility	High resolution separation and measurement of particle concentration and size	Cholesterol concentration cannot be not directly measured and requires special equipment and expertise

on Cholesterol Measurement has suggested that LDL-C values should not be corrected for the presence of other atherogenic lipoproteins so that they could also be kept under consideration, not only LDL-C, during the treatment regimen (11).

Vertical spin density gradient ultracentrifugation-based vertical auto-profile

In vertical spin density gradient ultracentrifugation method, lipoprotein particles are separated and analyzed in three distinguished steps. First, a two-layer density gradient is established by dispensing saline solution in a tube and then under-layering with diluted serum. Then the tubes containing two-layer density gradients are ultracentrifuged. Second, following centrifugation, different layers of lipoproteins (HDLs being the particles of highest density are located at the bottom, VLDLs being the particles of least density are located at the top, and LDLs having the density between HDLs and VLDLs are located at the middle of the tube) are drained from the bottom of the tube and analyzed for determining cholesterol concentration using a continuous flow of cholesterol-specific enzymatic reagent through a narrow bore tubing. This instrumentation is called vertical auto-profile (VAP) analyzer. Third, as the reaction mixture flows through the tubing, absorbance of the corresponding colored-product, which is directly proportional to the cholesterol concentration of each class of lipoproteins, is measured using a spectrophotometric detector.

Because it directly measures the concentration of cholesterol in different fractions of lipoproteins, vertical spin density gradient ultracentrifugation-based VAP gives a high accuracy of LDL-C. Another important aspect of vertical spin density gradient ultracentrifugation-based VAP is that it separates IDL and Lp (a) from LDL, therefore, the cholesterol concentration of LDL particles is not confounded with that from IDL and Lp (a). Thus, VAP may represent a better reference method of LDL-C quantitation than beta-quantitation (12, 13).

Gradient gel electrophoresis

Using gradient gel electrophoresis, not only the cholesterol concentration of lipoprotein but also the size of the lipoprotein particles can be determined. In this method, serum samples are mixed with a loading solution, and then loaded to 2%-16% polyacrylamide gradient gels. To determine the size of particle, different standards having different diameters are used, such as bovine albumin, thyroglobulin, and serum VLDL. Besides, it is also important to use an internal standard, e.g., thyroglobulin is added to each serum sample. To distinguish LDL, gels are stained with Sudan Red after electrophoresis. To measure the concentration of LDL-C, gels are treated with reagent containing cholesterol ester hydrolase, cholesterol oxidase, and catalase which results in the elimination of HDL, VLDL, and chylomicrons, whereas LDL is protected. Then, the concentration of LDL-C is determined using CHOD-PAP method. To determine the diameters of LDL particles, LDL bands are compared with the calibration curve plotted on the basis of migration of standards on the gel (14).

LDL particles are heterogeneous due to their variation in size, density, and lipid composition. Gradient gel electrophoresis recognizes two different phenotypes of LDL particles. First, phenotype A comprises of large and buoyant LDL particles with a size of more than 25.5 nm. Second, phenotype B comprises of small and dense LDL with a size of 25.5 nm or less. Small and dense LDLs are considered atherogenic because they readily penetrate the arterial wall. It has been reported that the risk of coronary artery disease (CAD) is increased 2 to 3-fold in patients with short and dense LDL (15, 16). Unlike other non-automated analytical methods of LDL measurement, gradient gel electrophoresis can be

used not only to determine the concentration of LDL-C but also the diameter of lipoprotein particle.

High-performance liquid chromatography

High-performance liquid chromatography can determine the lipoprotein profile which includes both size and composition. To separate the lipoprotein particles, serum or plasma samples are pumped into tandemly connected gel permeation columns. The size of the particles is determined based on the retention times of the peaks on an observed chromatogram. To determine the lipoprotein composition, column effluent is equally split into two lines by a micro splitter. Each effluent flowing through two individual split lines are then separately used to react with cholesterol or triglyceride reagents. Then, the concentration of cholesterol or triglyceride in an individual split line representing a particular class or subclass of lipoprotein particle is determined spectrophotometrically by continuously monitoring the absorbance (17, 18). Likewise gradient gel electrophoresis, high-performance liquid chromatography can be used to determine both size and composition of lipoprotein particles. Moreover, it can separate not only the classes but also the subclasses of particles. This method can identify six LDL subfractions based on their variation in particle size (16-30 nm) (17, 18).

Proton nuclear magnetic resonance spectroscopy

Because of a number of various analytical advantages, ^{1}H-NMR spectroscopy has emerged as a valuable technique for measuring lipoproteins in plasma and serum samples. In this method, ^{1}H-NMR uses the characteristic signals generated by different lipoprotein classes of different size as the basis of their quantification. Each class of lipoproteins has Triglycerides and cholesterol esters inside the particles and has limited mobility, giving rise to the broadening of the NMR signals based on the aggregate number of methyl groups. Cholesterol esters and triglycerides which are located at the core of particles contribute 3 methyl groups each, whereas phospholipids and unesterified cholesterol which are located at the surface of the shell contribute 2 methyl groups each. The size of the lipoprotein particle determines the number of methyl groups and thereby, the methyl NMR signals. Thus, the methyl NMR signals emitted by large and less dense lipoprotein particles (e.g., VLDL and LDL) are different from the methyl NMR signals emitted by smaller and denser lipoproteins (e.g., HDL).

These signals are independent of the varying composition and relative amounts of cholesterol esters, triglycerides, and phospholipids, and degrees of unsaturation of the lipid fatty acyl chains. Therefore, the methyl NMR signal generated by a particular class of lipoproteins provides a direct measurement of the concentration of that specific class (19-21). Patients with insulin resistance, observed in metabolic syndrome and type-2 diabetes, contains a relatively higher number of particles of small dense LDL (sdLDL). Therefore, LDL particle number is a better measure of LDL as compared to the LDL-C (22). Besides LDL particle number, HDL particle number measured by NMR is also an important parameter for CVD risk assessment. In fact, as per key epidemiological and clinical trials, NMR-measured HDL particle number is a better parameter of CVD risk assessment than HDL-C (23). A limitation of ^{1}H-NMR is that it does not separate different classes of lipoprotein, and therefore it only estimates, but does not truly measure, the class-specific concentration of cholesterol (20, 21).

Ion mobility

In ion mobility, also known as gas phase differential electrical mobility, gas phase electrophoresis

is used to separate lipoproteins based on their size. First, singly charged lipoprotein particles on aerosol are generated in the electrospray chamber. The particles are then carried in the airflow to the differential mobility analyzer. As the particles pass through the differential mobility analyzer, an electric potential across the sheath flow causes the particles to drift toward a collection slit. At any given electrical potential, particles of a particular size can successfully be transported through the collection slit and finally enter a separate air stream that carries them to a particle counter. In the counter, each particle is detected by light scattering. Then, the data is analyzed to provide results on particle dry diameter, particle concentration, and mass concentrations. Ion mobility can be used for high-resolution separation and direct quantification of full spectrum of different subclasses of LDL. Because ion mobility cannot isolate different fractions of lipoprotein particles, it is not useful for measuring class-specific cholesterol concentration. LDL-C is estimated based on total cholesterol and percentage of LDL out of total lipoproteins. Furthermore, multistep preanalytical sample processing required for lipoprotein isolation and ionization is an important limitation (24, 25).

AUTOMATED DIRECT MEASUREMENT

Unlike the analytical methods, automated direct measurement methods are easily adoptable to a clinical setting. Heterogeneous selective precipitation and homogeneous methods are the two well-known types of automated direct measurement of LDL-C (Table 2).

Selective precipitation

There are several methods of LDL-C measurement based on selective precipitation. One important method is to selectively precipitate LDL-C with polyvinyl sulfate or heparin at low pH and then directly measure cholesterol concentration in the precipitate. It can also be calculated as a difference between the concentration of total cholesterol and that in the supernatant (26). A more specific method is to use polystyrene beads coated with polyclonal antibodies to apo A-I and apo E to immunoprecipitate VLDL, IDL, and HDL and then measure LDL-C is in the filtrate (27). Selective precipitation method was in good agreement with beta-quantification, but due to the requirement of a separate pretreatment step, it is now outmoded by direct homogeneous methods (27).

Homogeneous methods

Direct homogeneous methods use autoanalyzers to selectively measure the cholesterol concentration in LDL particles. Since the inception of homogeneous assays in 1998, various methods are now commercially available used by different manufacturers differing in employed detergents, modified enzymes, and other reagents allowing selective blocking and solubilization of lipoprotein classes to achieve LDL specificity. In Kyowa Medex method, LDL-C concentration is directly measured by suppressing other lipoproteins. α-cyclodextrin sulfate is used to mask cholesterol in chylomicron and VLDL and polyoxyethylene-polyoxypropylene polyether is used to block the cholesterol in HDL. Thus, cholesterol from LDL selectively produces colored product measured spectrophotometrically (28, 29). In Waki and Deika-Senken method, LDL-C is selectively masked from the initial enzymatic reaction.

All the non-LDL-C produces hydrogen peroxide which is consumed by catalase. Deprotecting reagent removes the protecting agent from LDL. Then the LDL-cholesterol generate hydrogen peroxide which eventually produces a colored complex (29-32). Similarly, in International Reagents Corp. method, first reagent containing calixarene (a detergent) forms a soluble complex with LDL. Cholesterol esters of HDL-C and

Table 2 Merits and limitations of different methods of direct measurement of low-density lipoprotein cholesterol

Direct methods	Merits	Limitations
Selective precipitation	In good agreement with beta-quantification	Requires additional pre-treatment
Homogeneous methods	Fully automated and rapid Improved precision/accuracy from automated pipetting and no sample preparation	Cost for extra reagents

VLDL-C are hydrolyzed resulting in conversion of cholesterol to cholestenone hydrazone. Second reagent, containing deoxycholate, breaks up the LDL-calixarene complex allowing LDL-C to produce cholestenone and β-NADH (29, 30). In Daiichi method, esterase and oxidase present in the reagent react with the cholesterol from non-LDL producing colorless product. On the other hand, cholesterol from LDL generates hydrogen peroxide producing colored product (29, 30).

Direct homogeneous methods are fully automated, easy to use, and cost effective. Because of being automated, they have improved precision from non-manual pipetting, and accurate control of timing and temperature (30). However, direct homogeneous measurements are not free of inaccuracies, particularly in the case of dyslipidemias. Bias between 13% and 46% has been reported between different direct homogeneous methods (7, 33). Compared to the calculation methods, direct homogeneous methods require additional steps of measurement. Therefore, homogeneous methods must demonstrate obvious advantages in performance and economics to replace calculation methods.

CALCULATION METHODS

Because inclusion of LDL-C in basic lipid panel would result in an increased turnaround time and additional cost, it is a regular practice to calculate LDL-C from the currently used components of basic lipid panel. To date, Friedewald and Martin/Hopkins are the commonly used methods for calculating LDL-C. Recently, the Sampson and extended Martin/Hopkins equations have been reported to provide more accurate calculations of LDL-C at hypertriglyceridemia (Table 3).

Friedewald equation

Friedewald et al. published a groundbreaking article in 1972 which described an equation to calculate LDL-C concentration to avoid the use of tedious ultracentrifugation-based methods (34). Considering its lower cost and shorter turnaround, Friedewald calculation has currently become the most widely used method for routine quantification of LDL-C. In this method, LDL-C is calculated by subtracting the concentration of cholesterol within all lipoproteins other than LDL from the concentration of

Table 3 Merits and limitations of different methods of calculation of low-density lipoprotein cholesterol

Calculation methods	Merits	Limitations
Friedewald equation	Good alternative of direct assay Quick turnaround and less cost	Not acceptable when triglyceride > 400 mg/dL
Martin/Hopkins calculation	Gives a more accurate calculation than Friedewald due to the use of adjustable factor	Not acceptable when triglyceride > 400 mg/dL
Sampson equation	Applicable at the triglyceride concentration up to 800 mg/dL	Not free of cholesterol contami-nation from IDL-C, and Lp (a)
Extended Martin/Hopkins calculation	Applicable at the triglyceride concentration up to 800 mg/dL Greater accuracy than the Friedewald and Sampson	Not free of cholesterol contami-nation from IDL-C, and Lp (a)

total cholesterol. In fasting condition, the major lipoprotein particles are LDL, HDL, and VLDL. Therefore, subtraction of concentration of cholesterol in HDL and VLDL from the total cholesterol concentration represents the estimate of LDL-C. But, only total cholesterol, HDL-C, and triglycerides are included in the basic lipid panel. VLDL-C is not a part of basic lipid panel, but it can be calculated from the serum concentration of triglycerides. VLDL particles carry most of the circulating triglycerides in normal fasting condition. Cholesterol within VLDL particles are reported to be contained with triglycerides in a ratio of [triglycerides]:[cholesterol] = 5 (for mg/dL unit) or 2.26 (for mmol/L) (34-36). Therefore, VLDL-C is calculated by dividing the concentration of triglycerides (mg/dL or mmol/dL) by 5 or 2.26, respectively (equation III). Then, LDL-C is estimated by subtracting the concentration of HDL-C and calculated VLDL-C from the concentration of total cholesterol (equation IV).

$$\text{VLDL-C} = {}^{[\text{Triglycerides}]}/_{5} \quad \text{(III)}$$

$$\text{LDL-C (mg/dL or mmol/L)} = [\text{Total cholesterol}] - [\text{HDL-C}] - {}^{[\text{Triglycerides}]}/_{5 \text{ or } 2.26} \quad \text{(IV)}$$

In Friedewald calculation, it is assumed that the subject is fasting, and the triglyceride concentration is less than 400 mg/dL (37). The requirement of a fasting condition significantly reduces the likelihood of triglyceride contribution by chylomicron. But in non-fasting condition, circulating triglyceride is remarkably contributed

by chylomicron, 90% of which by mass is triglyceride (38).

In that case, the actual ratio of [triglycerides]:[cholesterol] in the blood would be higher than 5. Likewise, when triglyceride concentration is higher than 400 mg/dL (e.g., in hypertriglyceridemia), the actual ratio of [triglycerides]:[cholesterol] would also be higher than 5. In such conditions, [Triglycerides]/5 is not an appropriate estimate of VLDL-C. Under those circumstances, using [Triglycerides]/5 as a fixed factor would overestimate VLDL-C and thereby, underestimate LDL-C. In fact, the Friedewald calculation of VLDL-C has been found to be most accurate in patients with a triglyceride concentration of less than 200 mg/dL (39).

Martin/Hopkins calculation

In Friedewald calculation of LDL-C, triglyceride concentration is divided by a fixed factor to determine the concentration of VLDL-C assuming an invariable ratio of triglyceride:VLDL-C. Given the inaccuracy of the fixed denominator in the case of triglycerides levels higher than mg/dL, Martin/Hopkins calculation was formulated which replaces the fixed denominator with an adjustable factor X (equation V). This adjustable factor X changes following an empirically derived 180-cells strata based on the varying concentration of triglyceride up to 400 mg/dL and non-HDL up to 220 mg/dL (40). Although the use of this adjustable factor improves the accuracy of LDL-C calculation to some extent compared to the Friedewald equation, Martin/Hopkins equation is still not a completely accurate calculation method and inapplicable in the case of triglyceride level beyond 400 mg/dL (40, 41). On top of that, Martin/Hopkins calculation formula for LDL-C is not available to users/laboratories for free.

$$\text{LDL-C} = [\text{Total cholesterol}] - [\text{HDL-C}] - {}^{[\text{Triglycerides}]}/_{X} \quad \text{(V)}$$

Sampson equation

Sampson LDL-C equation, also known as the National Institutes of health equation, used TG and non–HDL-C as independent variables and multiple least squares regression to develop a bivariate quadratic equation for VLDL-C (equation VI). The equation for VLDL-C was then used in a second equation for LDL-C calculation (equation VII). Sampson calculation of LDL-C is similar to Friedewald calculation in terms of subtracting VLDL-C and HDL-C from total concentration of cholesterol. Additionally, Sampson equation includes an intercept and allows the coefficients to vary for each term which made this equation a better fit with beta-quantification compared to Friedewald equation.

Whereas negative biases are sometimes observed for hypertriglyceridemic patients in the cases of other calculation methods, Sampson calculation is almost free of such negative bias. Thus, the use of continuous variables has made Sampson equation a superior method of calculation at triglyceride concentration up to 800 mg/dL (42).

$$\text{VLDL-C} = {}^{[\text{Triglycerides}]}/_{8.59} + {}^{[\text{Triglycerides}] \times [\text{non-HDL-C}]}/_{2250} - {}^{[\text{Triglycerides2}]}/_{16500} \quad \text{(VI)}$$

$$\text{LDL-C} = {}^{[\text{Total cholesterol}]}/_{0.948} - {}^{[\text{HDL-C}]}/_{0.971} - \left({}^{[\text{Triglycerides}]}/_{8.56} + {}^{[\text{Triglycerides}] \times [\text{non-HDL-C}]}/_{2140} - {}^{[\text{Triglycerides}]\wedge 2}/_{16100}\right) - 9.44 \quad \text{(VII)}$$

Extended Martin/Hopkins calculation

Extended Martin/Hopkins calculation is a modified version of the Martin/Hopkins calculation. Likewise, Martin/Hopkins calculation, Extended Martin/Hopkins calculation uses an adaptable triglyceride to VLDL-C ratio instead of a fixed one used in Friedewald equation (equation V). Extended Martin/Hopkins equation was validated against vertical density gradient ultracentrifugation for LDL-C up to 800 mg/dL using an empirically defined table of 240/560/1040-cells of median ratios of TG:VLDL-C based on the varying number of TG and non-HDL-C strata (41). In a cross-sectional study, the extended Martin/Hopkins calculation was demonstrated to calculate LDL-C with a greater accuracy as compared with the Friedewald and Sampson equations in patients with triglyceride levels of 400 to 799 mg/dL (41).

LDL-C belongs to the category of non-HDL-C that contains all atherogenic lipoproteins, including chylomicron, VLDL, LDL, IDL and lipoprotein(a). In primary CVD prevention, a number of prospective observation studies have reported that non-HDL-C predicts risk with equal or superior performance compared to LDL-C. Since VLDL in non-HDL represents particles rich in triglyceride, which is an independent risk factor of CVD, current guidelines list non-HDL-C as secondary therapeutic target of CVD prevention in addition to LDL-C. The clinical utility of non-HDL-C is beyond the scope of this review (43-45).

CONCLUSION

Due to the long-established connection between LDL-C and CVD, it is critically important to accurately measure the concentration of LDL-C for a proper cardiovascular risk assessment and management. To date, there is a sizable preference of analytical, calculation, and direct methods for LDL-C measurement. Although each of these methods have their own merits over the others depending on the existing analytical or clinical setting, none of these methods are free from limitations in terms of operational expertise, accuracy, turnaround time, and cost. This review has briefly illustrated different methods of LDL-C measurement which gives a clearer understanding on available methods of LDL-C measurement in addition to their comparative application. Given the necessity of accuracy, shorter turnaround time, and affordability of LDL-C measurement, it demands further investigation to develop an improved alternative.

❖❖❖❖❖

Abbreviations

AHA/ACC: American Heart Association/American College of Cardiology; CDC: Centers for Disease Control and Prevention; CVD: cardiovascular diseases; FAs: fatty acids; HDL-C: high-density lipoprotein-cholesterol; IDL-C: intermediate-density lipoprotein-cholesterol; LDL-C: low-density lipoprotein-cholesterol; Lp (a): lipoprotein (a); NCEP: National Cholesterol Education Program; VLDL-C: very low-density lipoprotein-cholesterol.

❖❖❖❖❖

REFERENCE

1. Casares D, Escriba PV, Rossello CA. Membrane Lipid Composition: Effect on Membrane and Organelle Structure, Function and Compartmentalization and Therapeutic Avenues. Int J Mol Sci. 2019;20(9).

2. Rifai N. Lipoproteins and apolipoproteins. Composition, metabolism, and association with coronary heart disease. Arch Pathol Lab Med. 1986;110(8):694-701.

3. Linton MRF, Yancey PG, Davies SS, Jerome WG, Linton EF, Song WL, et al. The Role of Lipids and Lipoproteins in Atherosclerosis. In: Feingold KR, Anawalt B, Boyce A, Chrousos G, de Herder WW, Dhatariya K, et al., editors. Endotext. South Dartmouth (MA)2000.

4. Nelson RH. Hyperlipidemia as a risk factor for cardiovascular disease. Prim Care. 2013;40(1):195-211.

5. Grundy SM, Stone NJ, Bailey AL, Beam C, Birtcher KK, Blumenthal RS, et al. 2018 AHA/ACC/AACVPR/AAPA/ABC/ACPM/ADA/AGS/APhA/ASPC/NLA/PCNA Guideline on

the Management of Blood Cholesterol: Executive Summary: A Report of the American College of Cardiology/American Heart Association Task Force on Clinical Practice Guidelines. J Am Coll Cardiol. 2019;73(24):3168-209.

6. Bachorik PS, Ross JW. National Cholesterol Education Program recommendations for measurement of low-density lipoprotein cholesterol: executive summary. The National Cholesterol Education Program Working Group on Lipoprotein Measurement. Clin Chem. 1995;41(10):1414-20.

7. Contois JH, Warnick GR, Sniderman AD. Reliability of low-density lipoprotein cholesterol, non-high-density lipoprotein cholesterol, and apolipoprotein B measurement. J Clin Lipidol. 2011;5(4):264-72.

8. AJKJ Hainline KLSD. Manual of laboratory operations. 1982 U.S Bethesda, Md.

9. Nakamura M, Kayamori Y, Iso H, Kitamura A, Kiyama M, Koyama I, et al. LDL cholesterol performance of beta quantification reference measurement procedure. Clin Chim Acta. 2014;431:288-93.

10. Nordestgaard BG, Tybjaerg-Hansen A. IDL, VLDL, chylomicrons and atherosclerosis. Eur J Epidemiol. 1992;8 Suppl 1:92-8.

11. Expert Panel on Detection E, Treatment of High Blood Cholesterol in A. Executive Summary of The Third Report of The National Cholesterol Education Program (NCEP) Expert Panel on Detection, Evaluation, And Treatment of High Blood Cholesterol In Adults (Adult Treatment Panel III). JAMA. 2001;285(19):2486-97.

12. Kulkarni KR. Cholesterol profile measurement by vertical auto profile method. Clin Lab Med. 2006;26(4):787-802.

13. Kulkarni KR, Garber DW, Marcovina SM, Segrest JP. Quantification of cholesterol in all lipoprotein classes by the VAP-II method. J Lipid Res. 1994;35(1):159-68.

14. Ghassab RK, Gohari LH, Firoozray M, Yegane MN. Determination of Low Density Lipoprotein Particle Size by Polyacrylamide Gradient Gel Electrophoresis in Patients with Coronary Artery Stenosis. Laboratory Medicine. 2010;41(3):164-6.

15. Austin MA, Breslow JL, Hennekens CH, Buring JE, Willett WC, Krauss RM. Low-density lipoprotein subclass patterns and risk of myocardial infarction. JAMA. 1988;260(13):1917-21.

16. Sacks FM, Campos H. Clinical review 163: Cardiovascular endocrinology: Low-density lipoprotein size and cardiovascular disease: a reappraisal. J Clin Endocrinol Metab. 2003;88(10):4525-32.

17. Kanonidou C. Small dense low-density lipoprotein: Analytical review. Clinica Chimica Acta. 2021;520:172-8.

18. Mizutani H, Sako T, Arai N, Kuriyama K, Yoshimura I, Mori A, et al. Application of gel permeation HPLC for lipoprotein profiling in dogs. J Vet Med Sci. 2010;72(6):813-7.

19. Clouet-Foraison N, Gaie-Levrel F, Gillery P, Delatour V. Advanced lipoprotein testing for cardiovascular diseases risk assessment: a review of the novel approaches in lipoprotein profiling. Clin Chem Lab Med. 2017;55(10):1453-64.

20. Blake GJ, Otvos JD, Rifai N, Ridker PM. Low-density lipoprotein particle concentration and size as determined by nuclear magnetic resonance spectroscopy as predictors of cardiovascular disease in women. Circulation. 2002;106(15):1930-7.

21. Mora S, Otvos JD, Rifai N, Rosenson RS, Buring JE, Ridker PM. Lipoprotein particle profiles by nuclear magnetic resonance compared with standard lipids and apolipoproteins in predicting incident cardiovascular disease in women. Circulation. 2009;119(7):931-9.

22. Matyus SP, Braun PJ, Wolak-Dinsmore J, Jeyarajah EJ, Shalaurova I, Xu Y, et al. NMR measurement of LDL particle number using the Vantera Clinical Analyzer. Clin Biochem. 2014;47(16-17):203-10.

23. Matyus SP, Braun PJ, Wolak-Dinsmore J, Saenger AK, Jeyarajah EJ, Shalaurova I, et al. HDL particle number measured on the Vantera(R), the first clinical NMR analyzer. Clin Biochem. 2015;48(3):148-55.

24. Kanonidou C. Small dense low-density lipoprotein: Analytical review. Clin Chim Acta. 2021;520:172-8.

25. Caulfield MP, Li S, Lee G, Blanche PJ, Salameh WA, Benner WH, et al. Direct determination of lipoprotein particle sizes and concentrations by ion mobility analysis. Clin Chem. 2008;54(8):1307-16.

26. Mulder K, van Leeuwen C, Schouten JA, van Gent CM, Snel MT, Lahey J, et al. An evaluation of three commercial methods for the determination of LDL-cholesterol. Clin Chim Acta. 1984;143(1):29-35.

27. Jialal I, Hirany SV, Devaraj S, Sherwood TA. Comparison of an immunoprecipitation method for direct measurement of LDL-cholesterol with beta-quantification (ultracentrifugation). Am J Clin Pathol. 1995;104(1):76-81.

28. Sugiuchi H, Irie T, Uji Y, Ueno T, Chaen T, Uekama K, et al. Homogeneous assay for measuring low-density lipoprotein cholesterol in serum with triblock copolymer and alpha-cyclodextrin sulfate. Clin Chem. 1998;44(3):522-31.

29. Rifai N, Horvath AR, Wittwer CT. Tietz Textbook of Clinical Chemistry and Molecular Diagnostics. 6th ed: Elsevier; 2018.

30. Nauck M, Warnick GR, Rifai N. Methods for measurement of LDL-cholesterol: a critical assessment of direct

measurement by homogeneous assays versus calculation. Clin Chem. 2002;48(2):236-54.

31. Esteban-Salan M, Guimon-Bardesi A, de La Viuda-Unzueta JM, Azcarate-Ania MN, Pascual-Usandizaga P, Amoroto-Del-Rio E. Analytical and clinical evaluation of two homogeneous assays for LDL-cholesterol in hyperlipidemic patients. Clin Chem. 2000;46(8 Pt 1):1121-31.

32. Okada M, Matsui H, Ito Y, Fujiwara A, Inano K. Low-density lipoprotein cholesterol can be chemically measured: a new superior method. J Lab Clin Med. 1998;132(3): 195-201.

33. Miller WG, Waymack PP, Anderson FP, Ethridge SF, Jayne EC. Performance of four homogeneous direct methods for LDL-cholesterol. Clin Chem. 2002;48(3):489-98.

34. Friedewald WT, Levy RI, Fredrickson DS. Estimation of the concentration of low-density lipoprotein cholesterol in plasma, without use of the preparative ultracentrifuge. Clin Chem. 1972;18(6):499-502.

35. SI Units and the Friedewald Formula. Annals of Internal Medicine. 1992;117(10):876-.

36. Samman S, Truswell AS. The Friedewald equation for the determination of low-density-lipoprotein cholesterol: a special case. Am J Clin Nutr. 1993;58(6):928-9.

37. Zhao W, Chaffin C, Desmond RA, Hodges B, Daly TM, Andrew Robinson C, et al. Overestimation of HDL-cholesterol using a homogeneous “direct” assay. J Clin Lab Anal. 2004;18(1):42-4.

38. LaRosa JC, Chambless LE, Criqui MH, Frantz ID, Glueck CJ, Heiss G, et al. Patterns of dyslipoproteinemia in selected North American populations. The Lipid Research Clinics Program Prevalence Study. Circulation. 1986;73(1 Pt 2): I12-29.

39. Warnick GR, Knopp RH, Fitzpatrick V, Branson L. Estimating low-density lipoprotein cholesterol by the Friedewald equation is adequate for classifying patients on the basis of nationally recommended cutpoints. Clin Chem. 1990;36(1):15-9.

40. Martin SS, Blaha MJ, Elshazly MB, Toth PP, Kwiterovich PO, Blumenthal RS, et al. Comparison of a novel method vs the Friedewald equation for estimating low-density lipoprotein cholesterol levels from the standard lipid profile. JAMA. 2013;310(19):2061-8.

41. Sajja A, Park J, Sathiyakumar V, Varghese B, Pallazola VA, Marvel FA, et al. Comparison of Methods to Estimate Low-Density Lipoprotein Cholesterol in Patients With High Triglyceride Levels. JAMA Netw Open. 2021;4(10):e2128817.

42. Sampson M, Ling C, Sun Q, Harb R, Ashmaig M, Warnick R, et al. A New Equation for Calculation of Low-Density Lipoprotein Cholesterol in Patients With Normolipidemia and/or Hypertriglyceridemia. JAMA Cardiol. 2020; 5(5):540-8.

43. Mach F, Baigent C, Catapano AL, Koskinas KC, Casula M, Badimon L, et al. 2019 ESC/EAS Guidelines for the management of dyslipidaemias: lipid modification to reduce cardiovascular risk: The Task Force for the management of dyslipidaemias of the European Society of Cardiology (ESC) and European Atherosclerosis Society (EAS). European Heart Journal. 2019;41(1):111-88.

44. Pearson GJ, Thanassoulis G, Anderson TJ, Barry AR, Couture P, Dayan N, et al. 2021 Canadian Cardiovascular Society Guidelines for the Management of Dyslipidemia for the Prevention of Cardiovascular Disease in Adults. Can J Cardiol. 2021;37(8):1129-50.

45. [Detection, evaluation, and treatment of high blood cholesterol in adults]. Rev Panam Salud Publica. 2001;9(5): 338-44.

The Journal of the International Federation of Clinical Chemistry and Laboratory Medicine

eJIFCC

The exposure to human breast cancer cells altered 14 post-translational modifications of human serum albumin

Surya Kannan[1], Serhiy Souchelnytskyi[2,3]

[1] *College of Medicine, QU Health, Qatar University, Doha, Qatar*
[2] *Oranta Cancer Diagnostics AB, Uppsala, Sweden*
[3] *Lviv National University, Lviv, Ukraine*

ARTICLE INFO

Corresponding author:
Serhiy Souchelnytskyi
Oranta Cancer Diagnostics AB
Uppsala, 75263
Sweden
E-mail: serhiy8085@gmail.com

Key words:
human serum albumin,
post-translational modifications

ABSTRACT

Purpose

Serum albumin is in contact with practically all cells in the human body, including tumor cells in cancer patients. The purpose of this study was to explore whether cancer cells affect post-translational modifications (PTMs) of albumin.

Material and methods

Mass spectrometry was used to identify the PTMs. Purified human serum albumin was incubated with human breast cancer cells MDA-MB-231, MDA-MB-468, MCF7, or kept in water or in cell culture media. PTMs which were affected upon exposure of the albumin to cancer cells were identified. Three-dimensional analysis was performed to locate PTMs in albumin.

Results

We report here that an exposure to human breast cancer cells affected post-translational modifications (PTMs) of 14 peptides of human serum albumin (HSA). PTMs at 8 peptides were observed upon exposure of HSA to metastatic MDA-MB-231 and MDA-MB-468 breast cancer cells. PTMs at another 6 peptides were lost in MDA-MB-231 and MDA-MB-468 cells, while these 6 PTMs were observed in HSA exposed to conditionally tumorigenic MCF7 cells, or in HSA kept in water or a cell culture medium. Cancer cell altered phosphorylation, deamidation followed by methylation, acetylation, myristylation, palmitoylation, methylation, cysteine persulfide, and S-6-FMN cysteine modifications were detected in HSA. These PTMs locate predominantly in IB and IIA domains of HSA. Three-dimensional analysis showed that this region corresponds to the lipid-binding site and Sudlow's site 1.

Conclusion

Data reported here show that 14 PTMs of human serum albumin can be modified upon its exposure to human breast cancer cells.

❖❖❖❖❖

1. INTRODUCTION

Tumor cells modulate the matrix, the enzymatic and biochemical composition of the extracellular environment in a tumor [1, 2]. This modulation may include changes of post-translational modifications (PTMs) of proteins in the extracellular environment. PTMs may reflect the functional status of a tumor and serve as markers for the diagnostic and prognosis of cancer [3].

The number of reported PTMs in human serum albumin (HSA) is higher than 120 (reviewed in ref. [4]). The high number of PTMs indicates that there are many different forms of HSA due to different combinations of PTMs in a given HSA molecule. The diversity of PTM types is also broad and includes at least 30 types of PTMs, such as phosphorylation, acetylation, methylation, glycosylation, myristylation, palmitoylation, farnesylation, and PARylation [4-9]. Some of these PTMs in HSA have confirmed marker values for diagnosis and monitoring of diseases, e.g., the end glycation of HSA is the marker of diabetes [6-8]. Many other albumin PTMs do not have yet established links to physiological conditions. PTMs may be generated by enzymatic or chemical reactions. Phosphorylation, glycosylation, and ADP-ribosylation are examples of enzyme-dependent PTMs. Generation of advanced end glycation products is an example of non-enzymatic PTM. Oxidation of serum albumin at Cys34 is regarded as the marker of oxidative stress-related diseases [10, 11].

Serum albumin is the most abundant protein in human plasma [12, 13]. Albumin is highly abundant in the interstitial fluid of tumors, with albumin concentration reaching up to 60% of its concentration in plasma [12]. PTMs of albumin can be observed even in early-stage tumors, if these PTMs are stable in the interstitial fluid, lymph, and plasma. Protein acetylation and methylation are examples of such relatively stable PTMs [14]. Aggressive breast tumors often release circulating tumor cells in the bloodstream [15]. When the circulating tumor cells interact with albumin, it may be an additional opportunity to generate cancer relevant PTMs in albumin, in addition to PTMs that would be generated in the tumor. Therefore, presence of albumin in the interstitial fluid of tumors and in plasma, and the contact of albumin with tumor cells may lead to post-translational modifications of albumin. These tumor specific PTMs may serve as cancer markers.

Search for phosphorylation and acetylation in albumin from cancer patients identified a number of modified sites, even though the cancer

specificity of these PTMs has to be confirmed [4, 16-20]. The specificity issue is underlined by the possible impact of different non-cancerous conditions of the tested patients, e.g., diabetes, inflammatory diseases, renal or liver impairment. The use of an experimental model with only tumor cells may solve the specificity concern.

The published reports show that PTMs of albumin are frequent, and these PTMs may be a sensing mechanism for the status of a tumor. Therefore, it is important to explore whether human cancer cells affect PTMs profile of serum albumin. If PTMs of HSA are changed upon exposure to cancer cells, PTMs identification would be required for further clinical study of these PTMs as markers.

Here we report alterations of 14 PTMs of human serum albumin due to HSA exposure to human breast cancer cells.

2. MATERIALS AND METHODS

2.1. Materials

Human serum albumin was purchased from Abcam (Abcam ab205808, accession number P02768, 609 amino acids). Chemicals and reagents were purchased from Sigma Aldrich, Merk, and ThermoScientific, and were of analytical grade. This work was performed under an IBC permit from Qatar University (QU-IBC-2019/023). MCF7 (HTB-22), MDA-MB-231 (HTB-26), and MDA-MB-468 (HTB-132) human breast cancer cells were obtained from American Type Culture Collection (ATCC, Manassas, USA).

The cells used in this study were in culture for less than one year. The cells were regularly tested for contaminations by mycoplasma, bacteria, and fungi. The cells were cultured in DMEM medium supplemented with 10% fetal bovine serum, penicillin, and streptomycin, as recommended for these cells.

2.2. Preparation of albumin samples and electrophoresis

Aliquots of albumin were prepared in deionized (Millipore) water followed by glass-distilled water (pH 7.0-7.2), and stored frozen at -20^{0}C. Sodium dodecyl sulfate-polyacrylamide gel electrophoresis (SDS-PAGE) was performed as described earlier [9]. 10% acrylamide gel was used. Dithiothreitol (DTT) and iodoacetamide (IAA) pre-treatment of samples is frequently used in SDS-PAGE to break Cys-Cys bonds in proteins. However, this pre-treatment may also modify cysteine PTMs, as such we did not do pre-treatment of albumin samples with dithiothreitol (DTT) and (IAA). This preserved PTMs that could be affected by DTT and/or IAA. Staining with Coomassie Brilliant Blue R-250 was used to detect proteins separated in gels.

2.3. Cell culture and electrophoresis of albumin

Cells were seeded in 10 cm dishes to form confluent. The cells were washed 2 times with serum-free DMEM, then incubated with fresh serum-free DMEM for 3 hrs. The medium was changed to the fresh serum-free DMEM with added 5% human serum albumin. The cells were incubated for 24 hrs. The medium was collected and centrifuged for 10 min at 21,000 g (15,000 rpm). 10 μL of the cleared medium was subjected to sodium dodecyl sulfate-polyacrylamide gel electrophoresis (SDS-PAGE) as described earlier [9].

2.4. Mass spectrometry

MALDI-TOF MS (Ultraflextreme, Bruker Daltonics, Bremen, Germany) mass spectrometry was used for the analysis of albumin samples. Albumin samples were prepared by in-gel digestion with porcine mass spectrometry-grade trypsin (sequence grade, Promega, USA), as described previously [9]. In brief, protein bands of interest in gels were excised and collected

in tubes. Gels were destained, washed with water, 50mM ammonium bicarbonate, and 4 times with 100% acetonitrile. After the removal of acetonitrile, the gels were air-dried. Solution of trypsin (5 to 10 µl; 0.1-0.2 µg) was added to the dried gel, and incubated for 18-24 hrs at 37^0C. Digest of the protein was extracted by adding 30-50 µl of 50% acetonitrile and 0.1% trifluoracetic acid (TFA) in water. Extraction was for 2-3 hrs under gentle agitation. The extracted digest was loaded on a MALDI target (polished steel) with matrix α-cyano-4-hydroxycinnamic acid (Sigma Aldrich, USA).

Matrix-assisted laser-desorption ionization (MALDI) mass spectrometry was performed with Ultraflextreme instrument (Bruker Daltonics, Bremen, Germany). Mass spectra were collected in the range from 500 to 3,500 m/z values, positive mode, single protonated, and with a collection of a minimum of 10,000 laser shots for every single spectrum. For calibration, tryptic autodigestion peptides were used (842.51, 1045.56, and 2211.10 Da). Spectra were collected by using FlexControl software (Bruker Daltonics, Bremen, Germany). Analysis of spectra was performed with FlexAnalysis software (Bruker Daltonics, Bremen, Germany). Collected mass lists were used for identification by using ProFound and Mascot search engines. NCBIr database (version by October 2021) was used in the searches, and the significance of identification was set to $p<0.5$. Mass tolerance was +/-0.1 Da for peptide mass fingerprinting, the database was set to "human", with no restriction of pI, and molecular mass was set to +/- 50 kDa of the experimental migration position. For identification, the number of matched peptides and coverage of the identified protein with detected peptides were considered.

2.5. Prediction of PTMs

For the identification of modified peptides, we used FindMod tool that predicts PTMs in the experimentally measured peptide masses (https://www.expasy.org/resources/findmod) [21]. We included only PTMs that confirmed to the rules of PTMs identification by mass spectrometry, including statistical significance of identification set by FindMod to $p<0.5$ [21]. Manual curation of assigned PTMs was also performed to exclude false assignments. For example, if a PTM would interfere with the tryptic digestion and generation of a predicted peptide, such a PTM would be excluded. Mass spectrometry and PTMs assignment data were collected after 3 independent collections of cell culture experiments (see sections 2.1, 2.2, and 2.3) and analysis of mass spectra from independent samples from 2 mass spectrometry acquisitions and assignment of PTMs (see sections 2.4 and 2.5). Only reproducible data were used. Note that the mass spectrometry experiments, e.g., mass list generation and analysis, were set to statistical significance $p<0.5$.

2.6. Three-dimensional analysis of PTMs location

Protein Data Bank (PDB) was used to retrieve a 3-dimensional structure of human albumin. The structure deposited at PDB with accession number 1E78 for human serum albumin (doi: 10.2210 /pdb1E78/pdb) was used as a template for the analysis of identified PTMs. ChimeraX tool was used for allocation of the identified PTMs in the 3D structure of albumin (https://www.rbvi.ucsf.edu/chimerax) [22].

3. RESULTS

3.1. Preparation of albumin samples.

Presented here and our previously published [9] data, show that solubilization of HSA in water or in a cell culture medium DMEM did not affect the PTMs profile of albumin purified from the serum of healthy individuals. This allows efficient detection of PTMs in albumin incubated with human cancer cells, and comparison of its PTM profile with HSA that was kept solubilized in water or in

a cell culture medium (Figure 1). This comparison of PTMs profiles leads to the identification of PTMs affected by an exposure to cells.

We did not observe differences in migration in SDS-PAGE for HSA solubilized in water, medium, or exposed to different breast cancer cells (Figure 2A). This indicated the absence of PTMs affecting the molecular mass of HSA more than for a few thousands Da. The recovery of HSA incubated with the cells was estimated to be more than 95% of the initially added to the cells, and as compared to HSA prepared and kept in the medium without incubation with the cells. The low loss of HSA is due to adding HSA at a concentration that is similar to the concentration in human serum (i.e., 5%) [12, 13], and due to a relatively low albumin adhesion to the surface of the plates and cells.

As was expected, MCF7, MDA-MB-231, and MDA-MB-468 cells did not change their morphology, neither showed signs of cell death during incubation with 5% HSA in DMEM. These cells are extensively used in breast cancer research, and are known to tolerate incubation conditions that are similar to the used in this work. Incubation in a serum-free culturing medium for 24 hrs could inhibit cell proliferation but does not affect cellular viability and cellular tumorigenic properties.

Large quantities of recovered HSA after its incubation with cells, e.g., 30 to 50 µg in a single electrophoresis lane, allowed robust mass spectrometry analysis. The mass spectra provided confirmatory identification of human serum albumin (accession number P02768). The collected mass spectra of albumin samples showed a similar pattern of main peaks for all 5 experimental conditions (Supplementary Figure S1, this figure can be retrieved at https://doi.org/10.6084/m9.figshare.21552372.v1).

Figure 1 **Workflow of the project: the main steps of this study are shown**

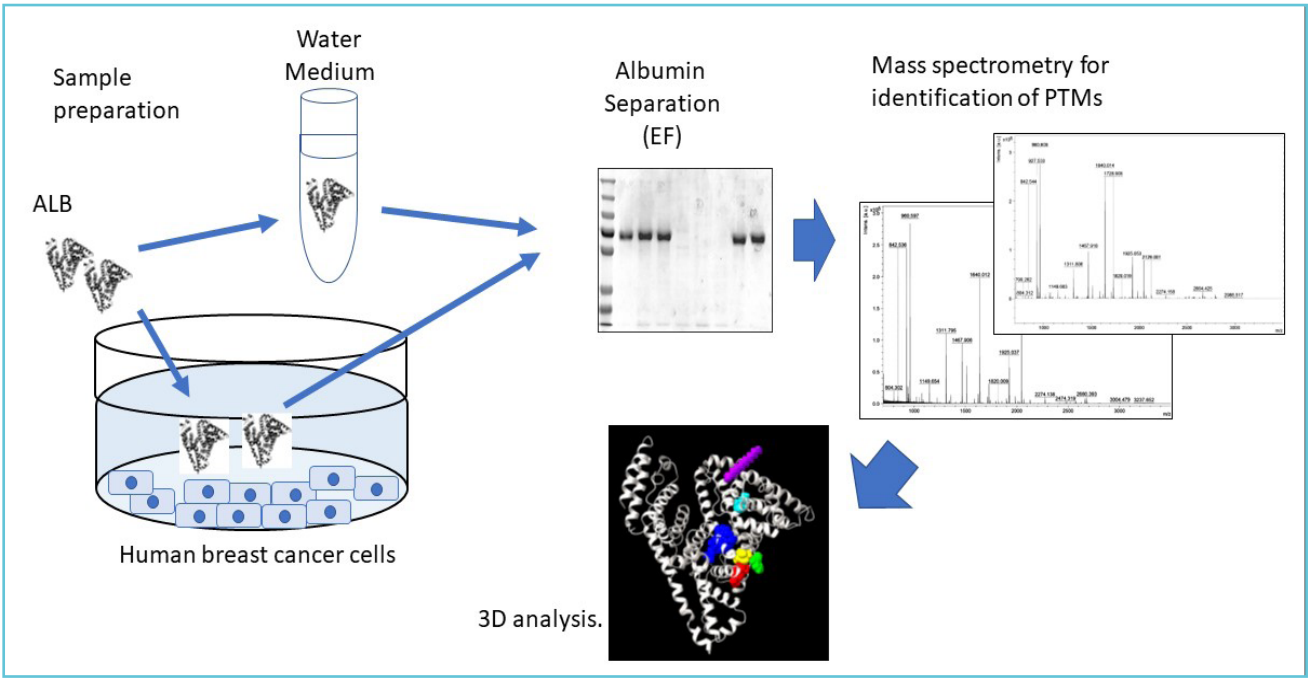

Samples were prepared by incubation of human serum albumin with human breast cancer cells, or by keeping albumin solubilized in water or a cell culture medium. The recovered albumin was separated by SDS-PAGE, and subjected to mass spectrometry for identification of post-translational modifications. Modeling of the location of the identified PTMs in the 3-dimensional model of human serum albumin was performed.

Figure 2 Separation of HSA and mass spectrometry analysis

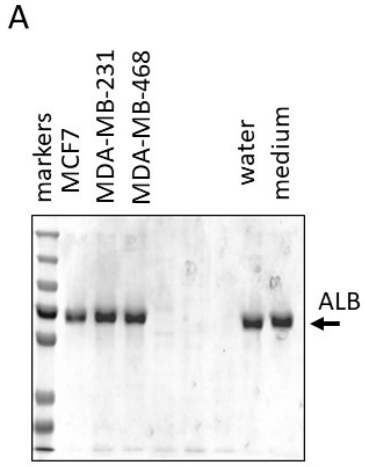

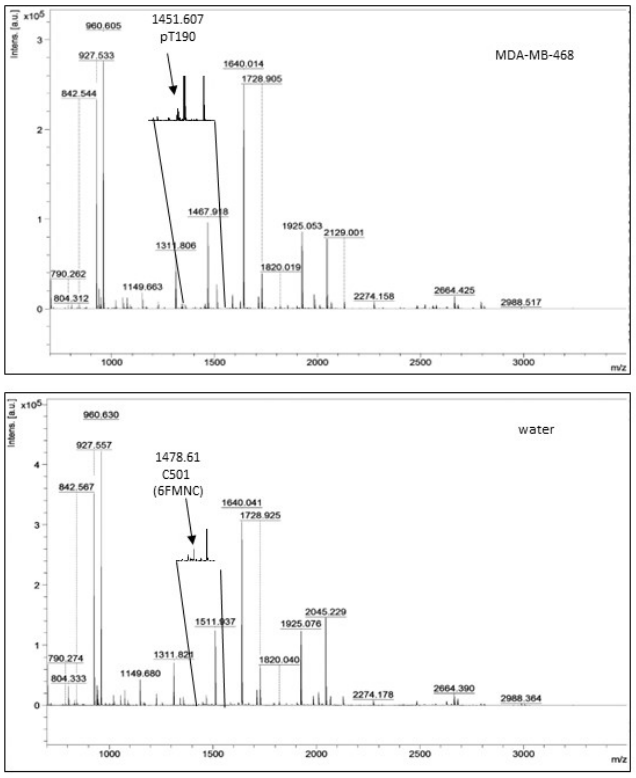

A) Separation of human serum albumin (ALB) samples in SDS-PAGE gel is shown. The arrow and annotation "ALB" indicate the migration position of HSA. The annotation of samples is indicated at the top of the gel. Migration of molecular mass markers is indicated as "markers". B) Two mass spectra show representative spectra of albumin recovered after exposure to MDA-MB-468 cells and water solubilized HSA. Representative mass spectra of all 5 types of albumin samples are shown in Supplementary Figure S1. The intensity of peaks and m/z values are indicated. Inserts show examples of peaks with assigned PTMs. See Table 1 for annotation of all PTMs.

After optimization experiments, the experiments with the established protocol were repeated 3 times and are presented here. Thus, the protocol of this study allowed the generation of reproducible and representative mass spectra of HSA of 5 tested conditions, e.g., albumin exposed to MDA-MB-231, MDA-MB-468, and MCF7 cells, or kept in water or in the cell culture medium.

3.2. Exposure of albumin to cancer cells altered PTMs in 14 peptides of albumin

The mass spectra of HSA exposed to human breast cancer cells, solubilized in water or in the cell culture medium were used to search for post-translational modification of HSA. We applied FindMod tool which is one of the most used tools for PTMs assignment with mass spectrometry data [21]. FindMod is known for the application of stringent criteria for PTMs prediction. We generated PTMs profiles for HSA retrieved in each experimental condition. Then, we removed all PTMs that were not affected by exposure of HSA to the cells in comparison to HSA in water or the cell culture medium. These removed PTMs were not altered by exposure to cells. We repeated mass spectrometry experiments with independent samples from 2 different experiments, and only reproducibly detected PTMs were considered for analysis.

The analysis showed 14 modified peptides of 8 types of PTMs (Table 1; Supplementary Table S1, this table can be retrieved at https://doi.org/10.6084/m9.figshare.21552414.v1).

We observed PTMs that discriminated HSA exposed to MDA-MB-231 and MDA-MB-468 from albumin exposed to MCF7 cells, or kept in water or in the cell culture medium. MDA-MB-231 and MDA-MB-468 cells represent aggressive breast cancer and form tumors in animal studies, while MCF7 cells are conditionally tumorigenic and much less aggressive [23, 24]. PTMs identified in HSA solubilized in water represent important controls of PTMs present in HSA from healthy individuals. The cell culture medium contains chemicals that theoretically may affect PTMs, e.g., by oxidation and chemical addition reactions. The Table 1 shows that the PTMs in HSA that originated from the healthy individuals were also present in the albumin solubilized in the cell culture medium. It means that the cell culture medium did not interfere with PTMs described in Table 1. However, the exposure of HSA to the cells affected these PTMs.

Eight PTMs were observed after exposure to aggressive cells, e.g., phosphorylation, palmitoylation, and cysteine persulfide modification. Other 6 PTMs were observed in albumin exposed to non-aggressive MCF7 cells and for HSA non-exposed to cells, e.g., deamidation followed by methylation, acetylation, and S-6-FMN cysteine modification (Table 1).

The distribution of the identified PTMs in the sequence of albumin showed localization of PTMs mostly in the IB and IIA domains of HSA (Figure 3).

Table 1 **Post-translational modifications of human serum albumin detected after exposure of HSA to breast cancer cells**

PTM*	Peptide	Position (peptide)	Position (site)	MCF7	MDA-MB-231	MDA-MB-468	Water	Medium
6FMNC	C**C**TESLVNR	500-508	C501	Yes	-	-	Yes	Yes
DEAME	CASL**Q**K	224-229	Q228	Yes	-	-	Yes	Yes
METH	YI**C**ENQDSISSK	287-298	C289	Yes	-	-	Yes	Yes
DEAME	ADLAKYICEN**Q**DSISSK	282-298	Q292	-	-	-	Yes	Yes
ACET	HPYFYAPELLFFA**K**R	169-183	K182	Yes	-	-	-	-
MYRI	LVRPEVDVMCTAFHDNEETFL**K**K	139-161	K160	Yes	-	-	-	-
PHOS	AEFAEV**S**K	250-257	S256	-	Yes	Yes	-	-
PHOS	YICENQD**S**I**SS**KLK	287-300	S294, S296, S297	-	Yes	-	-	-

PHOS	AAF**T**ECCQAADK	187-198	T190	-	-	Yes	-	-
PALM	AVMDDFAAFVEK**CC**K	570-584	C582, C583	-	Yes	Yes	-	-
ACET	EQL**K**AVMDDFAAFVEK	566-581	K569	-	Yes	Yes	-	-
CYSP	C**C**KHPEAK	461-468	C462	-	Yes	Yes	-	-
METH	ADLA**K**YICENQDSISSK	282-298	K286	-	Yes	Yes	-	-
MYRI	AAFTE**CC**QAADK	187-198	C192, C193	-	Yes	Yes	-	-

MCF7 are conditionally tumorigenic, and less aggressive as compared to invasive and highly tumorigenic MDA-MB-231 and MDA-MB-468 cells. PTMs in HSA that was solubilized in water or medium are shown to indicate the presence of these PTMs in HSA from healthy individuals (Water), and no impact on these PTMs of the chemicals in the cell culture medium (Medium). In bold and underlined are indicated modified amino acids. "Yes" indicates detection of a peptide, "-" indicates absence of a peptide. A peptide position in HSA sequence is indicated.

** 6FMNC, S-6-FMN cysteine modification; DEAME, deamidation followed by methylation; METH, methylation; ACET, acetylation; MYRI, myristoylation; PHOS, phosphorylation; PALM, palmytoylation; CYSP, cysteine persulfide modification.*

Figure 3 **Distribution of the identified 14 PTMs in the sequence of human serum albumin**

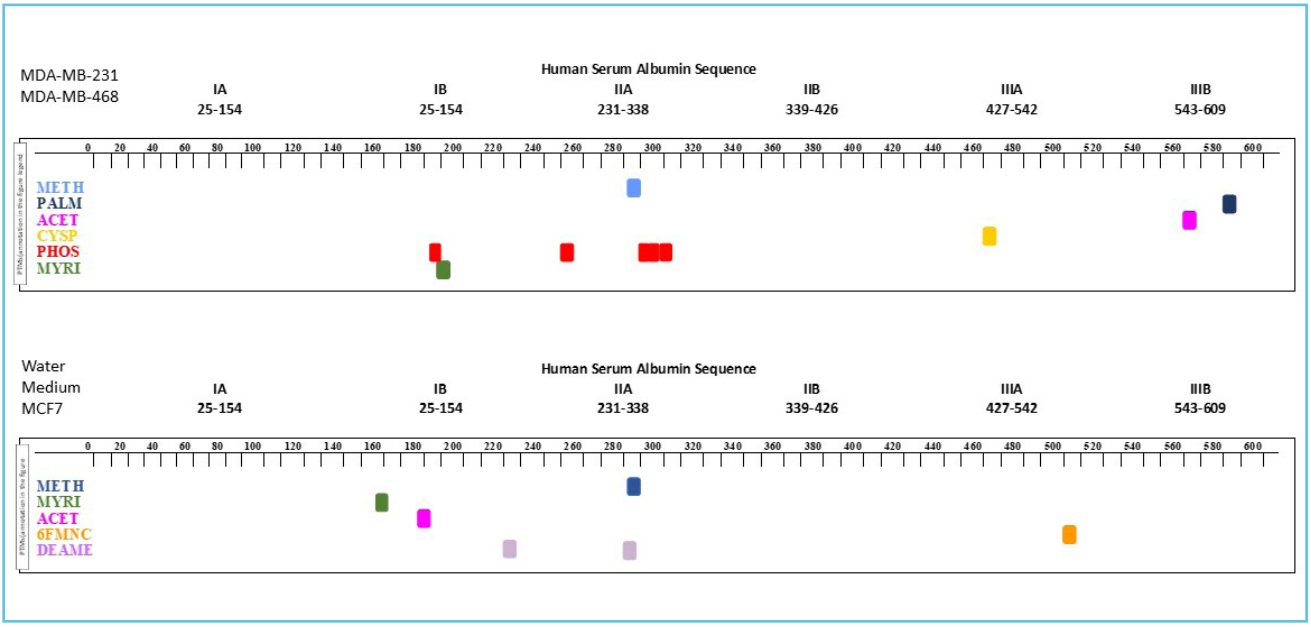

Panels show the distribution of PTMs annotated in Table 1. The upper panel shows 8 PTMs observed in HSA exposed to aggressive breast cancer cells MDA-MB-231 or MDA-MB-468. The lower panel shows 6 PTMs identified in HSA exposed to conditionally tumorigenic MCF7 cells, or kept in water, or in the cell culture medium. The sequence of HSA (accession number P02768) corresponds to a pro-form of albumin of 609 amino acids length. PTMs are colour coded, the same colour coding is used in Figures 3 and 4.

This contrasts with the relatively uniform distribution of PTMs in HSA from the serum of healthy individuals [4, 9, 18-20]. The focus on IB and IIA domains indicates functional implication of this region in modifications by cancer cells, by promotion of PTMs upon exposure to aggressive cancer cells, or by removal of PTMs. The 8 PTMs that appeared in HSA after its exposure to aggressive cancer cells have not been detected in HSA from healthy individuals [4, 9, 18-20].

3.3. Three-dimensional modeling shows location of PTMs at the Sudlow's site 1

The 3-dimensional model of human serum albumin [25, 26] is an excellent tool for the evaluation of the potential impact of identified PTMs on albumin functions. Structural regions involved in interactions with fatty acids, drugs, and metals have been identified in HSA [25-28]. We observed that the location of identified PTMs may affect lipid-binding sites in HSA by cysteine persulfide modification (CYSP), methylation (METH), and phosphorylation (PHOS) after exposure to MDA-MB-231 and MDA-MB-468 cells (Figure 4). In HSA incubated with MCF7 cells or kept in water or cell culture medium, one of the lipid-binding sites (Sudlow's site 1) is also affected by deamidation followed by methylation (DEAME), methylation (METH), and S-6-flavine mononucleotide (FMN) conjugation to cysteine (6FMNC) (Figure 4). 3D model shows the location of myristylation (MYRI) and palmitoylation (PALM) on the top of the 'heart' structure of HSA.

Figure 4 3-dimensional modelling of location of the 14 identified PTMs

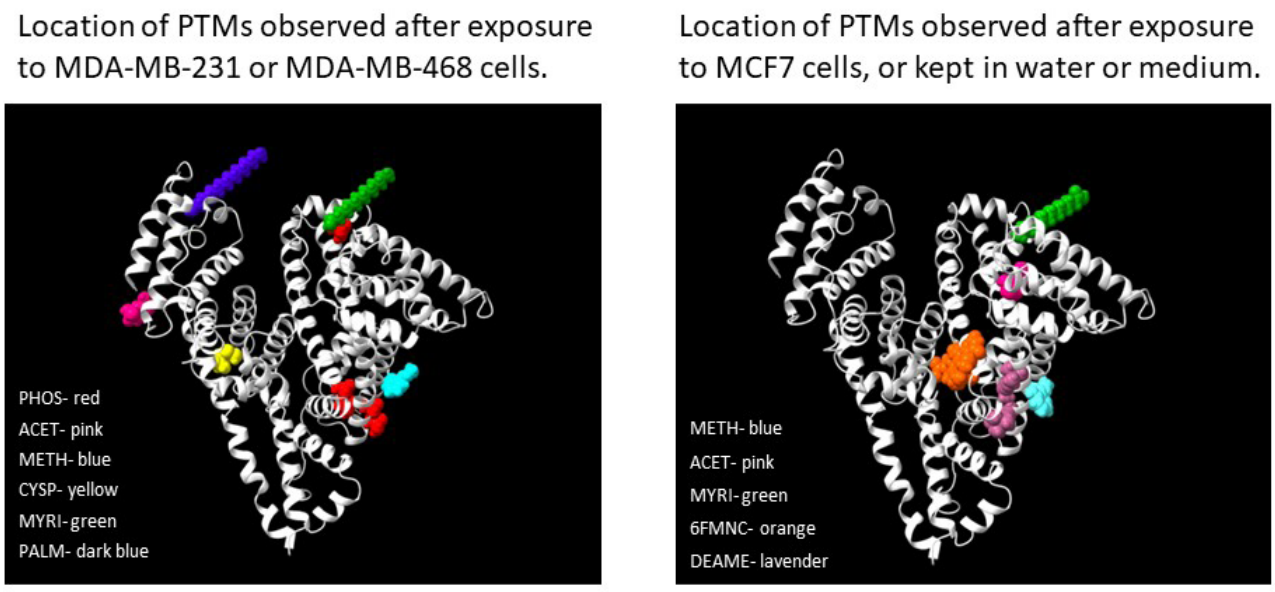

The left panel shows 3D modelling of the location of PTMs at 8 modified peptides that were observed in HSA exposed to MDA-MB-231 and MDA-MB-468 cells but not in HSA exposed to conditionally tumorigenic MCF7, or solubilized in water or in the cell culture media. The right panel shows 3D modelling of the location of PTMs at 6 modified peptides that were observed in HSA exposed to conditionally tumorigenic MCF7 cells or were kept in water and in the cell culture medium. PTMs are colour coded as indicated in the images. The 3D model of non-PTM modified human serum albumin, accession number 1E78 (doi: 10.2210/pdb1E78/pdb; 585 amino acids representing 25 to 609 amino acids of HAS, was retrieved from Protein Data Bank (PDB) under open access permit. ChimeraX tool was used to locate reported here PTMs in the 3D model of HSA.

These modifications (MYRI and PALM) are considered as a mechanism for tethering proteins to a membrane. It remains to be explored whether these modifications affect the distribution of albumin.

4. DISCUSSION

Our data show that HSA exposed to cancer cells acquires novel PTMs. Our identification of enhanced phosphorylation of HSA upon exposure to aggressive cancer cells (Figure 3; Table 1) is in an agreement with the enhanced activities of many kinases in growing tumors [29]. The reported here phosphorylation of HSA at T190, S256, S294, and S297 was observed in non-small cell lung cancer tumors [18]. Phosphorylation at S256, S294, and S296 was detected in pancreatic cancer tumors [19]. Phosphorylation at T190, S256, S294, and S296 were observed in samples of breast cancer tumors [20]. However, none of the published reports [18-20] showed a dependency of the phosphorylation on tumor cells, or in comparison to HSA from healthy individuals. Our data demonstrate that the phosphorylation mentioned in Table 1, was observed only after exposure of HSA to aggressive cancer cells, and no phosphorylation was observed in HSA exposed to conditionally tumorigenic MCF7 cells or in HSA kept in water or in the cell culture medium (Table 1). Our data suggest that the phosphorylation at T190, S256, S294, S296, and S297 may serve as a marker of advanced breast cancer.

The sequences surrounding the phosphorylated residia (Table 1, Figure 3, Supplementary Table S1) differ from consensus sequences reported for SerPro-targeting kinases. Only 1% of reported phosphorylation sites have functional information, e.g., information about a kinase and/or its functional role (www.phosphonet.ca). Therefore, the prediction of the kinase(s) of HSA and/or functional impact of the 3 identified phosphorylated peptides await further studies.

We observed HSA acetylation at K182 and K569 only after its exposure to cells (Table 1, Figure 3). Acetylation at K182 was observed in humans [16, 17] and at K569 in rats [30]. In humans, K182 acetylation was described in datasets of mass spectrometry studies of liver and colorectal cancer [16, 17]. These reports did not explore the dependency of K182 and K569 acetylation on tumorigenesis. Our data show that this acetylation is detected only after HSA contact with cancer cells.

Modifications with lipids were described for HSA [9]. Our finding of myristylation at C192 or C193 has not been described earlier. A tripeptide CCK with C582 and C583 was identified as palmitoylated, with C583 as the probable site of palmitoylation, due to unlikely trypsin cut with adjacent palmitoylated cysteine [9]. Detection of the peptide consisting of 15 amino acids, with a lysine before C582 and possible no-cut by trypsin after lysine followed by the palmitoylated C582, indicates that the C582 is the most probable palmitoylation site in HSA exposed to cancer cells. Both S-palmitoylation and S-myristylation were detected for HSA that was exposed to aggressive cancer cells MDA-MB-231 and MDA-MB-468 (Table 1, Figure 3). We also observed a lysine-myristylation at K160 in HSA exposed to conditionally tumorigenic MCF7 cells. N-myristylation is associated with cancer progression. The enzyme lysine myristoyltransferease NMT1 was associated with the aggressive development of human breast cancer [31]. The location of the modifications at the top of the “heart” structure of albumin (Figure 4) may indicate their potential interactions with membranes.

Ten methylation sites were reported for HSA [32], however, without a confirmed dependency on cancer. We observed methylation at C289,

and methylation after deamidation at Q228 and Q292 in HSA that was kept in water or the cell culture medium, or was incubated with MCF7 cells, but no detection of these PTMs in HSA that was incubated with aggressive cancer cells. (Table 1, Figure 3). Deamidation followed by methylation at Q292 was observed by us earlier in HSA [9]. This suggests that demethylation and/or inhibition of deamidation at Q292 could be associated with the exposure to aggressive cancer cells. K286 was found methylated in HSA incubated with MDA-MB-231 or MDA-MB-468 cells (Table 1, Figure 3). The detected cancer cell-relevant differences in methylation are in the Sudlow's site 1 in HSA (Figure 4), suggesting modifications of interactions via this site.

Cysteine persulfide modification is the result of the action of reactive sulfur species, and is one of the oxidation mechanisms of cysteine. Our data predicted the formation of a cysteine persulfide at C462 in HSA exposed to aggressive cancer cells (Table 1, Figure 3). No data about this PTM in HSA was reported earlier. However, Fukuoka *et al.* observed an increased level of cysteine persulfide in colon tumors, as compared to a normal colon tissue [33], which may indicate the relevance of this PTM to cancer. Doka *et al.* showed that cysteine persulfide modification is involved in the regulation of protein functions and growth factor responsiveness [34]. Our detection of cysteine persulfide modification in albumin exposed to aggressive cancer cells but not in HSA exposed to MCF7 cells, suggests that this modification may be explored as a marker of aggressive development of breast cancer.

S-6-flavine mononucleotide (FMN) conjugation to cysteine (6FMNC) at C501 in albumin is an example of another oxidation-dependent PTM. We observed this modification earlier in HAS from healthy individuals [9]. 6FMNC at C501 was absent in HSA after exposure to the aggressive cancer cells. Flavine mononucleotide is involved in the regulation of the redox potential in cells, and this modification may indicate 6FMNC modification of HSA due to higher oxidation potential in tumors or in the tumor microenvironment.

Hypoalbuminemia is a marker of aggressive development of cancer [12, 13, 35]. End glycation of HSA serves as a marker of diabetes [6, 8]. Oxidation of Cys34 in HSA is considered a sensor of oxidative stress-related diseases [10, 11]. These observations are sufficient proof of the clinical value of HSA PTMs. The 14 PTMs reported here show that HSA is engaged by the microenvironment of cancer cells. We show that the cells can affect PTMs of albumin. This is an important finding that opens for further study of PTMs clinical marker value.

❖❖❖❖❖

Conflict of interest

Authors declare that they have no competing interests.

Ethical approval

This work was performed under an IBC permit from Qatar University (QU-IBC-2019/023).

Availability of data and materials

Original files are freely available upon request. All data generated and analyzed during the study are included in this published article.

The Supplementary Figure S1 can be retrieved at: https://doi.org/10.6084/m9.figshare.21552372.v1.

Representative mass spectra of human serum albumin recovered in the 5 tested conditions are shown. The intensity of peaks and m/z values are annotated. The tested conditions are exposure of HSA to human breast cancer cells MDA-MB-231 (A), MDA-MB-468 (B), MCF7 (C), or HSA kept solubilized in water (D), or in the cell culture medium (E).

The Supplementary Table S1 can be retrieved at: https://doi.org/10.6084/m9.figshare.21552414.v1.

The Supplementary Table S1 shows expanded information about identified PTMs presented in Table 1. The information about the user mass, database mass, mass difference, modification mass difference, PTM name, miscut or not, peptide sequence, and position of modified peptides are indicated.

Acknowledgments

Partial support by the "Ove's Minnesfond", QUCG-CMED-20/21-1, QUCG-CMED-18/19-2, and QUST-2-CMED-2020-12 to S.S. is acknowledged.

Authors' contributions

1. Study Design: Serhiy Souchelnytskyi;
2. Data Collection: Surya Kannan;
3. Statistical Analysis: Surya Kannan, Serhiy Souchelnytskyi;
4. Data Interpretation: Surya Kannan, Serhiy Souchelnytskyi;
5. Manuscript Preparation: Surya Kannan, Serhiy Souchelnytskyi;
6. Literature Search: Surya Kannan, Serhiy Souchelnytskyi;
7. Funds Collection: Serhiy Souchelnytskyi.

❖❖❖❖❖

REFERENCES

1. Kim S-J, Khadka D, Seo JH. Interplay between Solid Tumors and Tumor Microenvironment. Front Immunol. 2022 May 30;13:882718. https://doi.org/10.3389/fimmu.2022.882718. eCollection 2022.

2. de Andrés JL, Griñán-Lisón C, Jiménez G, Marchal JA. Cancer stem cell secretome in the tumor microenvironment: a key point for an effective personalized cancer treatment. J Hematol Oncol. 2020 Oct 15; 13:136. https://doi.org/10.1186/s13045-020-00966-3.

3. Li W, Li F, Zhang X, Lin HK, Xu C. Insights into the post-translational modification and its emerging role in shaping the tumor microenvironment. Signal Transduction and Targeted Therapy. 2021 Dec 29; 6(1):422. https://doi.org/10.1038/s41392-021-00825-8.

4. Kannan S, Souchelnytskyi S. Review of Post-translational Modification of Human Serum Albumin. Curr Protein Pept Sci. 2022 Mar 17; 23(2):114-120. https://doi.org/10.2174/1389203723666220217150332.

5. Martin S, Pia E. In Vitro Phosphorylation of Serum Albumin by Two Protein Kinases: A Potential Pitfall in Protein Phosphorylation Reactions. Analytical Biochemistry. 1986 May 1; 154:395-399. https://doi.org/10.1016/0003-2697(86)90004-7.

6. Giglio RV, Lo Sasso B, Agnello L, Bivona G, Maniscalco R, Ligi D. Recent Updates and Advances in the Use of Glycated Albumin for the Diagnosis and Monitoring of Diabetes and Renal, Cerebro- and Cardio-Metabolic Diseases. Journal of Clinical Medicine. 2020 Nov 11; 9(11):3634. https://doi.org/10.3390/jcm9113634.

7. Qiu H, Jin L, Chen J, Shi M, Shi F, Wang M, et al. Comprehensive glycomic analysis reveals that human serum albumin glycation specifically affects the pharmacokinetics and efficacy of different anticoagulant drugs in diabetes. Diabetes. 2020 Jan 23; 69(4):760–770. https://doi.org/10.2337/db19-0738.

8. Anguizola J, Matsuda R, Barnaby OS, Hoy KS, Wa C, DeBolt E, et al. Review: Glycation of human serum albumin. Clinica Chimica Acta. 2013 Oct 21; 425:64–76. https://doi.org/10.1016/j.cca.2013.07.013.

9. Kannan S, Krishnankutty R, Souchelnytskyi S. Novel post-translational modifications of human serum albumin. Protein Pept Lett. 2022 Jun 2; 29(5):473-484. https://doi.org/10.2174/0929866529666220318152509.

10. Lepedda AJ, Zinellu A, Nieddu G, Muro P De, Carru C, Spirito R, et al. Human Serum Albumin Cys 34 Oxidative Modifications following Infiltration in the Carotid Atherosclerotic Plaque. Oxid Med Cell Longev. 2014 Mar 6;2014:690953. https://doi.org/10.1155/2014/690953.

11. Nagumo K, Tanaka M, Chuang VTG, Setoyama H, Watanabe H, Yamada N, et al. Cys34-cysteinylated human serum albumin is a sensitive plasma marker in oxidative stress-related chronic diseases. PLoS One. 2014 Jan 8; 9(1): e85216. https://doi.org/10.1371/journal.pone.0085216. eCollection 2014.

12. Caraceni P, Tufoni M, Bonavita ME. Clinical use of albumin. Blood Transfus. 2013 Aug 10; 11(SUPPL. 4):s18-25. https://doi.org/10.2450/2013.005s.

13. Fanali G, Di Masi A, Trezza V, Marino M, Fasano M, Ascenzi P. Human serum albumin: From bench to bedside.

Mol Aspects Med. 2012 Jun; 33(3):209-290. https://doi.org/10.1016/j.mam.2011.12.002.

14. Su X, Wellen KE, Rabinowitz JD. Metabolic control of methylation and acetylation. Curr Opin Chem Biol. 2016 Nov 28; 30:52-60. https://doi.org/10.1016/j.cbpa.2015.10.030.

15. Fridrichova I, Kalinkova L, Ciernikova S. Clinical Relevancy of Circulating Tumor Cells in Breast Cancer: Epithelial or Mesenchymal Characteristics, Single Cells or Clusters? Int J Mol Sci. 2022 Oct 12; 23(20):12141. https://doi.org/10.3390/ijms232012141.

16. Tucker M (2010) CST Curation Set: 8953; Year: 2010; Biosample/Treatment: tissue, liver/untreated; Disease: liver cancer; SILAC: -; Specificities of Antibodies Used to Purify Peptides prior to LCMS: acK Antibodies Used to Purify Peptides prior to LCMS: Acetylated-Lysine (Ac-K2-100) Rabbit mAb Cat#: 9814, PTMScan(R) Acetyl-Lys Motif (Ac-K) Immunoaffinity Beads Cat#: 1989 Curation sets: 8951, 8952. https://www.phosphosite.org/curatedInfoAction.action?record=11958524.

17. Li Y (2008) CST Curation Set: 4813; Year: 2008; Biosample/Treatment: tissue, colon/untreated; Disease: colorectal cancer; SILAC: -; Specificities of Antibodies Used to Purify Peptides prior to LCMS: acK Antibodies Used to Purify Peptides prior to LCMS: Acetylated-Lysine (Ac-K2-100) Rabbit mAb Cat#: 9814, PTMScan(R) Acetyl-Lys Motif (Ac-K) Immunoaffinity Beads Cat#: 1989 Curation sets: 4809, 4799, 4758, 4642, 3507, 3509. https://www.phosphosite.org/proteinAction.action?id=8316&showAllSites=true.

18. Schweppe DK, Rigas JR, Gerber SA. Quantitative phosphoproteomic profiling of human non-small cell lung cancer tumors. J Proteomics. 2013 Oct 8; 91:286-296. https://doi.org/10.1016/j.jprot.2013.07.023.

19. Britton D, Zen Y, Quaglia A, Selzer S, Mitra V, Löβner C, et al. Quantification of pancreatic cancer proteome and phosphorylome: indicates molecular events likely contributing to cancer and activity of drug targets. PLoS One. 2014 Mar 26; 9:e90948. https://doi.org/10.1371/journal.pone.0090948.

20. Mertins P, Mani DR, Ruggles KV, Gillette MA, Clauser KR, Wang P, et al. Proteogenomics connects somatic mutations to signalling in breast cancer. Nature. 2016 May 25; 534:55-62. https://doi.org/10.1038/nature18003.

21. Wilkins MR, Gasteiger E, Gooley AA, Herbert BR, Molloy MP, Binz PA, Ou K, Sanchez J-C, Bairoch A., Williams KL, Hochstrasser DF. High-throughput mass spectrometric discovery of protein post-translational modifications. Journal of Molecular Biology. 1999 Jun 11; 289(3):645-657. https://doi.org/10.1006/jmbi.1999.2794.

22. Pettersen EF, Goddard TD, Huang CC, Meng EC, Couch GS, Croll TI, et al. UCSF ChimeraX: Structure visualization for researchers, educators, and developers. Protein Sci. 2021 Jan; 30(1):70-82. https://doi.org/10.1002/pro.3943.

23. Huguet EL, McMahon JA, McMahon AP, Bicknell R, Harris AL. Differential expression of human Wnt genes 2, 3, 4, and 7B in human breast cell lines and normal and disease states of human breast tissue. Cancer Res. 1994 May 15; 54(10):2615-2621. PMID: 8168088.

24. Brinkley BR, Beall PT, Wible LJ, Mace ML, Turner DS, Cailleau RM. Variations in cell form and cytoskeleton in human breast carcinoma cells in vitro. Cancer Res. 1980 Sep; 40(9):3118-3129. PMID: 7000337.

25. Carter DC, He XM, Munson SH, Twigg PD, Gernert KM, Broom MB, et al. Three-dimensional structure of human serum albumin. Science. 1989 Jun 9; 244(4909):1195-1198. https://doi.org/10.1126/science.2727704.

26. He XM, Carter DC. Atomic Structure and chemistry of human serum albumin. Nature. 1992 Jul 16; 358(6383): 209-215. https://doi.org/10.1038/358209a0.

27. Curry S, Mandelkow H, Brick P, Franks N. Crystal structure of human serum albumin complexed with fatty acid reveals an asymmetric distribution of binding sites. Nat Struct Biol. 1998 Sep; 5(9):827-835. https://doi.org/10.1038/1869.

28. Ferraro G, Massai L, Messori L, Merlino A. Cisplatin binding to human serum albumin: a structural study. Chem Commun (Camb). 2015 Apr 8; 51(46):9436-9439. https://doi.org/10.1039/c5cc01751c.

29. Chu CN, Lee TKW. Targeting protein kinases in cancer stem cells. Essays Biochem. 2022 Sep 16; 66(4):399-412. https://doi.org/10.1042/EBC20220002.

30. Lundby A, Lage K, Weinert BT, Bekker-Jensen DB, Secher A, Skovgaard T, et al. Proteomic analysis of lysine acetylation sites in rat tissues reveals organ specificity and subcellular patterns. Cell Rep. 2012 Aug 30;2(2):419-431. https://doi.org/10.1016/j.celrep.2012.07.006.

31. Mackey JR, Lai J, Chauhan U, Beauchamp E, Dong W-F, Glubrecht D, et al. N-myristoyltransferase proteins in breast cancer: prognostic relevance and validation as a new drug target. Breast Cancer Res Treat. 2021 Jan 4;186(1):79-87. https://doi.org/10.1007/s10549-020-06037-y.

32. Rikova K (2013) CST Curation Set: 20096; Year: 2013; Biosample/Treatment: cell line, A549, H1355, H23, H441, H1792; Disease: -; TMT: Y; Specificities of Antibodies Used to Purify Peptides prior to LCMS: m1R Antibodies Used to Purify Peptides prior to LCMS: Mono-Methyl Arginine [mme-R] MultiMab(TM) Rabbit mAb mix Cat#: 8015. https://www.phosphosite.org/curatedInfoAction.action?record=49192900.

33. Fukuoka H, Andou T, Moriya T, Narita K, Kasahara K, Miura D, et al. Sulphur metabolism in colon cancer tissues: a case report and literature review. J Int Med Res. 2021 Nov

17;49(11):3000605211059936. https://doi.org/10.1177/03000605211059936.

34. Dóka E, Ida T, Dagnell M, Abiko Y, Luong NC, Balog N, et al. Control of protein function through oxidation and reduction of persulfidated states. Sci Adv. 2020 Jan 1; 6(1):eaax8358. https://doi.org/10.1126/sciadv.aax8358. eCollection 2020 Jan.

35. Nicholson JP, Wolmarans MR, Park GR. The role of albumin in critical illness. Br J Anaesth. 2000 Oct 1; 85(4): 599-610. https://doi.org/10.1093/bja/85.4.599.

The Journal of the International Federation of Clinical Chemistry and Laboratory Medicine

eJIFCC

Correlation between time to positive result of SARS-CoV-2 rapid antigen self-test and viral antigen concentration

Gian Luca Salvagno[1,2], Brandon M. Henry[3], Simone De Nitto[1,2], Laura Pighi[1,2], Giuseppe Lippi[1]

[1] *Section of Clinical Biochemistry and School of Medicine, University of Verona, Verona, Italy*

[2] *Service of Laboratory Medicine, Pederzoli Hospital, Peschiera del Garda, Verona, Italy*

[3] *Clinical Laboratory, Division of Nephrology and Hypertension, Cincinnati Children's Hospital Medical Center, Cincinnati, OH, USA*

ARTICLE INFO

Corresponding author:
Prof. Giuseppe Lippi
Section of Clinical Biochemistry
University Hospital of Verona
Piazzale L.A. Scuro, 10
37134 Verona
Italy
Phone: 0039-045-8122970
Fax: 0039-045-8124308
E-mail: giuseppe.lippi@univr.it

Key words:
COVID-19; SARS-CoV-2, laboratory medicine, diagnosis, immunoassay

ABSTRACT

Background

This study was planned to investigate how the positivization time of a SARS-CoV-2 rapid antigen self-test may correlate with SARS-CoV-2 nucleocapsid (N) antigen concentration measured with a quantitative laboratory-based immunoassay.

Methods

Paired nasopharyngeal (healthcare-collected) and nasal (self-collected) samples were taken from patients undergoing routine SARS-CoV-2 testing. The concentration of SARS-CoV-2 antigen nucleocapsid (N) was assayed with Liaison SARS-CoV-2 Antigen test, whilst the time of positivization of COVID-VIRO ALL rapid diagnostic test (RDT) was concomitantly measured and then compared SARS-CoV-2 viral load measured with Liaison SARS-CoV-2 Antigen test and expressed as Median Tissue Culture Infectious Dose (TCID50)/mL.

Results

The study sample consisted of 32 paired specimens which tested positive with COVID-VIRO ALL IN RDT and had SARS-CoV-2 N protein concentration measured with Liaison SARS-CoV-2 Antigen test. A highly significant correlation was found between SARS-CoV-2 viral antigen concentration and RDT positivization time (r=-0.64; 95%CI, -0.81 to -0.38; p<0.001). At the >1500 TCID50/mL threshold of the Liaison SARS-CoV-2 Antigen test, the positivization time of the COVID-VIRO ALL IN RDT displayed high accuracy (93.7%). A positivization time <42 sec enabled to identify patients with high SARS-CoV-2 antigen concentration (i.e., >1500 TCID50/mL) with 91.3% negative and 100% positive predictive values.

Conclusion

Self-testing using COVID-VIRO ALL IN RDT could be reliably used for garnering valuable information on the actual SARS-CoV-2 viral antigen concentration in respiratory samples.

❖❖❖❖❖

INTRODUCTION

The continued development and availability of fast, decentralized, relatively inexpensive and accurate severe acute respiratory syndrome coronavirus disease 2 (SARS-CoV-2) rapid diagnostic tests (RDTs) is imperative, since the volume of routine and urgent molecular tests that need to be performed all around the world largely outweigh the current capacity of most clinical laboratories. An ongoing worldwide survey promoted by the American Association for Clinical Chemistry (AACC), aimed at defining the state-of-the-art of the coronavirus disease 2019 (COVID-19) testing capacity, highlights that over two-third of responding laboratories are still facing problems in obtaining enough reagents and test kits for routine diagnosis of SARS-CoV-2 infection [1], thus paving the way to planning and validating alternative strategies that may overcome the bottleneck caused by the relatively long turnaround time and low throughput of molecular testing. Recent guidelines and recommendations, such as those of the World Health Organization (WHO) [2] and International Federation of Clinical Chemistry and Laboratory Medicine (IFCC) [3], have endorsed the possible use of SARS-CoV-2 RDTs under specific circumstance, such as for population screening (i.e., before large mass gatherings or prior to accessing healthcare facilities) and epidemiological purposes. One major and well-recognized limitation of these tests, along with their lower diagnostic accuracy [4], is represented by the generation of qualitative test results (i.e., negative or positive), which would then encumber the possibility to obtain information on SARS-CoV-2 viral load, a useful parameter for predicting infectivity, monitoring the course of disease and stratifying the risk of unfavourable disease progression [5]. Nonetheless, interesting evidence is emerging that the time to positive reaction of RDTs may be used for roughly predicting the SARS-CoV-2 viral load (i.e., the faster the positivization time, the higher the viral load) [6,7]. To this end, we planned this study to verify how the positivization time of a SARS-CoV-2 rapid antigen self-test may correlate with SARS-CoV-2 nucleocapsid (N) antigen concentration measured with a quantitative laboratory-based immunoassay.

MATERIALS AND METHODS

Study population

The study population consisted of a series of outpatients presenting to the Pederzoli Hospital in Peschiera del Garda (Verona, Italy) for undergoing routine SARS-CoV-2 testing between August 2 and September 3, 2022, when SARS-CoV-2 Omicron BA.5 prevalence was >90%. A

nasopharyngeal (healthcare-collected; Virus swab UTM Copan, Brescia, Italy) and nasal (self-collected; COVID-VIRO ALL) samples were taken upon patient admission, the former for being assayed in the local laboratory with Liaison SARS-CoV-2 Antigen test, the latter for performing COVID-VIRO ALL IN RDT, thus allowing faster screening of patients upon hospital presentation. All patients were instructed to correctly use the self-device by reading a quick utilization notice [8].

DiaSorin Liaison SARS-CoV-2 Antigen test

The immunochemical detection of SARS-CoV-2 in nasopharyngeal samples was carried out using DiaSorin Liaison SARS-CoV-2 Antigen test (DiaSorin, Saluggia, Italy), a fully-automated chemiluminescence sandwich-immunoassay (CLIA) that specifically developed for detecting SARS-CoV-2 nucleocapsid (N) protein in nasal and nasopharyngeal swabs, as described in details elsewhere [9]. The test, locally adapted for use on a DiaSorin LIAISON XL immunochemistry platform, displays an analytical sensitivity (i.e., limit of detection [LOD]) and a diagnostic threshold of 22.0 and 200 Median Tissue Culture Infectious Dose ($TCID_{50}$)/mL, respectively. A recent clinical investigation, assessing the cumulative diagnostic performance of this immunoassay during a period of SARS-CoV-2 Omicron predominance revealed that the diagnostic sensitivity and specificity were 0.93 and 1.00, respectively [10].

COVID-VIRO ALL IN RDT

COVID-VIRO ALL IN (AAZ-LMB, Boulogne-Billancourt, France) is a vertical flow immunoassay based on immunochemical detection of SARS-CoV-2 core (C) antigen in nasal specimens. The device could be used by healthcare professionals but is also suitable for self-testing due to its relatively simplicity of use, as comprehensively described elsewhere [11]. Briefly, after inserting the soft sponge at the upper part of the device in each nostril for 15 sec, the test kit is directly activated by pressing firmly the bottom of the holder (and hence without the need to twist the specimen in the reaction buffer and applying drops of the sample to the device, as for most RDTs), which breaks the buffer capsule and starts the reaction. After 15 min, the presence of two-coloured bands in the control (C) and test (T) windows reflects test positivity, their combined absence mirrors test failure, while the presence of a single coloured band in the control (C) windows defined test negativity. The testing procedure typically takes around 1 min and test results are within 15 min. According to data published in a recent clinical assessment this test, the positive predictive value (PPV) and negative predictive value (NPV) were 100% and 96.2%, respectively [11]. For this specific study, the positivization time of the RDT was measured with a manual chronometer by a healthcare professional, defined as the period between device activation to appearance of a coloured band in the test (T) windows, always accompanied by simultaneous presence of a coloured band in the (C) control window.

Statistical analysis

Test results were finally reported as median values and interquartile range (IQR). The agreement between antigen nucleocapsid concentration measured with Liaison SARS-CoV-2 Antigen test and time of positivization of COVID-VIRO ALL RDT was analyzed using Spearman's correlation and receiver operating characteristic (ROC) curve analysis. Since the test results displayed a non-normal distribution as assessed by Shapiro-Wilk test, they were transformed using natural logarithms before being analyzed. The correlation between the two measures could obviously only be conducted using COVID-VIRO ALL IN RDT positive samples, in which a numeric value of positivization time could be measured. The following statistical analysis was carried out

with Analyse-it software (Analyse-it Software Ltd, Leeds, UK). The study was conducted in accordance with the Declaration of Helsinki, under the terms of relevant local legislation, and was part of larger study protocol previously approved by the Ethical Committee of Verona and Rovigo Provinces (971CESC; Approved July 25, 2016).

RESULTS

The study sample consisted of 32 consecutive paired specimens which tested positive with COVID-VIRO ALL IN RDT (appearance of two bands in the control and test windows, respectively) and having also SARS-CoV-2 N protein concentration measured with Liaison SARS-CoV-2 Antigen test (median age 44 years, IQR 35-52 years; 75% women). The median SARS-CoV-2 viral antigen concentration was 1006 (IQR, 339-7169) TCID50/mL, whilst the median time of positivization of COVID-VIRO ALL IN RDT was 64 (IQR, 35-156) sec. No correlation was found between presence of symptoms (n=20) and TCID50/mL values (r=0.01; 95%CI, -0.34 to 0.36; p=0.940).

The association between SARS-CoV-2 viral antigen concentration and RDT positivization time is shown in Figure 1, evidencing a highly significant inverse correlation between these two measures (r= -0.64; 95%CI, -0.81 to -0.38; p<0.001).

At the >1500 $TCID_{50}$/mL threshold of Liaison SARS-CoV-2 Antigen test, which was earlier shown to reflect high viral antigen concentration and thereby greater risk of both infectivity and unfavourable clinical outcomes [12,13.], the diagnostic accuracy of COVID-VIRO ALL IN RDT positivization time was 93.7% (95%CI, 79.2 to 99.2%), with an area under the curve (AUC) of 0.88 (95%CI, 0.71 to 1.00; p<0.001) (Figure 2).

The best cut-off for predicting SARS-CoV-2 viral antigen concentration >1500 TCID50/mL was <42 sec of RDT positivization, which was associated with 91.3% (95%CI, 75.0-97.4%) NPV and 100% (95%CI, 100-100%) PPV, respectively.

DISCUSSION

Several lines of evidence now attest that the use of SARS-CoV-2 RDTs may represent a potential solution to overcome the current shortage of technical (and even human) resources needed as the COVID-19 pandemic progresses unremittingly [14]. The surge of SARS-CoV-2 infections sustained by recent and highly mutated lineages, especially BA.4/5 and BA.2.75 [15], is imposing a dramatic pressure on medical laboratories and other testing facilities, thus persuading several governments and health organizations worldwide to endorse the use of decentralized self-testing for widespread community testing as well as for optimizing the length of quarantine and/or isolation [16,17].

The generation of qualitative data, in terms of negative or positive test results, which are usually reflected by absence or presence of a colored band in the test window of the device, is a widely recognized shortcoming of RDTs, which does not implicitly consent to garner information on the actual viral load expressed by positive subjects. A tentative solution to this limitation has been provided by two preliminary investigations. Akashi et al. measured the positivization time of the QuickNavi™-COVID19 Ag RDT in 84 consecutive patient nasopharyngeal samples [6], and found a linear association between the viral load (i.e., cycle threshold values of SARS-Cov-2 N2 gene) and time to achieve a positive result (p< 0.001). Predictably, the positivization time of the RDT was longer in samples bearing a high viral load (cycle threshold values ≤31). In a following investigation, Salvagno et al. measured the positivization time of Roche SARS-CoV-2 Rapid Antigen Test in 106 patients with SARS-CoV-2 infection [7], and also found a significant correlation between the cycle thresholds values

of SARS-CoV-2 E and S genes and the RDT positivization time (r= 0.70; p<0.001), displaying an overall agreement of nearly 71% for identifying samples with high viral load (i.e., cycle thresholds values <20).

Taken together, the results of the present investigation support and extended the validity of these earlier findings, using a different SARS-CoV-2 RDT (most suited to be used as a self-test), self-administered, and in a period characterized by high prevalence of the SARS-CoV-2 Omicron BA.5 lineage.

In brief, we confirmed that SARS-CoV-2 viral antigen concentration and RDT positivization time obtained with self-testing are highly inversely correlated (i.e., r= -0.64), such that the sooner the coloured band will appears in the test window, the higher is the viral load expressed

Figure 1 **Spearman's correlation between positivization time of COVID VIRO ALL IN rapid diagnostic test (RDT) and viral load expressed as Median Tissue Culture Infectious Dose (TCID50)/mL and measured with DiaSorin Liaison SARS-CoV-2 Antigen test**

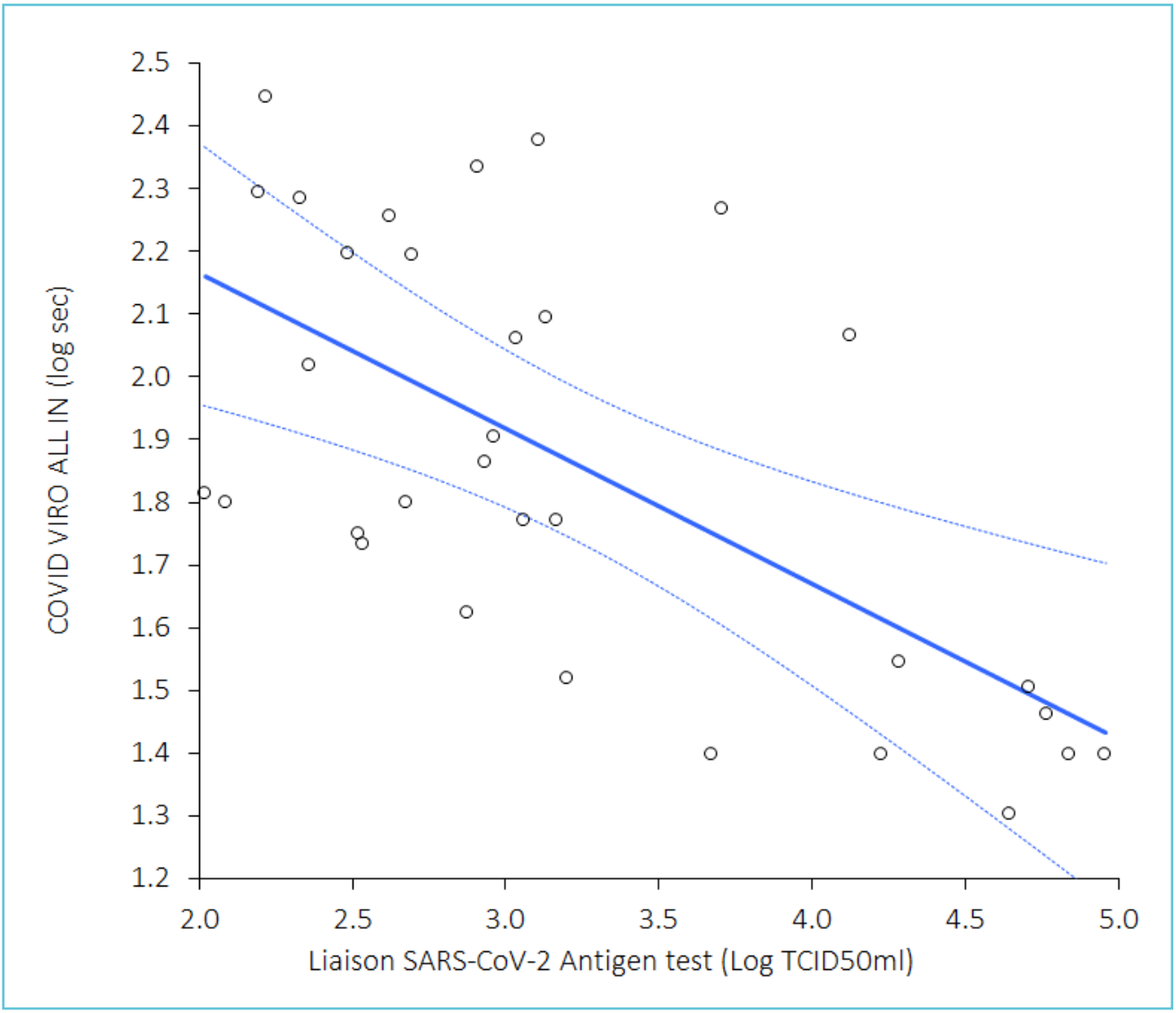

Figure 2 **Receiver operating characteristics (ROC) curve analysis of positivization time of COVID VIRO ALL IN rapid diagnostic test (RDT) for identifying samples with >1500 SARS-CoV-2 Median Tissue Culture Infectious Dose ($TCID_{50}$)/mL**

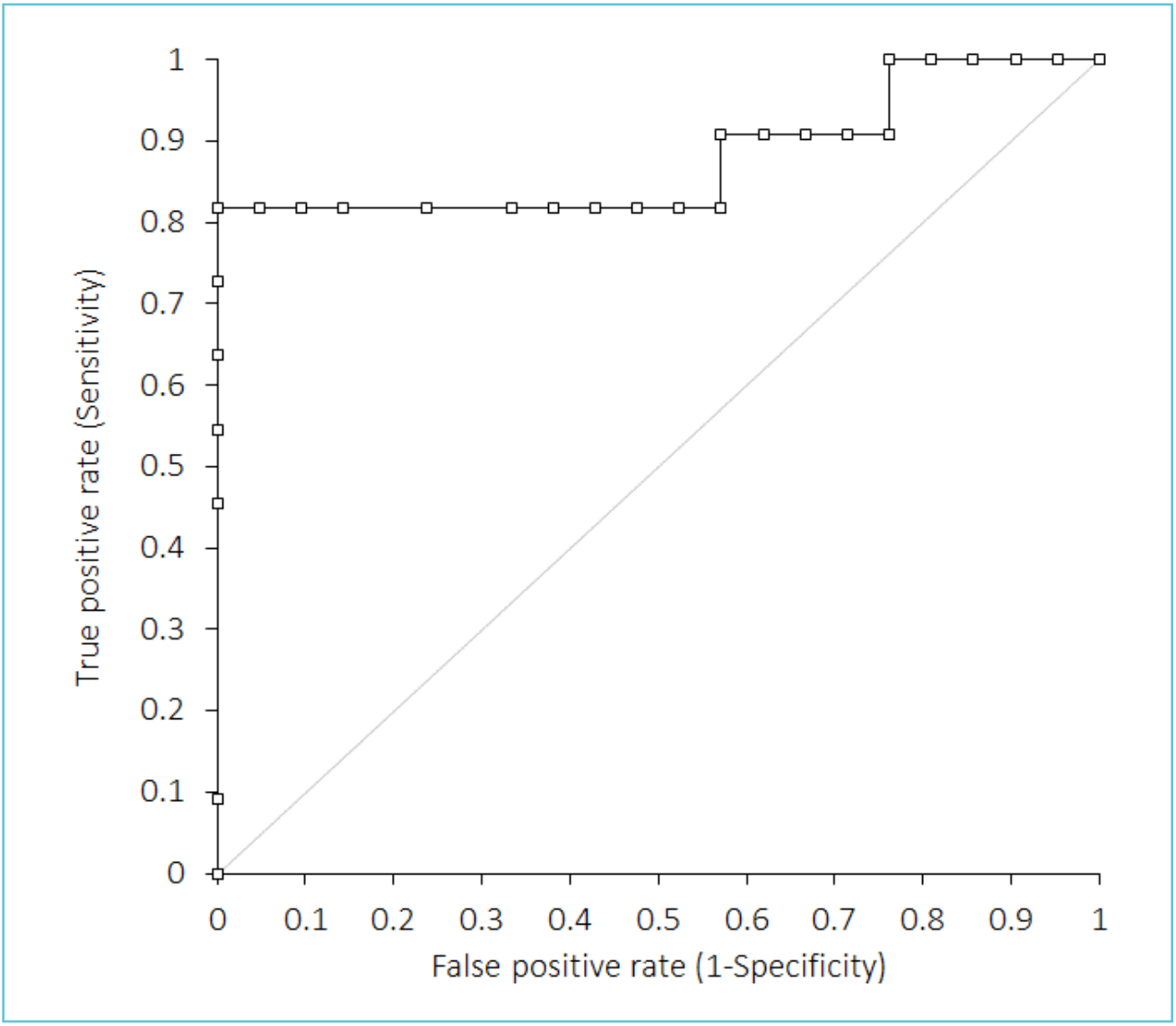

as SARS-CoV-2 N protein concentration. We also found that setting a positivization time of this device at <42 sec may enable identification of patients with high viral antigen concentration (i.e., >1500 $TCID_{50}$/mL) with over 90% NPV and 100% PPV, respectively. Interestingly, we also noticed that the IQR of COVID VIRO RDT positivization was much shorter (i.e., 35-156 sec) that the time window suggested by the manufacturer for test result availability (i.e., 15 min). This is a general aspect of all SARS-CoV-2 flow lateral immunoassays, in that the time window for reading results provided by manufacturers is typically longer than the effective time of positivization. This is probably due to legal reasons, for ensuring that the patients will wait a sufficient amount of time before reading the final test results.

CONCLUSIONS

The evidence that emerged from this study, combined with earlier published data which demonstrated that negativity or positivity of SARS-CoV-2 antigen tests may reflect the absence or presence of replication-competent virus [18], ultimately suggests that measuring the positivization time of the novel and user-friendly COVID-VIRO ALL IN RDT could be used for garnering valuable information on the actual SARS-CoV-2 viral RNA [19] and antigen concentration, even outside a specific healthcare setting, and thus providing a possible solution to relief the high workload currently caused by the ongoing COVID-19 pandemic [20].

❖❖❖❖❖

Acknowledgments

The authors acknowledge the staff of the Service of Laboratory Medicine of the Pederzoli Hospital (Peschiera del Garda, Italy) for the skill technical assistance.

Conflicts of interest

The authors declare no conflict of interest.

❖❖❖❖❖

REFERENCES

1. American Association for Clinical Chemistry. Coronavirus Testing Survey. Available at: https://www.aacc.org/science-and-research/covid-19-resources/aacc-covid-19-testing-survey. Last Accessed, September 20, 2022.

2. World Health Organization. Antigen-detection in the diagnosis of SARS-CoV-2 infection. Available at: https://www.who.int/publications/i/item/antigen-detection-in-the-diagnosis-of-sars-cov-2infection-using-rapid-immunoassays. Last accessed, September 20, 2022.

3. Lippi G, Favresse J, Gromiha MM, SoRelle JA, Plebani M, Henry BM. Ad interim recommendations for diagnosing SARS-CoV-2 infection by the IFCC SARS-CoV-2 variants working group. Clin Chem Lab Med 2022;60:975-981.

4. Tapari A, Braliou GG, Papaefthimiou M, Mavriki H, Kontou PI, Nikolopoulos GK, et al. Performance of Antigen Detection Tests for SARS-CoV-2: A Systematic Review and Meta-Analysis. Diagnostics (Basel) 2022;12:1388.

5. Lippi G, Plebani M. The many clinical advantages of reporting the cycle threshold (Ct) value. Ann Transl Med 2022;10:427.

6. Akashi Y, Kiyasu Y, Takeuchi Y, Kato D, Kuwahara M, Muramatsu S, et al. Evaluation and clinical implications of the time to a positive results of antigen testing for SARS-CoV-2. J Infect Chemother 2022;28:248-251.

7. Salvagno GL, Henry BM, De Nitto S, Pighi L, Lippi G. Association between viral load and positivization time of a SARS-CoV-2 rapid antigen test in routine nasopharyngeal specimens. J Med Biochem. 2022;41:513-517. https://doi.org/10.5937/jomb0-35482.

8. AAZ-LMB. Instruction Leaflet. Available at: https://www.autotest-sante.com/medias/fichiers/notice_autotest_covid_viro_all_in_en.pdf. Last accessed, September 20, 2022.

9. Salvagno GL, Gianfilippi G, Fiorio G, Pighi L, De Nitto S, Henry BM, et al. Clinical Assessment of the DiaSorin LIAISON SARS-CoV-2 Ag Chemiluminescence Immunoassay. EJIFCC 2021;32:216-223.

10. Uster S, Topalli Z, Sasse T, Suter-Riniker F, Barbani MT. Evaluation of the DiaSorin LIAISON SARS-CoV-2 antigen assay on nasopharyngeal swabs in two different SARS-CoV-2 pandemic waves in Switzerland: The impact of the Omicron variant on its performance. J Clin Virol Plus 2022;2:100095.

11. Prazuck T, Gravier A, Pires-Roteira D, Theillay A, Pallay S, Colin M, et al. Evaluation of a new "all in one" SARS-CoV-2 antigen-detecting rapid diagnostic test and self-test: Diagnostic performance and usability in child and adult populations. J Med Virol 2022;94:4097-4106.

12. Fernández-Rivas G, Barallat J, Gonzalez V, Martinez S, Bordoy AE, Jimenez L, et al. Analytical Performance of Quantitative DiaSorin Liaison SARS-COV-2 Antigen Test for the Asymptomatic Population. Front Public Health 2022;9:788581.

13. Lefever S, Indevuyst C, Cuypers L, Dewaele K, Yin N, Cotton F, et al. Comparison of the Quantitative DiaSorin Liaison Antigen Test to Reverse Transcription-PCR for the Diagnosis of COVID-19 in Symptomatic and Asymptomatic Outpatients. J Clin Microbiol 2021;59:e0037421.

14. Mattiuzzi C, Henry BM, Lippi G. Making sense of rapid antigen testing in severe acute respiratory syndrome coronavirus 2 (SARS-CoV-2) diagnostics. Diagnosis (Berl). 2020 Nov 26:dx-2020-0131. https://doi.org/10.1515/dx-2020-0131. Epub ahead of print.

15. Mattiuzzi C, Henry BM, Lippi G. Regional Association between Mean Air Temperature and Case Numbers of

Multiple SARS-CoV-2 Lineages throughout the Pandemic. Viruses 2022;14:1913.

16. Herbert C, Shi Q, Kheterpal V, Nowak C, Suvarna T, Durnan B, et al. Use of a Digital Assistant to Report COVID-19 Rapid Antigen Self-test Results to Health Departments in 6 US Communities. JAMA Netw Open 2022;5:e2228885.

17. Jeong YD, Ejima K, Kim KS, Joohyeon W, Iwanami S, Fujita Y, et al. Designing isolation guidelines for COVID-19 patients with rapid antigen tests. Nat Commun 2022;13:4910.

18. De Angelis G, Menchinelli G, Liotti FM, Marchetti S, Salustri A, Vella A, et al. SARS-CoV-2 Antigen Test Results to Infer Active or Non-Active Virus Replication Status in COVID-19 Patients. Diagnostics (Basel) 2022;12:1338.

19. Salvagno GL, Henry BM, Bongiovanni G, De Nitto S, Pighi L, Lippi G. Positivization time of a COVID-19 rapid antigen self-test predicts SARS-CoV-2 viral load: a proof of concept. Clin Chem Lab Med. 2021 https://doi.org/10.1515/cclm-2022-1058.

20. Nagy B Jr. Foreword: Current laboratory aspects of COVID-19. eJIFCC 2022;33:75-8.

The Journal of the International Federation of Clinical Chemistry and Laboratory Medicine

eJIFCC

A macro-TSH: a clinical diagnostic dilemma

Xikombiso Nkuna[1], Zodwa Dire[2], Siyabonga Khoza[1]

[1] *Department of Chemical Pathology, National Health Laboratory Service and University of the Witwatersrand, Johannesburg, South Africa*

[2] *Division of Endocrinology, Department of Internal Medicine, School of Clinical Medicine and University of the Witwatersrand, Johannesburg, South Africa*

ARTICLE INFO

Corresponding author:
Siyabonga Khoza
Department of Chemical Pathology
National Health Laboratory Service
and University of the Witwatersrand
7 York Rd, Parktown, 2193
Johannesburg
South Africa
E-mail: siyabonga.khoza@nhls.ac.za

Key words:
immunoassays, macroTSH, interferences

ABSTRACT

Isolated increase in thyrotropin stimulating hormone (TSH) in a clinically euthyroid patient may be caused by the formation of a macromolecule between TSH and autoantibodies causing discordant thyroid function test results. Despite the effort to eliminate interferences in immunoassays, these assays are still vulnerable to different interferences. Immunoassay interferences may cause erroneous results and lead to misdiagnosis which may subject a patient to unnecessary investigations and treatment. Immunoassays are affected by multiple substances; these may be endogenous or exogenous such as heterophile antibodies, autoantibodies, macromolecules, and human anti-mouse antibodies. This case reports a 47-year-old African woman who presented with a persistent elevated TSH with thyroid hormones within normal reference limits. She was found to have a macro-TSH which was associated with IgA paraprotein.

INTRODUCTION

An increased TSH in the presence of normal free T4 (fT4) commonly suggests subclinical hypothyroidism. However, other causes such as TSH resistance, poor compliance to thyroxine, recovery phase of non-thyroidal illness, and assay interference need to be excluded (1). Automated immunoassays are prone to various interferences resulting in erroneous results. Some of these assay interferences include heterophile antibodies, anti-mouse antibodies, and macromolecules e.g., macro-TSH. Macro-TSH is a macromolecule as a result of the complex binding of TSH to immunoglobulins, which results in increased TSH. Even though macro-TSH has poor biological activity, and circulates longer, it retains the ability to react with antibodies used in immunoassays, causing falsely elevated results (1, 2). This case reports a 47-year-old South African woman who presented with a persistent elevated TSH with thyroid hormones within normal reference limits. She was found to have a macro-TSH which was associated with IgA Kappa paraprotein. This case reports the potential interference on assays, if not identified, may have adverse effects on the patient clinical outcomes. Also, it emphasises the need for laboratory professionals to work closely with clinicians.

CLINICAL-DIAGNOSTIC CASE

A 47-year-old woman was referred to the Endocrine Unit, for evaluation of abnormal thyroid function test results. She denied any history of weight gain, hoarseness of voice, and cold intolerance. She reported no headaches and blurred vision. She reported no personal or family history of thyroid or autoimmune diseases. Examination was unremarkable.

Thyroid function tests revealed markedly elevated thyrotropin stimulating hormone (TSH) with free thyroxine (fT4) and free triiodothyronine (fT3) within reference intervals. Her anti-thyroid peroxidase antibodies were negative (Table 1). Since she was clinically euthyroid, no medication was prescribed.

Due to discordant thyroid function results on repeated measurements with no symptoms suggestive of thyroid disorder in the patient, an interference was suspected. In our patient, thyroid function tests were measured using a Roche Cobas c602 (Roche Diagnostics, Mannheim, Germany, Figure 1A).

To screen for laboratory interference, the measurements of TSH and fT4 from the same serum sample were repeated on Siemens Advia Centaur (Siemens Medical Solutions Diagnostics, USA) which utilizes a two-site sandwich immunoassay using direct chemiluminometric technology (Figure 1B). TSH levels were significantly lower compared to Roche platform (Table 1) while fT4 remained within reference intervals; this further strengthened the suspicion of the presence of interference.

We further performed serial dilutions (1/2, 1/5, 1/10, and 1/20) of the serum using a diluent recommended by the manufacturer. We obtained non-linear results which suggested the presence of assay interference (Table 2). Unfortunately, non-linear recovery cannot differentiate the heterophile antibodies from macro-TSH and rheumatoid factor interferences.

To exclude macro-TSH, the serum of the patient was subjected to polyethylene glycol (PEG) 6000 solution (25% w/v) using a well described procedure commonly used for macroprolactinemia. Briefly, in this procedure an equal amount of the patient sample and PEG solution was mixed and incubated for 10 minutes at room temperature. Then the mixture was centrifuged at 10900 rpm (9430 g) speed for precipitation to occur and the supernatant was analysed. The post-PEG TSH was 2.92 mIU/L (reference interval, 0.27-4.20 mIU/L, 2.9% recovery) suggesting that the interfering antibodies were in the macro-form.

Figure 1 The schematic representation of differences between Roche Cobas (A) and Siemens's (B) TSH assays

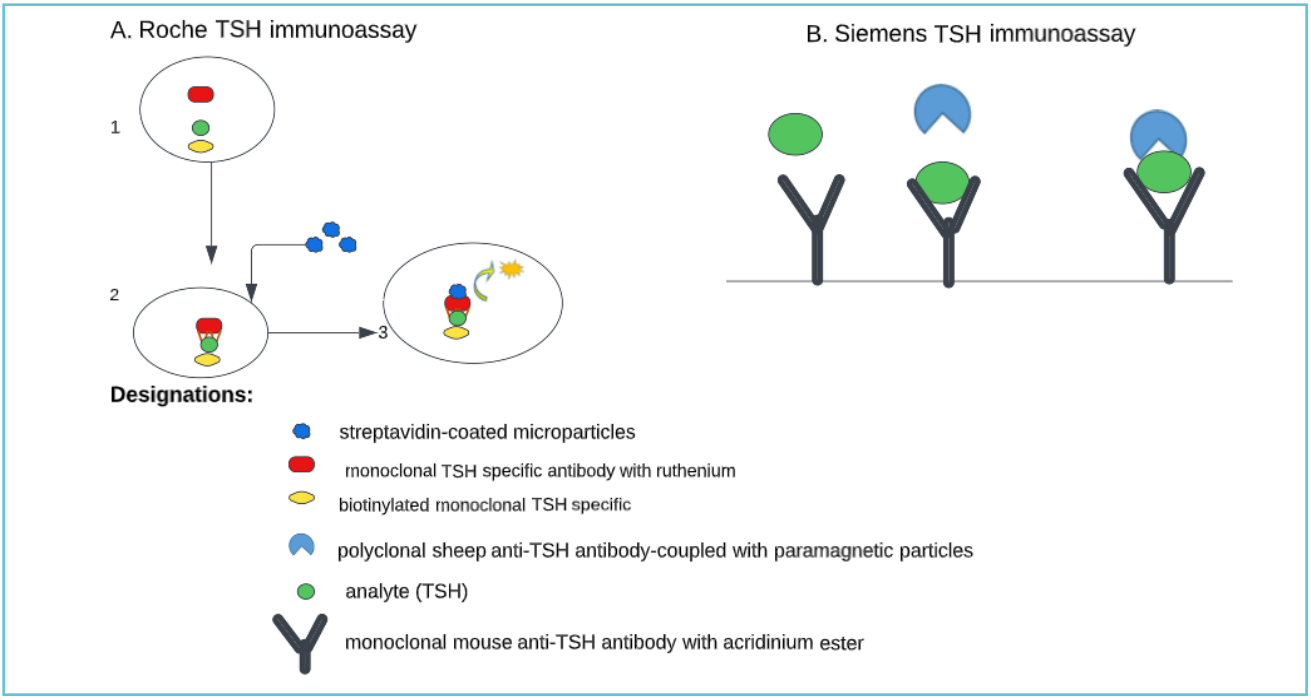

A. *TSH in the sample is incubated with biotinylated monoclonal TSH-specific antibody and a monoclonal TSH specific antibody labelled with ruthenium (1) to form a sandwich complex (2). Streptavidin-coated microparticles are added, a complex becomes bound to the solid phase via interaction of biotin and streptavidin inducing chemiluminescent emission (3).*

B. *TSH binds firstly to a monoclonal mouse anti-TSH antibody with acridinium and secondly to a polyclonal sheep anti-TSH antibody-coupled with paramagnetic particles, measuring the concentration using the chemiluminometric technology.*

Table 1 Measurements of thyroid function test on different instruments

	On admission (Roche)	1-month later (Roche)	1-month later (Siemens)	5-months later (Roche	1-year later (Roche)	Reference intervals
Test	**Results**					
TSH	>100.0	>100.0	7.40	>100.0	>100.0	0.27-4.20 mIU/L
fT4	17.2	14.3	14.2	12.9		12.0-22.0 pmol/L
fT3	4.9			4.7		3.1-6.8 pmol/L
Anti-TPO Abs		5				<34 U/mL

TSH, thyroid-stimulating hormone, fT4, thyroxine, fT3, free triiodothyronine, Anti-TPO Abs, Anti-thyroid peroxidase antibodies.

Table 2 TSH results after serial dilutions analyzed on Roche instrument

Test	Without Dilution	1/2 Dilution	1/5 Dilution	1/10 Dilution	1/20 Dilution	Reference Intervals
TSH	>100	>100	103.2	113.6	115.6	0.27-4.20 mIU/L

Table 3 Biochemical results before and after polyethylene glycol (PEG) precipitation

Test	Before PEG	After PEG	Reference Intervals (RI)
TSH	99.54	2.92	0.27-4.20 mIU/L
Prolactin	510.7	136.0	4.8- 23.3 µg/L (Post-PEG 3.5-18 µg/L)

TSH, thyroid-stimulating hormone, PEG, polyethylene glycol.

Figure 2 Serum immunofixation image depicting two IgA Kappa monoclonal gammopathy (arrows)

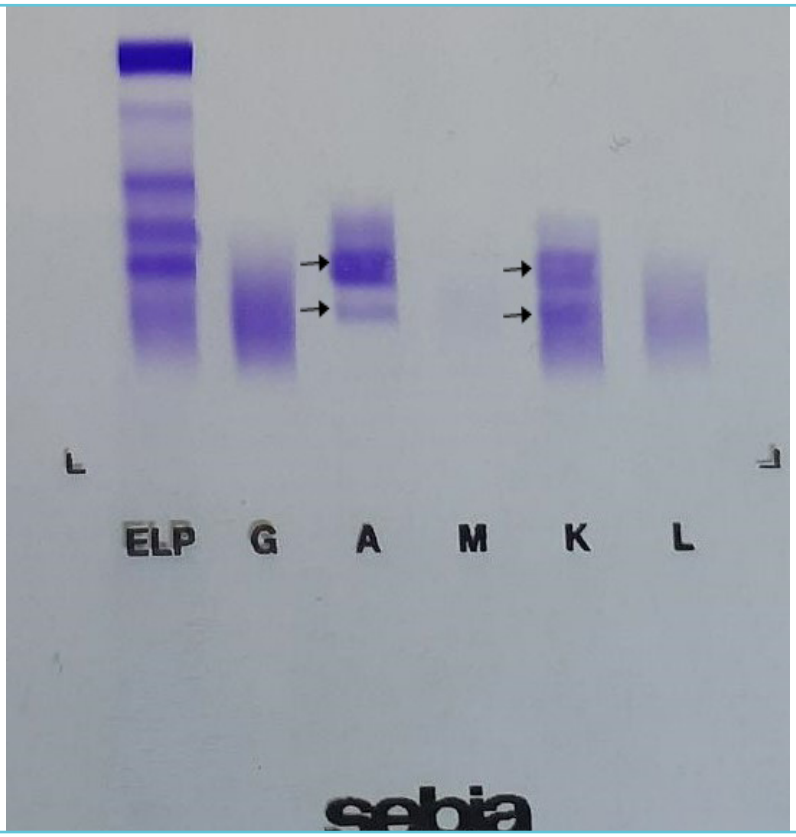

The recovery of TSH post-PEG was calculated as (post-PEG TSH ÷ pre-PEG TSH) x 100%. Because we suspected the presence of a high molecular weight interfering substance might affect other hormones, we ordered prolactin, since macroprolactin is commonly encountered in clinical practice compared to other hormones. Prolactin concentrations were markedly high 510.7 µg/L (4.8- 23.3) using Roche Cobas e602 (Table 3). She was not pregnant or breastfeeding or any medication known to increase prolactin. The post-PEG prolactin was 136 µg/L (post-PEG intervals: 3.5- 18) which is 26.6 % recovery (Table 3). No further investigation was done since the patient was not complaining of the headaches and had no blurred vision that would have suggested a prolactinoma.

To further characterize interfering antibodies, immunoglobulins were ordered. The immunoglobulins results show markedly elevated IgA: 9.39 g/L (0.7-4 g/L) while IgG: 12.32 g/L (7-16 g/L) and IgM: 0.40 g/L (0.4- 2.3 g/L) were within the reference intervals. These results suggested the presence of TSH-IgA macro-TSH interferences. This was further confirmed with the immunofixation which confirmed the presence of two IgA Kappa paraproteins (Figure 2).

DISCUSSION

Interferences in the measurement on immunoassays are common [1, 2]. Since interferences are common, grossly increased TSH should be investigated when the isolated elevation is not consistent with the rest of thyroid function tests and the clinical presentation.

Commonly, immunoassays are interfered with by endogenous and exogenous substances. Substances such as heterophile antibodies, human anti-mouse/animal antibodies, anti-streptavidin antibodies, mega doses of biotin, and rheumatoid factors have been implicated [2].

The increased use of biotin supplementation, especially mega doses has created huge challenges on laboratory assays [3]. The effect of biotin on immunoassays has been recognised by manufacturers. In particular, Roche assays have been improved to tolerate higher biotin levels without significant interferences. In our patient, the new versions TSH, fT4 and fT3 assays were utilised making biotin interference unlikely. Also, high biotin levels cause a negative interference on TSH [3], which was not the case in our patient. In addition to biotin interference, heterophile antibodies needs to be considered. Heterophile antibodies are classified as a group of natural antibodies and autoantibodies, and have ability to react with heterogeneous and poorly defined antigens of different compounds. They either affect the antigen binding to the antibody in immunoassay or act as an antigen due to polyreactive nature [2]. To elucidate the presence of heterophile antibodies, firstly, the sample can be analysed on the different platform. Secondly, the serial dilution to demonstrate nonlinear results in the presence of interfering antibodies. Thirdly, the test is analysed after incubation with heterophile blocking agents/tubes [4], these agents aid in removal of heterophile antibodies.

Repeating analysis on another analyzer by a different manufacturer often reveals the presence of interference. Assays from alternative manufacturers are mostly likely to use different antibodies and targeting at different epitopes [5]. In our case we analysed the same patient sample on a different instrument and TSH results were different, providing the clue to possible interference.

Another approach to screen for interference is through serial dilution using recommended manufacturer specific diluents. Nonlinear serial dilution provides a clue of the presence of the interference [6]. We observed a nonlinear dilution pattern, indicating assay interference.

This method is not perfect, only 60% of patients may show lack of linearity [5, 6].

Macromolecules such as macroprolactin and macro-TSH have been described as causes of immunoassay interference [7, 8]. Macro-TSH is estimated to have prevalence between 0.6-1.6% [6]. When monomeric TSH combines with immunoglobulin (Ig), commonly IgG forms macro-TSH. Unlike the monomeric, bioactive form which is 28 kDa, macro-TSH has a large molecular weight of approximately 150 kDa. Because of the molecular weight, the renal clearance of macro-TSH is markedly reduced, hence circulating longer. The immunoreactivity of the TSH-Ig complex is retained [6, 9, 10]. Currently, the available immunometric assays will not be affected to the same degree by macro-TSH as shown as shown in our patient (Siemens TSH was 7mU/L, while Roche TSH was >100mU/L). Therefore, macro-TSH has the ability to react with antibodies used for measurement causing elevated TSH. However, the biological activity of macro-TSH is low, and the patient remains clinically euthyroid [9]. The pitfall of this procedure is that interferences from other molecules such as heterophile antibodies and rheumatoid factors may give similar results. In addition, linear dilutions have been reported in the presence of macro-TSH. We were able to demonstrate non-linear recovery in our patient. Unfortunately, we were not able to exclude the presence of heterophile antibodies due to unavailability and cost of heterophile blocking tubes.

The common and easy method to screen for macroprolactin is the use of polyethylene glycol (PEG) precipitation which has been adapted to screen for macro-TSH [11]. Briefly, the PEG solution is added to patient serum. Even though PEG precipitation is easy to use, the low recovery needs to be confirmed by gel filtration chromatography. However, the latter is costly and not widely accessible. Compared to other methods, PEG precipitation is commonly performed because of ease of use, cost effective, and correlates well to gel chromatography which is considered a gold standard for macroprolactin [12] but it remains to be seen if same result will be achieved for macro-TSH. At this stage, there is no single method that reliably identifies macro-TSH. Therefore, various diagnostic strategies are often applied to rule out the presence of macro-TSH [13].

Once macro-TSH was detected in this patient, we searched for the involvement of other hormones. Since prolactin is a frequently detected macroform, it was performed of which was found to be elevated as well. The patient had no clinical features that suggested hyperprolactinaemia and not on medication known to increase prolactin. The post-PEG was higher above the upper limits of post-PEG reference intervals suggesting true hyperprolactinaemia even though 26.6% which is less than the 40% cut-off commonly used. Studies are now advocating for use of post-PEG reference intervals rather than recovery percentage after precipitation to establish the presence of true hyperprolactinaemia or macroprolactin [14]. At this stage no reference intervals for post-PEG TSH have been established. Despite the absence of a protocol to screen macro-TSH, Mills et al. has suggested that macro-TSH should be suspected when TSH is >10mIU/L with thyroid hormones within the reference intervals [8]. However, this approach may be costly since the prevalence of macro-TSH is low.

CONCLUSIONS

In conclusion, this case demonstrated the importance of considering interferences when biochemical results, especially analyzed on immunoassays are discordant with the clinical presentation before costly and potentially invasive investigations are performed. In addition, strong interaction between clinicians and

laboratory professionals is necessary to identify interferences and costly investigations.

TAKE-HOME MESSAGES/ LEARNING POINTS

1. Isolated TSH with normal thyroid hormones should trigger the suspicion of the interference, especially in the clinical euthyroid patient.
2. Some immunoassays are unable to differentiate macroTSH from the bioactive TSH molecule.
3. MacroTSH is a rare phenomenon that should be exclude to avoid unnecessary management and possible invasive investigations. Therefore, collaboration between clinician and laboratory professional is vital.
4. Measurement of TSH after addition of PEG precipitation can reveal the presence of macroTSH. This method has been used for diagnosis of macroprolactin due to low cost and high accessibility.

❖❖❖❖❖

Author disclosures & contributions

Written informed consent was obtained from patient for publication of this case.

Ethical clearance was obtained from the Medical Human Research Ethics Committee, University of the Witwatersrand - clearance certificate no. M210758.

X Nkuna wrote the first draft of the manuscript. X Nkuna, Z Dire, and SP Khoza edited the submitted manuscript. All authors reviewed and approved the final manuscript for publication.

The authors declare that they have no competing interests.

❖❖❖❖❖

REFERENCES

1. Levy MJ, Koulouri O, Gurnell M. How to interpret thyroid function tests. Clin Med (Lond). 2013; 13:282–6.

2. Tate J, Ward G. Immunoassay interferences. Clin Biochem Rev 2004; 25:105-20.

3. Zhang Y, Wang R, Dong Y, Huang G, Ji B, Wang Q. Assessment of biotin interference in thyroid function tests. Medicine. 2020; 99: e19232.

4. Paczkowska K, Otlewska A, Loska O, Kolačkov K, Belanowski M, Daroszewski J. Laboratory interference in the thyroid function test. Endokrynol Pol. 2022, 71(6): 551-560.

5. Ward G, Simpson A, Boscato L, Hickman PE. The investigation of interferences in immunoassays. Clinical Biochemistry. 20176;50.

6. Favresse J, Burlacu M-C, Maiter D, Gruson D. Interferences with thyroid function immunoassays: clinical implications and detection algorithm. Endocrine Reviews. 2018; 39:830-50.

7. Gulbahar O, Degertekin CK, Akturk M, Yalcin MM, Kalan I, Atikeler GF, et al. A Case With Immunoassay Interferences in the Measurement of Multiple Hormones. J Clin Endocrinol Metab. 2015; 100:2147-53.

8. Mills F, Jeffrey J, Mackenzie P, Cranfield A, Ayling R. An immunoglobulin G complexed form of thyroid stimulating hormone (macro thyroid-stimulating hormone) is a cause of elevated serum thyroid-stimulating hormone concentration. Ann Clin Biochem. 2013; 50:416-20.

9. Hattori N, Ishihara T, Shimatsu A. Variability in the detection of macroTSH in different immunoassays systems. European Journal of Endocrinology. 2016; 174:9-15.

10. Loh TP, Kao SL, Halsall DJ, Toh SES, Chan E, Ho CS, et al. Macro-Thyrotropin: A Case Report and Review of Literature. JCEM. 2012; 97:1823-8.

11. Giusti M, Conte L, Repetto AM, Gay S, Marroni P, Mittica M, et al. Detection of Polyethylene Glycol Thyrotropin (TSH) Precipitable Percentage (Macro-TSH) in Patients with a History of Thyroid Cancer. Endocrinol Metab (Seoul) 2017; 32:460-5.

12. Beltran L, Fahie-Wilson MN, McKenna TJ, Kavanagh L, Smith TP. Serum Total Prolactin and Monomeric Prolactin Reference Intervals Determined by Precipitation with Polyethylene Glycol: Evaluation and Validation on Common ImmunoAssay Platforms Clinical Chemistry. 2008; 54: 1673–81.

13. Ohba K, Maekawa M, Iwahara K, Suzuki Y, Matsushita A, Sasaki S, et al. Abnormal thyroid hormone response

to TRH in a case of macro-TSH and the cut-off value for screening cases of inappropriate TSH elevation. Endocr J. 2020; 67:125-30.

14. Šostarić M, Bokulić A, Marijančević D, Zec I. Optimizing laboratory defined macroprolactin algorithm. Biochem Med (Zagreb). 2019; 29:020706.

The Journal of the International Federation of Clinical Chemistry and Laboratory Medicine

eJIFCC

Deletion in the BCL11B gene and intellectual developmental disorder with speech delay, dysmorphic facies, and t-cell abnormalities – a case report

Adriel Roa-Bautista[1]*, Mónica López-Duarte[2], Nerea Paz-Gandiaga[3]*, David San Segundo Arribas[1], J. Gonzalo Ocejo-Vinyals[1]

[1] *Division of Immunology, Marques de Valdecilla University Hospital, University of Cantabria, IDIVAL, Santander, Cantabria, Spain*

[2] *Division of Hematology, Marques de Valdecilla University Hospital, University of Cantabria, IDIVAL, Santander, Cantabria, Spain*

[3] *Division of Genetics, Marques de Valdecilla University Hospital, University of Cantabria, IDIVAL, Santander, Cantabria, Spain*

** These authors share first authorship.*

ARTICLE INFO

Corresponding author:
Adriel Roa-Bautista, MD, MHSc
Division of Immunology
Marques de Valdecilla University Hospital
University of Cantabria
IDIVAL, Santander, Cantabria (39008)
Spain
Phone: +34 640 55 57 65
E-mail: adrielantonio.roa@scsalud.es

Key words:
BCL11B gene mutation, type 2 innate lymphoid cells, facial dysmorphia, immune disorder

ABSTRACT

Herein we described a retrospective analysis of a 13-year-old female patient with facial dysmorphia and immune disorder caused by BCL11B gene mutation. The patient upon physical examination presented a particular face (thin eyebrows, small mandible, and widened eye distance), delayed language and motor development. Supplementary examination showed expansion of CD8+, absence of type 2 Innate Lymphoid Cells, increased IgG and altered distribution of T cells. Genetic testing revealed a heterozygous frameshift variation in exon 4 of the BCL11B gene; c.1887_c.1893delCGGCGGG (p.Gly630Glyfs*91). Finally, a BCL11B gene mutation could lead to abnormal development of the nervous and immune systems, therefore, it is necessary to consider this syndrome in patients with the clinical and immunological phenotype described below.

INTRODUCTION

The Chromatin Remodeling Complex Subunit BCL11B is essential for the normal development of the immune and central nervous system, participating in processes of activation, differentiation, cell apoptosis and working as a modulator of early thymocyte development [1].

Currently, the scientific literature has few reports on BCL11B germline variants, Punwani et al. (2016) reported a male infant carrying a nonsense mutation in BCL11B with severe developmental delay, absent corpus callosum, craniofacial anomalies, and severe combined immunodeficiency (SCID)[2], while Lessel et al. (2018) reported 13 patients with distinct heterozygous mutations in BCL11B, all exhibit intellectual disability, developmental delay, and impaired T-cell development [3].

Finally, variants in BCL11B are associated with an autosomal dominant pattern of inheritance with immunodeficiency 49 (IMD49), describing a syndrome produced by a heterozygous mutation in this gene. IMD49 is related to severe combined immunodeficiency and intellectual disability. In the same manner is associated with Intellectual developmental disorder with dysmorphic facies, speech delay, and T-cell abnormalities [4].

CLINICAL CASE

A 13-year-old female patient, result of a twin pregnancy, with no paternal history of consanguinity or autoimmune diseases had a history of late independent ambulation (17 months), delay in language development (single words at 41 months), abnormal psychomotor development accompanied by dysmorphic facies, psoriasiform dermatitis with focal spongiosis, compatible with subacute eczema, left lacrimal obstruction and primary VZV infection during childhood.

She was admitted at nine months due to vomiting, liquid stools and significant paleness. A battery of laboratory tests was carried out where normochromic-normocytic anemia was observed, accompanied by consumption of haptoglobins, a positive direct Coombs test (IgG) and positive irregular antibodies. Eventually, autoimmune hemolytic anemia (AHA) was diagnosed. One month later, she was admitted to the emergency room due to symptoms similar to the one described previously, where a hemoglobin (Hb) of 5.3mg/dl was found, which later dropped to 3.7mg/dl. These AHA episodes later recurred at one year of life. Two years later, she was admitted due to ecchymosis secondary to a viral illness and was diagnosed with idiopathic thrombocytopenic purpura (ITP). Finally, the diagnosis of Evans syndrome was established, and the patient remained under closed control until she was five years old, when she again presented with ecchymosis and petechial accompanied by platelets <10,000/mm^3.

At six years of age, the patient was diagnosed with hypothyroidism due to autoimmune thyroid diseases (AITD), short stature and precocious puberty, for which replacement therapy was started with Levothyroxine 75 mcg/day and monthly administration of Decapeptyl 0.8 ml. AITD was diagnosed due to positivity to thyroid peroxidase antibodies (TPOAb), thyroglobulin antibodies (TgAb) and thyroid stimulating hormone receptor antibodies (TRAb).

At the age of nine, the patient was again admitted due to petechial on the chest and extremities, accompanied by intermittent abdominal pain, with the symptoms ceasing after administration of immunosuppressive treatment.

During that year, the patient debuted with vesicular and some bullous lesions grouped on an erythematous base compatible with herpes zoster, affecting several dermatomes from L2 to L5. Initially treated with oral and topical medication, but due to lack of response, she was

admitted for intravenous treatment with subsequent improvement.

Additionally, at 13, she was admitted with a platelet count of 6,000 per µl and symptoms similar to previous events. During this episode, the patient was referred to the clinical immunology team. The patient presented dysmorphic facial features on physical examination, including myopathic facies, thin eyebrows, small palpebral fissure, prominent nose, extended filter, thin upper lip, and abnormal dentition, with a visible slowing of the verbal processing of information and difficulty in the development of cognitive tasks (Table 1).

From an immunological point of view, an expansion of CD8+ with an anergic/senescent phenotype (CD8+CD62L-CD45RA+), absence of type 2 Innate Lymphoid Cells (ILC), increased IgG, altered distribution of T cells, low levels of NK cells (Figure 1, Table 2) and anti-nuclear antibodies (homogeneous pattern AC-1 ICAP 1/320) was observed. Extractable nuclear antibodies (ENA) test was performed obtaining positivity to anti-SSa/Ro, more specifically for Ro52 cytoplasmatic protein, anti dsDNA, anti-histone or anti nucleosome antibody tests were not performed. Even though the pathogenic role of the Ro antigen in autoimmune disorders is not fully dilucidated [5] it has been reported in few patients with autoimmune thyroiditis [6].

Previous cytogenetic analysis revealed normal female karyotype. Chromosomal array analysis by comparative genomic hybridization (CGH) was performed with negative result for pathogenic copy number variations. Genomic DNA of the proband, and both parents was extracted from peripheral blood for genetic analysis.

Clinical whole exome sequencing (WES) was achieved revealing a germline heterozygous deletion within exon 4 of the BCL11B gene. The variation involved a deletion which consequently generated a frameshift mutation in the DNA sequence and a premature stop codon, which is expected to results in a truncated protein

Table 1 Description of the clinical features

Neurological features	Skin disorders	Morphological changes	Autoimmune alteration	Immunological findings
Abnormal psychomotor development (Late independent ambulation)	Psoriasiform dermatitis	Short stature	Evan syndrome (Thrombocytopenia and hemolytic anemia)	Expansion of CD8+ with anergic/ senescent phenotype
Delay in language development	Left lacrimal duct obstruction	Myopathic facies	Autoimmune thyroid disease (AITD)	Deficiency of innate lymphoid cells type 2
Slowing of the verbal processing of information	Primary infection with varicella zoster virus with reactivation later in life	Thin eyebrows	Positive antinuclear antibodies (ANA) with Ro52 positive	Altered distribution of T cells
Difficulty in the development of cognitive tasks		Small palpebral fissure		Low NK cells
		Prominent nose		
		Thin upper lip		
		Abnormal dentition		

Table 2 Analytical results

Determination	Rank	Result
Expanded lymphocyte subpopulations		
CD3	[62.6-80.4%]	↑ 90.38
CD4	[32.6-51.5%]	¯ 30.65
CD8	[19-29%]	↑ 58.56
CD4/CD8	[1.21-2.64%]	¯ 0.52
CD19	[11.9-21%]	¯ 6.72
NK	[4.3-16.2%]	¯ 0.77
Absolute number of lymphocytes	[1340-3173 cells/ul]	↑ 4498
Absolute number CD3	[954-2332 cells/ul]	↑ 4042
Absolute CD4 number	[610-1446 cells/ul]	1379
Absolute number CD8	[282-749 cells/ul]	↑ 2634
Absolute number CD19	[173-685 cells/ul]	299
Absolute number NK	[87-504 cells/ul]	¯ 3. 4
Expanded memory T subpopulations		
T Recent Thymic Migrants Cells	[31-81%]	¯ 9.26
CD4 naïve	[37-97%]	¯ 21.32
CD4 TCM	[13-76%]	22.93
CD4 TEM	[0.49-25%]	↑ 54.71
CD4 TEMRA	[0-5.8%]	1.05

CD4 Regulatory T cells	[4-20%]	¯ 1.14
CD8 naïve	[20-95%]	¯ 5.99
CD8 TCM	[0.42-18%]	0.91
CD8 TEM	[4-100%]	¯ 1.29
CD8 TEMRA	[9-65%]	↑ 91.81
T Recent Thymic Migrants Cells Abs	[150-1500 cells/ul]	374
CD4 naïve Abs	[200-1700 cells/ul]	294
CD4 TCM Abs	[120-740 cells/ul]	316
CD4 TEM Abs	[5-210 cells/ul]	↑ 754
CD4 TEMRA Abs	[0-51 cells/ul]	14
CD4 Regulatory T cells Abs	[33-190 cells/ul]	¯ 16
CD8 naïve Abs	[78-640 cells/ul]	158
CD8 TCM Abs	[16-810 cells/ul]	24
CD8 TEM Abs	[16-810 cells/ul]	¯ 3. 4
CD8 TEMRA Abs	[35-420 cells/ul]	↑ 2418
Innate Lymphoid Cells (ILCs) subpopulation		
ILC 1	%	0.172
ILC 2	%	¯ 0
ILC 3	%	0.132

Absolute number, Abs. Terminally Differentiated Effector Memory T Cells, TEMRA. T helper cells, Th. Innate lymphoid cells, ILCs. Central Memory T Cells, TCM. Effector memory T cells, TEM.

¯,↑ Used to illustrate levels of the different determination, low and high respectively.

(NM_138576.3: c.1887_1893delCGGCGGG; p.(Gly630Thrfs*91). The variant was absent from the gnomAD databases and pathogenicity score prediction software analysis disclosed that the variant could be a disease causing variant. The variant has been previously reported as pathogenic in a 2-year-old boy and is described in the ClinVar database as a pathogenic variant (ID 1275761) diagnosing Intellectual Developmental Disorder with Speech Delay, Dysmorphic Facies, and T-Cell Abnormalities [1]. PCR and Sanger sequencing was finally applied to validate the mutation and the pedigree analysis (Figure 2.A). The results showed that the mutation in BCL11B arose de novo, which was not observed in both parents (Figure 2. B). This study was approved by the Ethics Committee of the Marques de Valdecilla University Hospital, and informed written consent was obtained from the parents of the patient.

Figure 1 **Flow cytometry panel of peripheral blood mononuclear cells (PBMCs) obtained from index case**

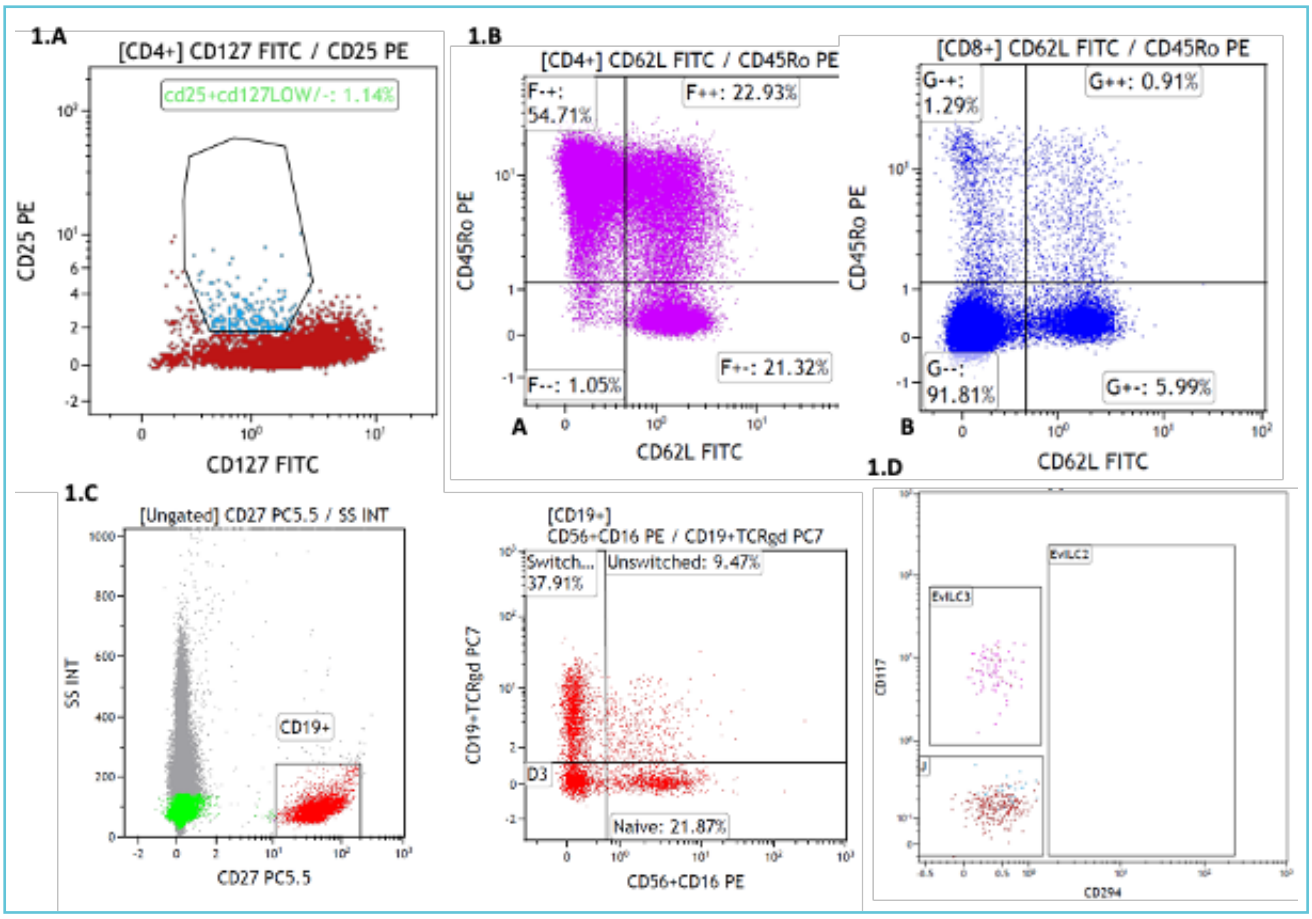

***Graph 1.A**, Panel for regulatory T cells (T reg), obtaining a total of 1.14% of CD4+CD25+CD27low cells.*

***Graph 1.B**, Panel for subtypes of memory T cells (T men), obtaining a total of CD4+ (A) lymphocytes (purple) of 21.32% naive T cells; 22.93% of central memory T cells (TCM); 54.71 of effector memory T cells (TEM) and 1.05% of recent thymic migrating T cells (TEMRA). For CD8 (B) lymphocytes (blue), 5.99% of naive T cells; 0.91% of TCM; 1.29% of TEM and 91.81% of TEMRA.*

***Graph 1.C**, Panel for B memory (B men), obtaining a total of 21.87% of naive B cells; 9.47% of unswitched B cells and 37.91 of switched B cells.*

***Graph 1.D**, panel for innate lymphoid cells (ILCs), obtaining an absence of type 2 ILCs (EvILC2).*

Figure 2 Genetic study of the index case

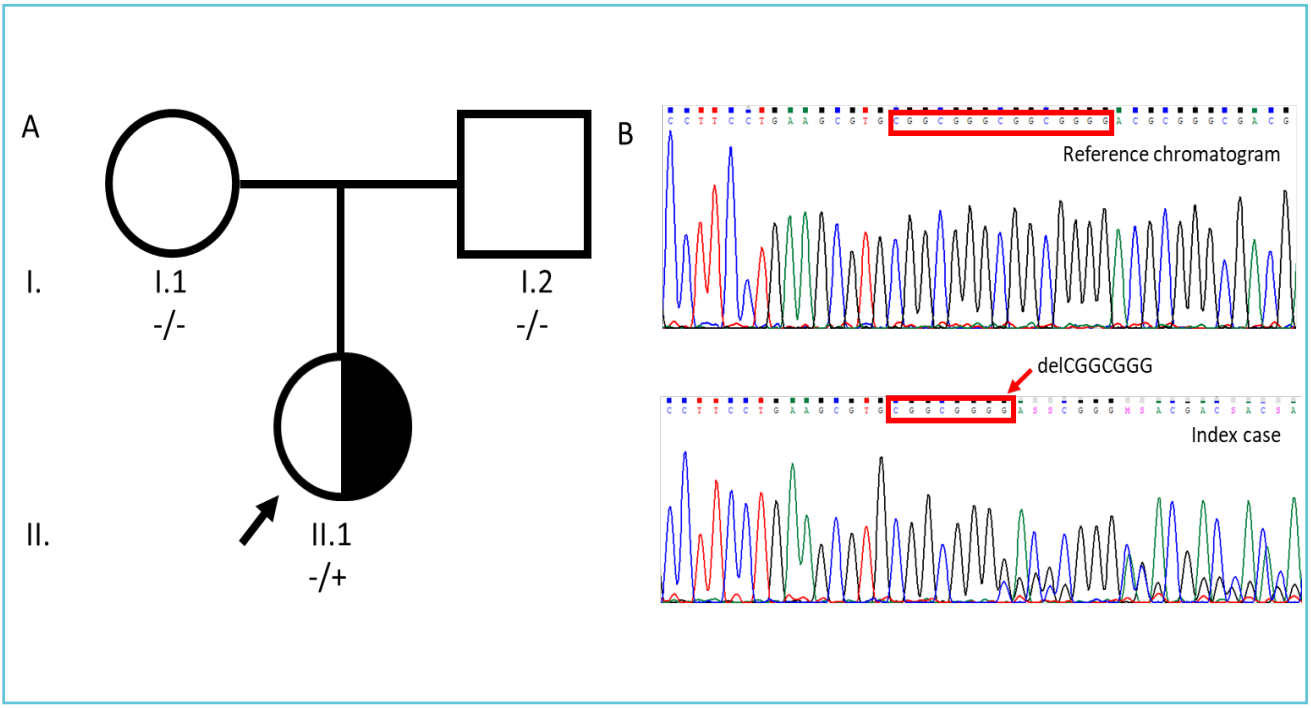

A. *Pedigree and mutation analysis of the family. Deletion arose de novo in heterozygosity in affected proband pointed with an arrow.*

B*. Sanger sequencing showing that the index case (II.1) carried a frameshift mutation (c.1887_1893delCGGCGGG), which was not found in reference chromatogram observed in both parents (I.1 and I.2).*

DISCUSSION

Variants in BCL11B are associated with Intellectual Developmental Disorder with Speech Delay, Dysmorphic Facies, and T-Cell Abnormalities. This syndrome is characterized by psychomotor developmental delay, intellectual disability, speech delay, autistic features, anxiety, and other behavioral abnormalities. Some of the cases described in the literature usually present slight delay in walking, with spasticity and abnormal movements [7][8].

Other peculiarities of this disorder are dysmorphic characteristics, which include thin eyebrows, small palpebral fissure, hypertelorism, epicanthal folds, prominent nose, and dental anomalies. Although this disorder is not an immunodeficiency, frequent infections, allergies or asthma have been observed [8].

From an immunological perspective, these patients may present an increase in eosinophils, alterations in the T cell compartment, a decrease in type 2 ILCs and, in some cases, exaggerated response of T helper 2 cells. Importantly, in our case, we described low counts of NK cells with a reshaping in the distribution of T cell. Alteration levels in NK cell has been previously discussed by Holmes TD et al (2021) [9]. This paper exposed the possible role of BCL11b in driving the differentiation of NK cells, finding that loss of BCL11b could substantially impact the generation and durability of mouse and human adaptive NK cells, suggesting the role of this gene in adaptive NK cell differentiation [9].

We also described variations in the percentage and total number of T cell lymphocyte, finding elevated absolute number of T cells lymphocyte, but more importantly, low levels of CD4+,

CD8+ naïve T cells, and regulatory T cells, resembling data described by Yang, Sai et al (2020) [10]. This discrepancy of our results, with few clinical cases reported in the literature, exposed the heterogeneity of this syndrome, and the function of the gene. Admittedly, BCL11b deficient mice show an arrest at the double negative stage of the thymocyte development [11]. Surprisingly, according to Lessel, Davor et al (2018), all analyzed individuals in their cohort (n=13) exhibited a severe reduction of peripheral ILC2 and impaired T cell development, but only two described low T cell percentage [3].

The variant identified in heterozygosis it is a loss-of-function variant that generates a premature stop codon that presumably causes the loss of 175 amino acids of the normal protein, thus being able to generate a non-functional truncated protein [12].

Our study of the patient with a mutation in BCL11B adds new data to the small group of subjects reported with this pathology, thus contributing to clinical advice and surveillance of this group of patients.

LEARNING POINTS

- Mutation on BCL11B must be considered when patients present a physical or immunological phenotype similar to the one we previously described.
- A heterozygous variant within exon 4, NM_138576.3: c.1887_1893delCGGCGGG p. (Gly630Thrfs*91) of the BCL11B gene has been currently described in the literature as a plausible cause of this syndrome.
- A multidisciplinary approach to patients with Intellectual Developmental Disorder with Speech Delay, Dysmorphic Facies, And T-Cell Abnormalities, including immunologists, hematologists, pediatricians, etc., is essential for a comprehensive approach to this syndrome.

❖❖❖❖❖

Disclosure

All authors contributed significantly to the analysis and interpretation of data, revising and approving the article. All authors declare no conflicts of interest.

❖❖❖❖❖

REFERENCES

1. Yan, S.; Wei, Y.S.; Yang, Q.Y.; Yang, L.; Zeng, T.; Tang, X.M.; Zhao, X.D.; An, Y.F. [A case report of BCL11B mutation induced neurodevelopmental disorder and literature review]. Zhonghua er ke za zhi = Chinese J. Pediatr. 2020, 58, 223–227, doi:10.3760/CMA.J.ISSN.0578-1310.2020.03.012.

2. Punwani, D.; Zhang, Y.; Yu, J.; Cowan, M.J.; Rana, S.; Kwan, A.; Adhikari, A.N.; Lizama, C.O.; Mendelsohn, B.A.; Fahl, S.P.; et al. Multisystem Anomalies in Severe Combined Immunodeficiency with Mutant BCL11B. N. Engl. J. Med. 2016, 375, 2165–2176, doi:10.1056/NEJMOA1509164.

3. Lessel, D.; Gehbauer, C.; Bramswig, N.C.; Schluth-Bolard, C.; Venkataramanappa, S.; van Gassen, K.L.I.; Hempel, M.; Haack, T.B.; Baresic, A.; Genetti, C.A.; et al. BCL11B mutations in patients affected by a neurodevelopmental disorder with reduced type 2 innate lymphoid cells. Brain 2018, 141, 2299–2311, doi:10.1093/BRAIN/AWY173.

4. Qiao, F.; Wang, C.; Luo, C.; Wang, Y.; Shao, B.; Tan, J.; Hu, P.; Xu, Z. A De Novo heterozygous frameshift mutation identified in BCL11B causes neurodevelopmental disorder by whole exome sequencing. Mol. Genet. genomic Med. 2019, 7, doi:10.1002/MGG3.897.

5. Yoshimi, R.; Ueda, A.; Ozato, K.; Ishigatsubo, Y. Clinical and pathological roles of Ro/SSA autoantibody system. Clin. Dev. Immunol. 2012, 2012, doi:10.1155/2012/606195.

6. Miyagawa, S.; Tanaka, M.; Okamoto, S.; Ishihara, T.; Nakajima, M.; Taira, K.; Yoshioka, A.; Asada, H. Autoimmune thyroid disease in anti-Ro/SS-A-positive children with annular erythema: report of two cases. Br. J. Dermatol. 2004, 150, 1005–1008, doi:10.1111/J.1365-2133.2004.05926.X.

7. Daher, M.T.; Bausero, P.; Agbulut, O.; Li, Z.; Parlakian, A. Bcl11b/Ctip2 in Skin, Tooth, and Craniofacial System. Front. cell Dev. Biol. 2020, 8, doi:10.3389/FCELL.2020.581674.

8. Prasad, M.; Balci, T.B.; Prasad, C.; Andrews, J.D.; Lee, R.; Jurkiewicz, M.T.; Napier, M.P.; Colaiacovo, S.; Guillen Sacoto, M.J.; Karp, N. BCL11B-related disorder in two canadian children: Expanding the clinical phenotype. Eur. J. Med. Genet. 2020, 63, doi:10.1016/J.EJMG.2020.104007.

9. Holmes, T.D.; Pandey, R.V.; Helm, E.Y.; Schlums, H.; Han, H.; Campbell, T.M.; Drashansky, T.T.; Chiang, S.; Wu, C.Y.; Tao, C.; et al. The transcription factor Bcl11b promotes both canonical and adaptive NK cell differentiation. Sci. Immunol. 2021, 6, doi:10.1126/SCIIMMUNOL.ABC9801.

10. Yang, S.; Kang, Q.; Hou, Y.; Wang, L.; Li, L.; Liu, S.; Liao, H.; Cao, Z.; Yang, L.; Xiao, Z. Mutant BCL11B in a Patient With a Neurodevelopmental Disorder and T-Cell Abnormalities. Front. Pediatr. 2020, 8, doi:10.3389/FPED.2020.544894.

11. Wakabayashi, Y.; Watanabe, H.; Inoue, J.; Takeda, N.; Sakata, J.; Mishima, Y.; Hitomi, J.; Yamamoto, T.; Utsuyama, M.; Niwa, O.; et al. Bcl11b is required for differentiation and survival of alphabeta T lymphocytes. Nat. Immunol. 2003, 4, 533–539, doi:10.1038/NI927.

12. Walker, J.A.; Oliphant, C.J.; Englezakis, A.; Yu, Y.; Clare, S.; Rodewald, H.R.; Belz, G.; Liu, P.; Fallon, P.G.; McKenzie, A.N.J. Bcl11b is essential for group 2 innate lymphoid cell development. J. Exp. Med. 2015, 212, 875–882, doi:10.1084/JEM.20142224.

The Journal of the International Federation of Clinical Chemistry and Laboratory Medicine

eJIFCC

A case of clinical confusion due to erroneous M-protein quantifications: to splice or skim?

Pak Cheung Chan[1,2], Amir Karin[3,4], Signy Chow[5,6]

[1] *Division of Clinical Biochemistry, Department of Laboratory Medicine and Molecular Diagnostics, Sunnybrook Health Sciences Centre, Toronto, Canada*
[2] *Department of Laboratory Medicine and Pathobiology, University of Toronto, Toronto, Canada*
[3] *Division of Clinical Chemistry, Department of Pathology and Laboratory Medicine, Vancouver Coastal Health, Vancouver, Canada*
[4] *Department of Pathology and Laboratory Medicine, The University of British Columbia, Vancouver, Canada*
[5] *Division of Hematology, Department of Medicine, Sunnybrook Health Sciences Centre, Toronto, Canada*
[6] *Department of Medicine, University of Toronto, Toronto, Canada*

ARTICLE INFO

Corresponding author:
Pak Cheung Chan
Division of Clinical Biochemistry
Department of Laboratory Medicine
and Molecular Diagnostics (DLMMD)
Sunnybrook Health Sciences Centre (CG76A)
2075 Bayview Ave
Ontario M4N3M5
Canada
E-mail: pc.chan@utoronto.ca

Key words:
serum protein electrophoresis, M-protein quantification, perpendicular drop, tangential skim, monoclonal gammopathy

ABSTRACT

An M-protein identified on electrophoresis is conventionally quantified by integrating the M-spike from baseline (PD), invariably including some irrelevant/background proteins. The use of an alternative approach that skims the M-spike tangentially thereby excluding the background proteins (TS), however, has been scanty. We report herein a case in which PD overestimated the M-proteins inconsistently, leading to confusion over relapse in a multiple myeloma patient.

At diagnosis, a 65-year old male had an IgG kappa M-spike of 44 g/L which decreased to 6 g/L (PD) following chemotherapy. Six weeks after autologous stem cell transplantation (ASCT), two M-spikes measuring respectively 10 and 5 g/L emerged. Together with decreases in hemoglobin and blood cell counts, a relapse was suspected. Bone marrow examinations, however, did not reveal any significant plasmacytosis or clonal restriction. Re-analyses by TS reduced the

original M-protein estimations by 12% and 88% pre- and post-ASCT respectively, and corroborated the disease activity/status consistently.

❖❖❖❖❖

Abbreviations

M-spike: monoclonal spike; PD: perpendicular drop (M-spike integration from baseline); TS: tangential skim (M-spike integration from a tangential line drawn between two inflection points); SPE: serum protein electrophoresis; CZE: capillary zone electrophoresis; AGE: agarose gel electrophoresis; MM: multiple myeloma; BM: bone marrow; ASCT: autologous stem cell transplant; ISS: International Staging System; RSV: Respiratory Syncytial Virus; Hb: hemoglobin.

❖❖❖❖❖

INTRODUCTION

Quantification of monoclonal immunoglobulins (M-proteins) by serum protein electrophoresis (SPE) plays an important role in the diagnosis, prognosis and management of monoclonal gammopathies such as monoclonal gammopathy of undetermined significance (MGUS), multiple myeloma (MM), and Waldenström's macroglobulinemia [1-3]. It is conventionally performed by integrating the areas under the demarcated M-protein peak (M-spike) on the electrophoretogram all the way to baseline perpendicularly, hence referred to as the perpendicular-drop (PD) method. This approach invariably includes both the M-protein and uninvolved background proteins above baseline, leading to a variable degree of overestimation depending on the amount of background proteins present. While an alternative tangential-skim (TS) method that excludes most of the background proteins has been described and shown to be more reliable, especially at low M-protein concentrations [4-7], its adoption in clinical practice has remained surprisingly scanty [9-11]. We, herein, describe a case of clinical confusion over relapse and stem cell transplant failure in a multiple myeloma patient whose M-protein was monitored by PD. This case also exemplifies the susceptibility of PD to errors due to background proteins (mostly uninvolved polyclonal immunoglobulins), particularly when they change over the course of a monoclonal gammopathy.

CLINICAL-DIAGNOSTIC CASE

A 65-year-old male was referred to Hematology with a one-year history of bony pain, particularly in the left femur. An X-ray demonstrated osteolytic lesions and SPE demonstrated an IgG kappa M-protein of 46 g/L. His medical history also included thalassemia minor, gout, hypertension and hernia. Myeloma survey confirmed osteolytic/sclerotic lesions on left femur and evidence of involvement of other areas including the left tibia, right clavicle, right femur head, left T1 vertebral body and right proximal tibia. MRI provided further evidence of myelomatous infiltrations within the marrow with additional focal lesions at T8, T10 and T11. Initial blood work at our centre showed significant anemia (Hb 109 g/L), an IgG kappa M-spike of 44 g/L (PD integration on the Sebia Capillarys II Electrophoretic System), reduced IgA and IgM, elevated beta2-microglobulin at 3 mg/L and a grossly elevated free kappa to free lambda ratio of >100 (The BindingSite). Bone marrow examinations reported 10% clonally-restricted plasma cells and cytogenetic studies detected translocations between chromosomes 11 and 14, t(11, 14). A diagnosis of stage 1 (ISS) MM was formally made. He received prophylactic intramedullary nailing of the femur, followed by radiation therapy. He was treated with 4 cycles of chemotherapy comprising of Cyclophosphamide, Bortezomib and Dexamethasone (CyBorD) with a plan for autologous stem cell transplant (ASCT). He achieved a partial response with the M-spike decreased to 6 g/L and a normal free light chain

ratio of 1.64 (0.26-1.65). ASCT was then arranged at a regional referral centre. He unfortunately developed deep vein thrombosis requiring anticoagulation and his ASCT was delayed by one month. He received an additional cycle of CyBorD prior to transplant.

Four weeks after ASCT, he developed autoimmune hemolytic anemia, which was thought to be related either to medication (colchicine) or a viral infection (RSV). He also developed two flares of gout post-transplant. Six weeks after ASCT, routine lab monitoring at our centre showed a large increase in total IgG to 30 g/L (by immunoturbidimetry), and two M-spikes (both of the same original IgG kappa isotype) measured 10 and 5 g/L, respectively (PD), had emerged on SPE. The free light chain ratio increased to 5.64 while both RBC and platelet counts were decreased. This was initially attributed to a brisk immune reconstitution. As he was also monitored by the transplant centre at ten weeks post-transplant, the two increased M-spikes were confirmed at their laboratory using a gel-based electrophoresis system (Sebia Hydrasys Electrophoresis System); both demonstrated the same IgG kappa isotype as his original disease and measured 9.6 and 8.6 g/L (PD), respectively. By then, Hb had dropped to 67 g/L and platelet numbers to $72x10^9$/L. The clinical picture was somewhat confounded by another gout flare occurring at the same time as well as a new onset of scrotal bleeding. However, given the confirmation of M-protein increases at two institutions more than 4 weeks apart, a relapse post-transplant was suspected. He was started on second line treatment and a bone marrow aspirate and biopsy was performed a week later to confirm the suspected myeloma progression.

The bone marrow examination surprisingly revealed no significant plasmacytosis (1%) or clonal restriction. At the same time, SPE once again demonstrated two M-spikes at 9.5 and 8.3 g/L, respectively (gel-based, PD). Attempts to reconcile the conflicting findings led to discussions with the Clinical Biochemist overseeing electrophoresis, and resulted in re-analyses of all M-spikes originally quantified by PD since diagnosis using the alternative TS method. TS yielded much lower M-protein concentrations than PD; an average reduction of 12% and 88% pre- and post-ASCT, respectively. TS eliminated the M-spike overestimations due to background polyclonal immunoglobulins and gave consistent results that corroborated the disease status and other laboratory findings. See Table 1 for a summary of general laboratory findings. PD overestimated the M-protein concentrations inconsistently over the course of the disease as the background polyclonal immunoglobulin concentrations changed, particularly after ASCT. Selected electrophoretograms at different time points and the trending of M-protein concentrations are shown in Figure 1 and 2, respectively.

DISCUSSION

M-protein quantification plays an important role not only in diagnosing but also in prognosticating

Table 1 Laboratory findings at selected time points following the diagnosis of multiple myeloma

Tests	At Diagnosis*	At ASCT	6 weeks post-ASCT	10 weeks post-ASCT	11 weeks post-ASCT# (BM exam)	Reference interval
Total Proteins, g/L	100	60	80	83	82	64-83

Albumin, g/L	36	36	37	34	34	35-50
Creatinine, µmol/L	98	64	74	72	74	44-106
LDH, IU/L	121	203	370	296	425	100-250
Hb, g/L	109	79	83	67	91	130-180
RBC, 10^{12}/L	5.18	3.75	3.59	2.85	3.77	4-6
WBC, 10^{9}/L	4.6	8.2	5.9	3.8	3	4-11
Platelet, 10^{9}/L	152	214	105	72	94	150-400
IgG, g/L	57.9	8.99	30.22	-	-	6.00-16.00
IgA, g/L	<0.2	0.23	0.4	-	-	0.70-4.00
IgM, g/L	0.14	0.21	0.4	-	-	0.40-2.50
sFLC						
FK, mg/L	212.5	10.5	98.2	-	-	3.3-19.4
FL, mg/L	<2.0	6.4	17.4	-	-	5.7-26.3
FK/FL ratio	>100	1.64	5.64	-	-	0.26-1.65
M-protein, g/L						
CZE (PD)	44.3	6	10.3, 5.4	-	-	ND
AGE (PD)	-	4.4	-	9.6, 8.6	9.5, 8.3	ND
M-protein, g/L (Re-analysis)						
CZE (TS)	43.4	4.9	0.8, 0.9	-	-	ND
AGE (TS)	-	3.6	-	1, 1	0.9, 1	ND

**Diagnosis confirmed with BM examination, followed by 5 cycles of Cyclophosphamide, Bortezomib and Dexamethasone; # Initiation of second line chemotherapy with Daratumumab, Lenalidomide and Dexamethasone; ASCT: autologous stem cell transplant; LDH: lactate dehydrogenase; Hb: hemoglobin; sFLC: serum free light chain assays; FK: free kappa light chain; FL: free lambda light chain; CZE: capillary electrophoresis; AGE: agarose gel electrophoresis; PD: perpendicular drop (the default method); TS: tangential skim; ND: not detected.*

Figure 1 **Electrophoretograms showing M-spike quantifications using both PD and TS methods at selected time points during the course of disease**

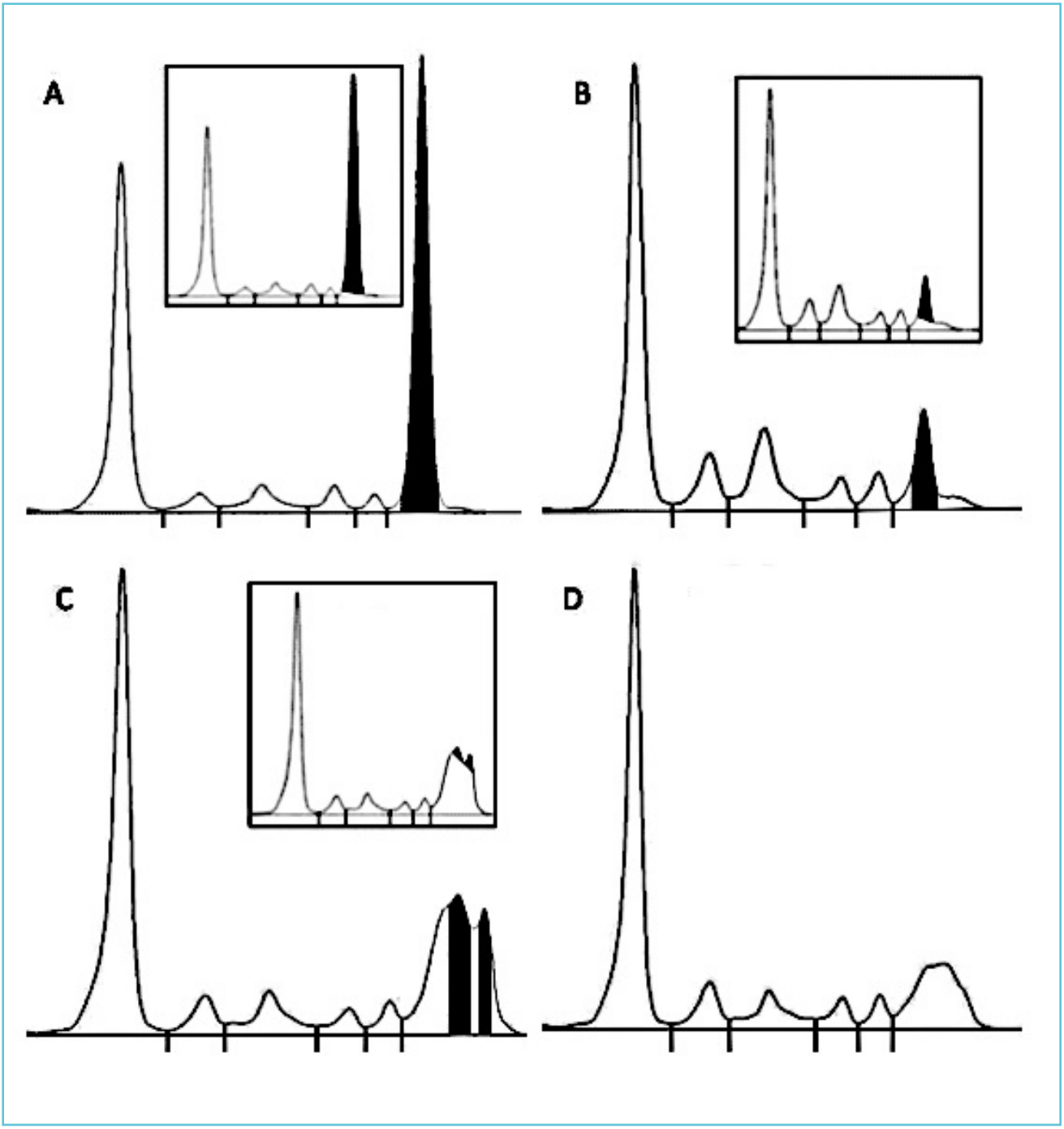

M-protein concentrations were estimated by demarcating the corresponding M-spikes (highlighted) using the perpendicular drop (PD) and subsequently the tangential skim (TS) (inset) methods at different time points during the course of treatment: (A) when a diagnosis of multiple myeloma was first established, (B) At autologous stem cell transplant (ASCT), (C) 11 weeks post-ASCT when a bone marrow (BM) examination was performed for the suspicion of disease progression, and (D) 15 weeks post-ASCT when the M-spikes were barely discernible. Major serum protein fractions from left to right were albumin, alpha1, alpha2, beta1, beta2 and gamma.

Figure 2 **Trending of M-protein concentrations as determined by PD and TS on two different electrophoretic systems**

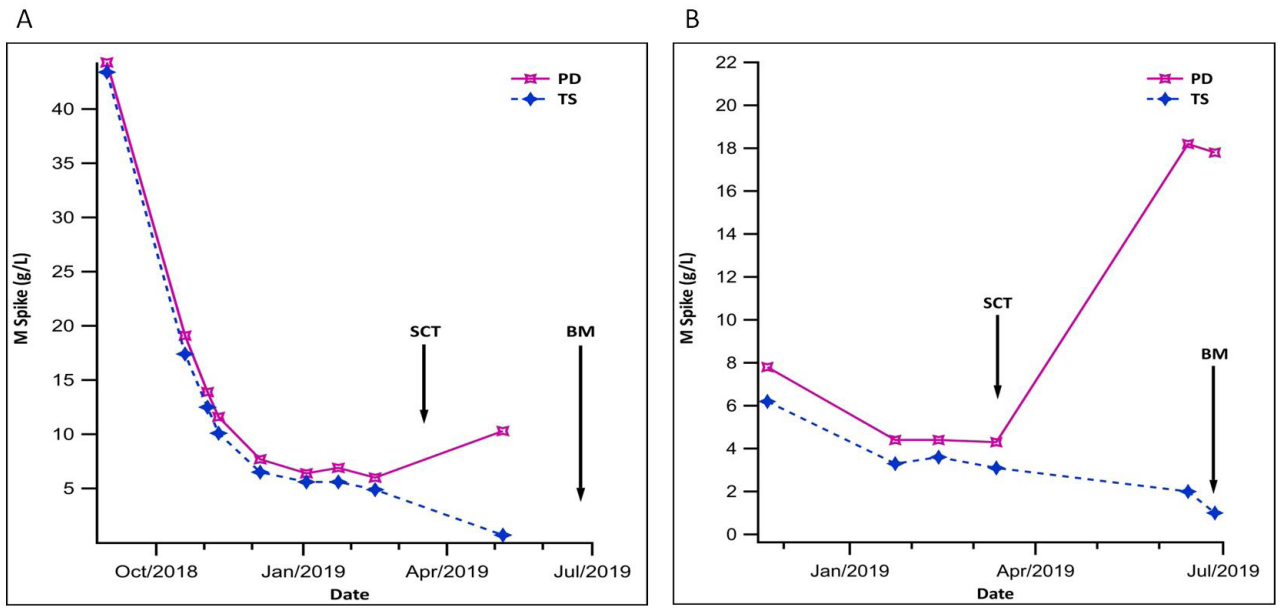

(A) Trending of M-protein concentrations as determined by both PD and TS methods on a capillary electrophoresis platform at the home institution since diagnosis; (B) Trending of M-protein concentrations by both PD and TS methods using agarose gel electrophoresis at the referral centre where stem cell transplant (SCT) was performed. BM: bone marrow examination.

and monitoring monoclonal gammopathies. For instances, M-protein greater than 15 g/L is a predictor for disease progression in MGUS [12] while < 30 g/L in the absence of end organ damage defines MGUS and ≥ 30 g/L is considered smoldering or active MM, depending on the presence of end organ damage [1,2]. In patients with MM undergoing treatment, a 25 % decrease in M-protein concentration is considered as a minimal response, while a 50 % decrease as partial, and a decrease of 90 % or more as a very good partial response [2]. A measurable disease is defined as having a serum M-protein ≥ 10 g/L and/or an M-protein excretion in urine of ≥ 200 mg/24 h, and that it should be tracked by changes in the M-protein concentration [13].

While SPE is generally preferred over total immunoglobulin determinations for estimating the M-protein concentrations, most clinical guidelines do not explicitly specify which SPE integration method should be used [1-3]. Yet, drastic differences between PD & TS have been reported based on observations from patient studies [5, 12] as well as spiked sample analyses [6, 8]. These studies have highlighted the differential effects of background proteins (mostly polyclonal immunoglobulins in the gamma fraction of SPE) on M-protein estimations by PD and TS, with the former being most adversely affected when the background is high.

In disease diagnosis and monitoring, when the M-protein concentration is relatively high and/or the background protein concentration is low and stable, there is little clinical impact as the difference between PD and TS is minimal. However, when the background protein concentrations change during the disease course, the accuracy of the M-protein determination can be

jeopardized leading to confusion. In the current case, the patient had suppressed polyclonal immunoglobulins due to immune paresis at diagnosis but the uninvolved immunoglobulin concentrations increased, likely due to a combination of the successful ASCT and the inter-current conditions including, but not necessarily limited to, the gout flare-ups and the autoimmune hemolytic anemia. Moreover, changes in the concentrations of these uninvolved immunoglobulins during the course of a monoclonal gammopathy may occur more often than what we anticipate, and the causes are plenty: infections, autoimmune diseases, inflammatory conditions, SCT, as well as immune paresis caused by expanding tumors and/or chemotherapy. Unfortunately, as demonstrated in this case, these uninvolved immunoglobulins may affect the M-protein determination by PD to such an extent that the care providers can be misled into performing additional invasive investigations. TS is a simple but robust alternative that would obviate such scenarios without introducing extra cost in laboratory instrumentation or analysis. However, PD continues to be recommended by some authorities for routine M-protein determinations on the sole basis of a marginally improved reproducibility [13, 14]. This factor alone is unlikely to translate to clinical benefit, especially if the patient is monitored at the same institution.

In summary, we reported a case in which the PD method of M-protein determination produced erroneous results that led to clinical confusion, unwarranted investigations and an unnecessary change in the care path. The alternative TS approach was shown to produce results that were in line with the patient's clinical development and other laboratory findings such as the bone marrow examination results. While our case provided one particular scenario in which the use of TS could have prevented the confusion over relapse, the resistance of TS to the interferences of background proteins in general would provide more consistent and reliable M-protein estimations especially for disease monitoring, and should, thus, merit a wider acceptance into routine practice.

LEARNING POINTS/ TAKE-HOME MESSAGES

- Changes in concentrations of polyclonal immunoglobulins affect adversely the accuracy of the conventional M-protein quantification by PD in electrophoresis.
- Polyclonal immunoglobulin concentrations do change over the course of a monoclonal gammopathy, probably more often than we expect, and can cause erroneous M-protein quantifications, leading to confusion over disease activity and treatment response.
- TS requires no extra hardware or software for implementation, and remains one of the most reliable and accessible approaches for minimizing the effect of polyclonal immunoglobulins on M-protein quantifications.

❖❖❖❖❖

Disclosures & authors' contributions

Disclosures: No conflicts of interests declared by all authors.

Contributions:

Chan: Inception, data analysis, manuscript drafting & review; Amir: Data collection and analysis, manuscript review; Chow: Case discovery, manuscript review.

❖❖❖❖❖

REFERENCES

1. Bergstrom DJ, Kotb R, Louzada ML, Sutherland HJ, Tavoularis S, Venner CP. Consensus Guidelines on the Diagnosis of Multiple Myeloma and Related Disorders: Recommendations of the Myeloma Canada Research

Network Consensus Guideline Consortium. Clinical Lymphoma, Myeloma & Leukemia. 2020;20 (7):e352-67.

2. Lakshman A, Rajkumar SV, Buadi FK, et al. Risk stratification of smoldering multiple myeloma incorporating revised IMWG diagnostic criteria. Blood Cancer J. 2018;8:59

3. Kastritis E, Leblond V, Dimopoulos MA, et al. Waldenström's macroglobulinaemia: ESMO Clinical Practice Guidelines for diagnosis, treatment and follow-up. Annals of Oncology. 2018;29 (Supplement 4): iv41–iv50

4. Keren DF, Schroeder L. Challenges of measuring monoclonal proteins in serum. Clin Chem Lab Med. 2016; 54(6):947–961.

5. Schild C, Wermuth B, Trapp-Chiappini D, Egger F, Nuoffer JM. Reliability of M protein quantification: comparison of two peak integration methods on Capillarys 2. Clin Chem Lab Med. 2008;46:876-877.

6. Turner KA, Frinack JL, Ettore MW, et al. An international multi-center serum protein electrophoresis accuracy and M-protein isotyping study. Part I: factors impacting limit of quantitation of serum protein electrophoresis. Clin Chem Lab Med. 2020;58:533–546.

7. Cárdenas Fernández MC, Pérez Surribas D, Pérez Garay R, et al. Vertical cutoff methods in serum protein electrophoresis for the measurement of monoclonal protein concentrations: Which is best?. Clin Chim Acta. 2020; 510:573-580.

8. Jacobs JFM, Turnera KA, Graziani MS, et al. An international multi-center serum protein electrophoresis accuracy and M-protein isotyping study. Part II: limit of detection and follow-up of patients with small M-proteins. Clin Chem Lab Med. 2020;58(4):547–559.

9. Genzen JR, Murray DL, Abel G, et al. Screening and Diagnosis of Monoclonal Gammopathies: An International Survey of Laboratory Practice. Arch Pathol Lab Med. 2018; 142:507-515.

10. Tate J, Graziani MS, Willrich M, Jacobs H, Moss M. Report of Survey conducted by IFCC WG Harmonisation of Interpretive Commenting EQA (WG-ICQA) subgroup: Results of an international survey of the reporting of protein electrophoresis and serum free light chains, and quantification of small monoclonal proteins. IFCC 2017

11. Wijeratne N, Tate JR, Wienholt L, Mollee P. Report of the Survey Conducted by RCPAQAP on Current Practice for Paraprotein and Serum Free Light Chain Measurement and Reporting: a Need for Harmonisation. Clin Biochem Rev. 2019;40:31-42.

12. Miller JJ, Taher J, Kulasingam V, Chan PC. To skim or splice? Comparing the quantification of M-proteins using two peak-integration protocols across multiple electrophoresis platforms. Clin Biochem. 2022:102:44-49

13. Dejoie T, Lakomy D, Caillon H, Pegourié B, Decaux O. IFM (Intergroupe francophone du myélome) recommendations for uniform interpretation of serum and urine protein electrophoresis in multiple myeloma diagnosis and follow-up. Ann Biol Clin (Paris). 2016;74:429-41.

14. Tate JR, Smith JD, Wijeratne N, Mollee P. Proposed Addendum to 2012 Recommendations for Standardised Reporting of Protein Electrophoresis in Australia and New Zealand. Clin Biochem Rev. 2019;40 (1):23-30.

The Journal of the International Federation of Clinical Chemistry and Laboratory Medicine

eJIFCC

Anti-HMGCR myopathy without exposure to statins: a case report

Jorge Ferriz Vivancos, Marta Fandos Sánchez, Pilar Teresa Timoneda Timoneda, Goitzane Marcaida Benito

Department of Clinical Biochemistry, Hospital General Universitario Valencia, Valencia, Spain

ARTICLE INFO

Corresponding author:
Jorge Ferriz Vivancos
Department of Clinical Biochemistry
Hospital General Universitario Valencia
Valencia
Spain
E-mail: ferriz_jor@gva.es

Key words:
myopathy, elevated CK values, HALIP, statins

ABSTRACT

Anti-HMGCR, which was first identified in 2010, has emerged as an important mechanism of myopathogenesis in patients with exposure to statins. The availability of new detection methods has expanded the phenotypic spectrum with a subtype of population that hasn't been exposed to the drug and whose clinical, analytical, and pathological manifestations are similar. The observation by immunofluorescence of a highly specific pattern known as HALIP (HMGCR Associated Liver Immunofluorescence Pattern) can be useful in the detection of these antibodies.

INTRODUCTION

Idiopathic inflammatory myopathies (IIM) are a group of low-prevalence diseases resulting from autoimmune inflammation and muscle damage. They can be categorized into polymyositis, dermatomyositis, autoimmune necrotizing myopathy, and inclusion body myositis based on clinical and myopathological features (1).

More than 15 myositis-specific antibodies (MSA) are considered important in the mechanism underlying IIMs. Among the antibodies responsible for these diseases, we find anti-3-hydroxy-3-methylglutaryl coenzyme A reductase (anti-HMGCR), an enzyme involved in cholesterol synthesis. Statins, a medication frequently used to treat hypercholesterolemia and other lipid metabolic disorders, are typically linked to the development of these antibodies in patients who have received this pharmacotherapy.

The association of anti-HMGCR and statins gives rise to a myopathy histologically compatible with immune-mediated necrosis, whose clinical manifestations are proximal, symmetric, and progressive muscle weakness with hight creatine kinase (CK) values (>1,000-10,000 U/L) (2).

The new chemiluminescence tests (CIA) available on the market, which allow quantifying of anti-HMGCR levels, have increased the determinations of these antibodies, which has resulted in the appearance of new subsets of patient populations, such as children and young people not exposed to statins. The identification of a new immunofluorescence pattern, called HALIP (HMGCR Associated Liver Immunofluorescence Pattern), can also guide its diagnosis.

We present the case of a 17-year-old male where incidental finding of hypertransaminasemia and HALIP led to the diagnosis of anti-HMGCR myopathy. This myopathy in persons not taking statins is an infrequent finding.

CASE REPORT

A 17-year-old male with no clinical history or treatment of interest went to Urgent Care due to abusive alcohol intake. Neurological, cardiovascular, and imaging exams without alterations. Laboratory tests revealed moderate leukocytosis (19.500/mL) and increased alanine transaminase (ALT) of 199 U/L (reference interval 3-50 U/L), so he was referred to Gastroenterology Service.

In the analytical liver function follow-up, elevated values of transaminase were maintained with an ALT value of 233 U/L and aspartate aminotransferase (AST) value of 161 U/L (reference interval 5-50 U/L), although total bilirubin (TB), alkaline phosphatase (ALP) and gamma-glutamyl transferase (GGT) levels were normal. Other analytical parameters and infectious serology were without significant alterations. A liver biopsy was performed in which minimal inflammatory infiltrates were found, with dilation, sinusoidal congestion, and slight dilation of the centrilobular veins.

To exclude the possibility of autoimmune liver disease, a study of antinuclear antibodies (ANAs) was performed by IFA using HEp-2 cells (ANA-Mosaik 1A EUROPattern, Euroimmun®) where no pattern was detected at 1/80 titer. Autoimmune liver blot (EUROLINE Autoimmune Liver Diseases, Euroimmun®), which was negative, and triple tissue IFA (Mosaic Basic Profile 3C EUROPattern, Euroimmun®) were also requested. The presence of immunofluorescence in the cytoplasm of dispersed hepatocytes of rat liver was evidenced with a centrilobular distribution, a pattern known as HALIP (Figure 1).

Given this finding, CK (4738 U/L, reference interval 46-171 U/L) and aldolase (42.8 U/L, reference level<7.6 U/L) were determined. Anti-HMGCR (321.6 CU, reference level<20 CU) were also quantified by Quanta Flash CIA assay® HMGCR (Inova, Werfen®).

Figure 1 HALIP: pattern of immunofluorescence in the cytoplasm of hepatocytes with centro-lobular distribution (yellow arrow) in rat liver stain (dilution 1/80)

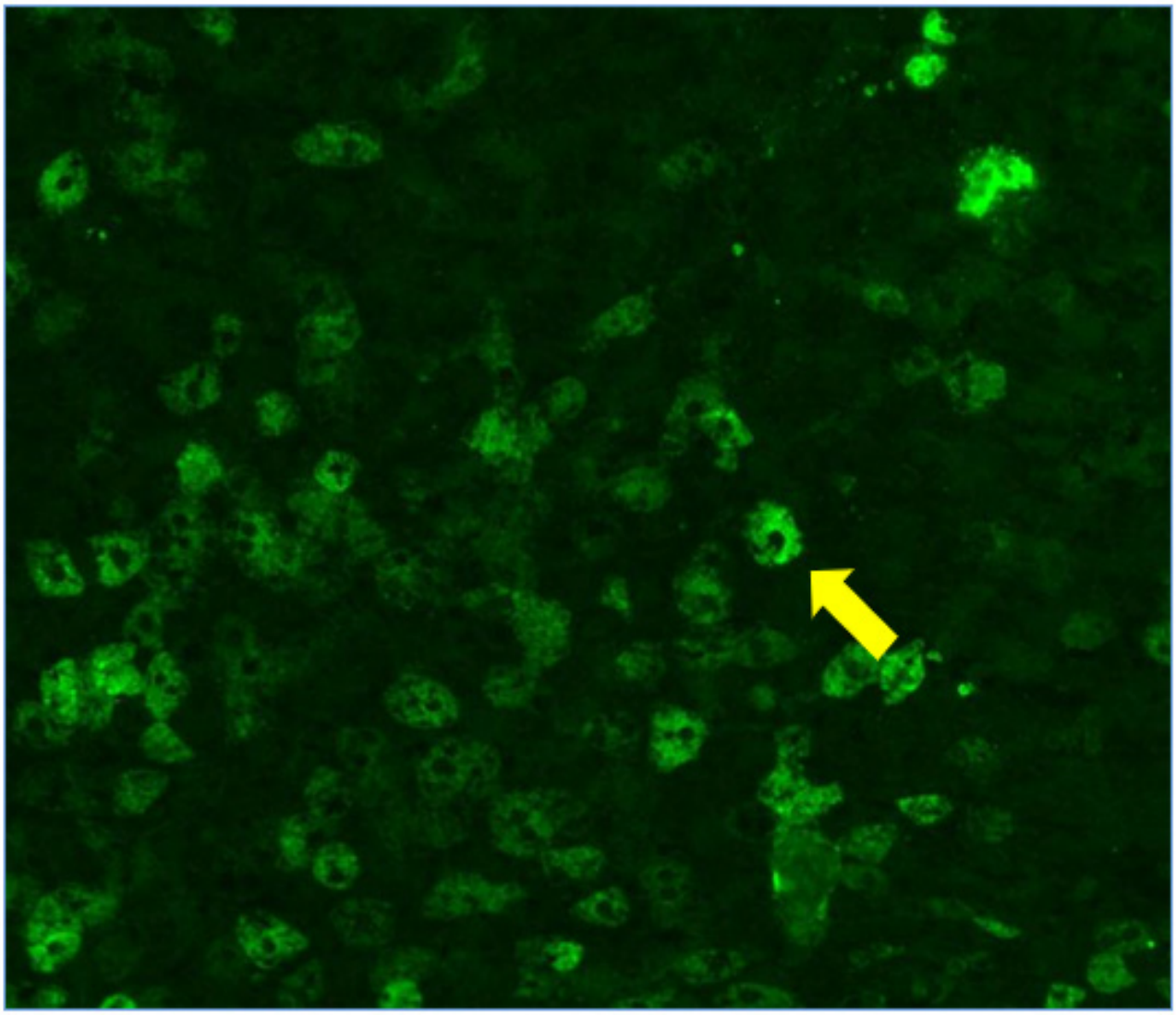

The patient was finally treated by the Neurology Service and a neurological evaluation revealed a loss of scapular strength with unusual movements during the examination.

A muscle MRI and electromyography were performed with no pathological findings, and a muscle biopsy, with a report of "Unequivocal immunostaining with autoimmune necrotizing inflammatory myopathy: C5b9 deposits in necrotic fibers and preserved myofiber membrane" (Figure 2).

Anti-HMGCR led to the diagnosis of autoimmune necrotizing myopathy and the patient was treated with immunoglobulins and low-dose corticosteroids with favorable evolution. During follow-up, CK and anti-HMGCR levels were monitored. Although concentrations decreased after treatment, they remained elevated (Figure 3).

Figure 2 **(I) Hematoxylin and eosin stain of muscle biopsy with necrotic and regenerative muscle fibers (orange arrow). (II) Immunostaining with sarcolemmal C5b–9 (MAC) deposits in necrotic fibers (red arrow)**

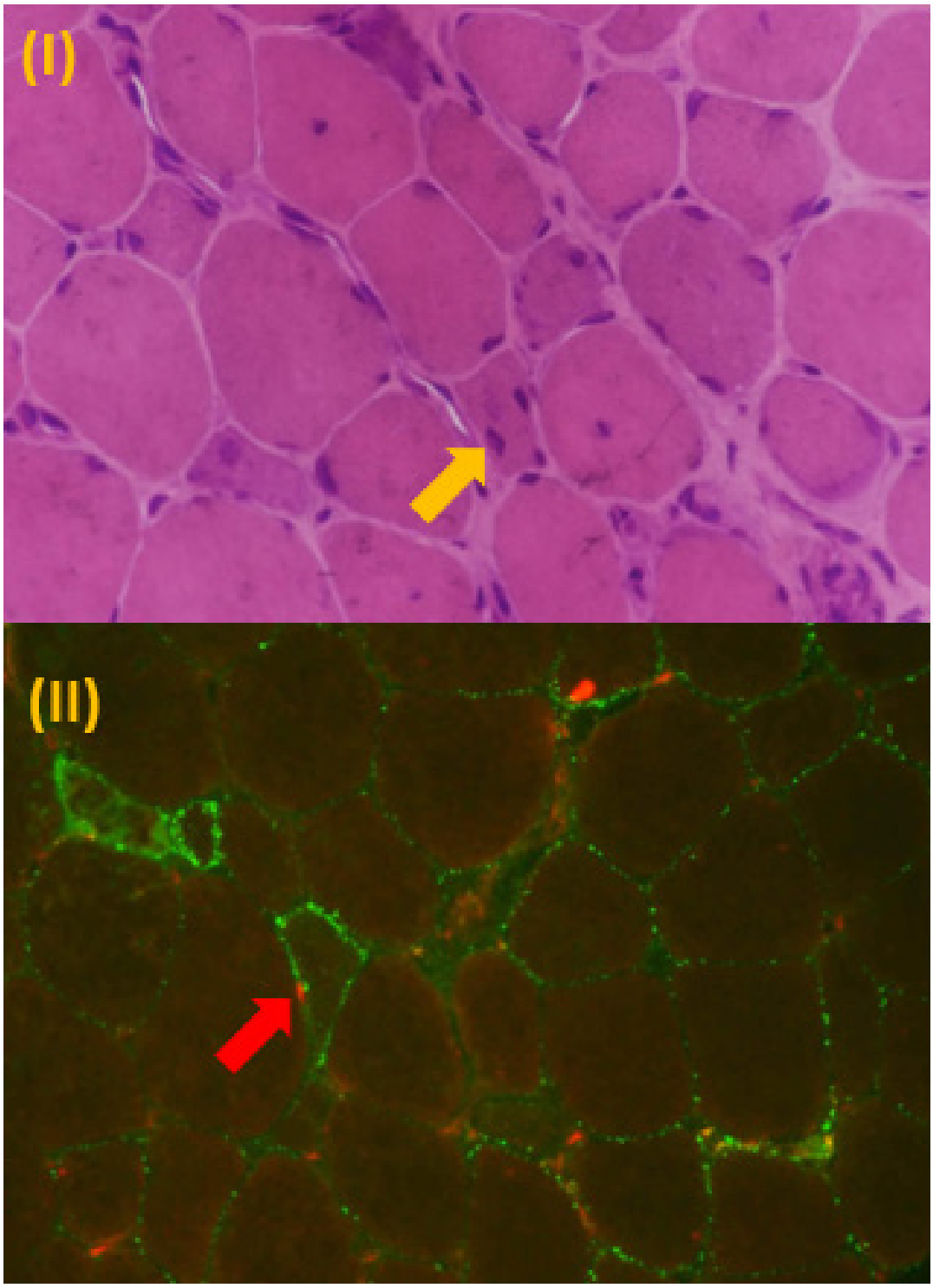

Figure 3 **CK levels (I) and anti-HMGCR levels (II) during follow-up after Urge Care (Day 1)**

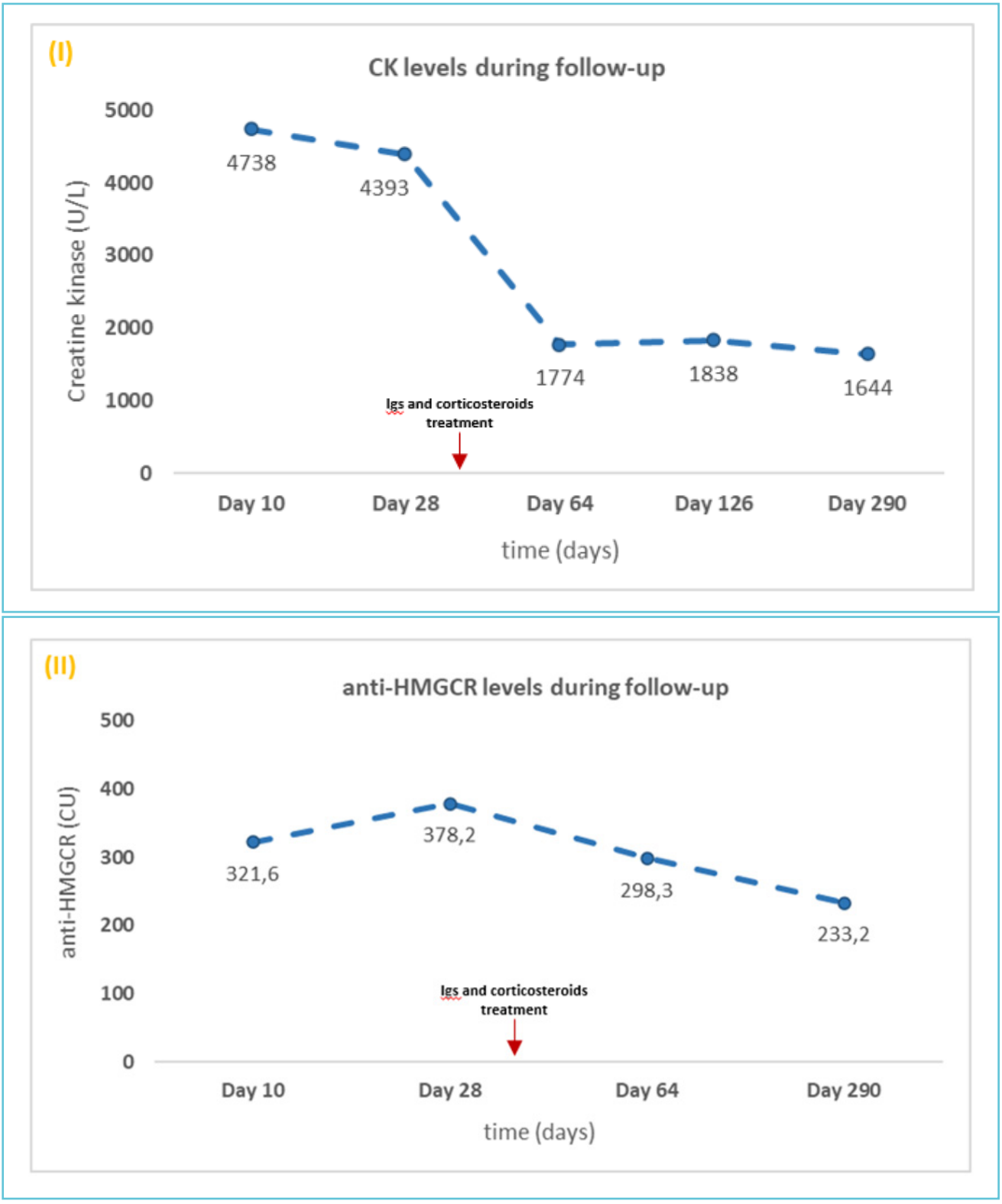

DISCUSSION

The intake of statins, one of the most frequently prescribed drugs, has increased worldwide in recent years, which has also caused an increase in the incidence of its intolerance, which is around 9.1% (3). One of its most frequent side effects is muscular toxicity (4), which includes anti-HMGCR myopathy, a rare condition that is caused by the action of antibodies against this essential enzyme of cholesterol synthesis. An increase in the HMGCR expression as a consequence of HMGCR inhibition by statins has been suggested as a possible cause of muscle toxicity (5).

Anti-HMGCR antibodies were first described in 2010 in a population of patients with a biopsy consistent with necrotizing myopathy and negative for other autoantibodies (6). Although they were initially associated with taking statins, due to their higher prevalence in this type of patient compared to other myopathies (2-3 of every 100,000 patients treated with statins), new subtypes of patients such as unexposed adults, adolescents, and even children were emerging (2). The estimated incidence of anti-HMGCR is 1.94-10.3 per million adults per year, depending on the testing criteria (7) and the proportion of patients who have been exposed to statins and have anti-HMGCR antibodies positive varies by geographic region, ranging from 44.4% to 72.7% in the European population, with a similar percentage in the North American population, and a lower association in Asian populations (8), where higher consumption of foods rich in natural statins, such as mushrooms or red tea, may act as triggers of non-drug anti-HMGCR myopathy (2).

Genetics can also play a role in anti-HMGCR myopathy. A higher predisposition has been observed in adults with the MHC class II allele DRB1∗11:01, whereas this risk is associated with DRB1∗07:01 in pediatric patients (9-10). However, given the high prevalence of this loci in the general population (7-15%), its determination in this type of patient does not seem useful.

Patients without exposure to statins have similar clinical symptoms to patients exposed to these drugs, although it has been shown that young patients have more severe disease and slower recovery (11). The titers of anti-HMGCR antibodies in IIM patients were also significantly higher in statin users (12). Some patients may have sustained elevated CK levels without muscle weakness, and in both groups, CK levels correlated with muscular strength (13). Although the appearance of HALIP could suggest the presence of autoimmune hepatitis due to immunofluorescence in hepatocytes, few cases have been described in the literature associating these antibodies with liver disease (14).

Unlike other mechanisms of intolerance to statins, drug withdrawal does not usually resolve patient symptoms, and immunosuppressants and intravenous immunoglobulins are necessary to prevent disease progression. The measurement of CK is useful during the monitoring of the disease, but not anti-HMGCR, which usually does not normalize despite clinical improvement (2).

Anti-HMGCR were initially discovered by immunoprecipitation, which remains the gold standard technique, but other techniques such as ELISA and CIA are currently used for their determination. A more common alternative to the above tests is indirect immunofluorescence on triple tissue with rat liver, in search of the characteristic HALIP (HMGCR-Associated Liver Indirect Immunofluorescence Pattern). This pattern has demonstrated high specificity (98.7%) (15-16), making it a fast and cheap alternative for screening myopathies in patients treated with statins.

The determination of anti-HMGCR is a highly specific test (99.7%) and it is not found in patients with other related diseases. Its study, either by CIA or HALIP, should be included in the differential diagnosis of IIM that includes a population of any age with suspected myopathy and not limited to statin users.

TAKE-HOME MESSAGES

- In patients treated with statins, anti-HMGCR antibodies may develop with symptoms of necrotizing autoimmune myopathy. This condition has also been observed in patients without exposure to statins.
- The finding of the HALIP pattern, specific to this type of myopathy, constitutes a fast and cheap alternative in its diagnosis.

❖❖❖❖❖

Compliance with ethical standards

Conflict of interest: The authors have declared that no conflict of interest exists.

Author contributions: All authors were involved in the diagnosis and management of this case.

Funding: The authors have not declared a specific grant for this research from any funding agency or source in the public, commercial or not-for-profit sectors.

❖❖❖❖❖

REFERENCES

1. Cheeti A, Brent LH, Panginikkod S. Autoimmune Myopathies. In: StatPearls. Treasure Island (FL): StatPearls Publishing; November 22, 2021.

2. Mohassel P, Mammen AL. Anti-HMGCR Myopathy. J Neuromuscul Dis. 2018;5(1):11-20. doi:10.3233/JND-170282

3. Bytyçi I, Penson PE, Mikhailidis DP, et al. Prevalence of statin intolerance: a meta-analysis [published online ahead of print, 2022 Feb 16]. Eur Heart J. 2022;ehac015. doi:10.1093/eurheartj/ehac015

4. Toth PP, Patti AM, Giglio RV, et al. Management of Statin Intolerance in 2018: Still More Questions Than Answers. Am J Cardiovasc Drugs. 2018;18(3):157-173. doi:10.1007/s40256-017-0259-7

5. Mammen AL, Chung T, Christopher-Stine L, et al. Autoantibodies against 3-hydroxy-3-methylglutaryl-coenzyme A reductase in patients with statin-associated autoimmune myopathy. Arthritis Rheum. 2011;63(3):713-721. doi:10.1002/art.30156

6. Christopher-Stine L, Casciola-Rosen LA, Hong G, Chung T, Corse AM, Mammen AL. A novel autoantibody recognizing 200-kd and 100-kd proteins is associated with an immune-mediated necrotizing myopathy. Arthritis Rheum. 2010;62(9):2757-2766. doi:10.1002/art.27572

7. Joseph VMK, Rose EC, Edwards CJ, et al. Anti-3-hydroxy-3-methylglutaryl-coenzyme A reductase antibodies: incidence using different testing criteria, and case series. Clin Exp Rheumatol. 2022;40(2):298-303. doi:10.55563/clinexprheumatol/5y19bb

8. Allenbach Y, Drouot L, Rigolet A, et al. Anti-HMGCR autoantibodies in European patients with autoimmune necrotizing myopathies: inconstant exposure to statin. Medicine (Baltimore). 2014;93(3):150-157. doi:10.1097/MD.0000000000000028

9. Mammen AL, Gaudet D, Brisson D, et al. Increased frequency of DRB1*11:01 in anti-hydroxymethylglutaryl-coenzyme A reductase-associated autoimmune myopathy. Arthritis Care Res (Hoboken). 2012;64(8):1233-1237. doi:10.1002/acr.21671

10. Kishi T, Rider LG, Pak K, et al. Association of Anti-3-Hydroxy-3-Methylglutaryl-Coenzyme A Reductase Autoantibodies With DRB1*07:01 and Severe Myositis in Juvenile Myositis Patients. Arthritis Care Res (Hoboken). 2017;69(7):1088-1094. doi:10.1002/acr.23113

11. Tiniakou E, Pinal-Fernandez I, Lloyd TE, et al. More severe disease and slower recovery in younger patients with anti-3-hydroxy-3-methylglutaryl-coenzyme A reductase-associated autoimmune myopathy. Rheumatology (Oxford). 2017;56(5):787-794. doi:10.1093/rheumatology/kew470

12. Musset L, Allenbach Y, Benveniste O, et al. Anti-HMGCR antibodies as a biomarker for immune-mediated necrotizing myopathies: A history of statins and experience from a large international multi-center study. Autoimmun Rev. 2016;15(10):983-993. doi:10.1016/j.autrev.2016.07.023

13. Werner JL, Christopher-Stine L, Ghazarian SR, et al. Antibody levels correlate with creatine kinase levels and strength in anti-3-hydroxy-3-methylglutaryl-coenzyme A reductase-associated autoimmune myopathy. Arthritis Rheum. 2012;64(12):4087-4093. doi:10.1002/art.34673

14. Palamuthusingam D, Mantha M, Dheda S. HMG CoA reductase inhibitor associated myositis and autoimmune hepatitis. Intern Med J. 2017;47(10):1213-1215. doi:10.1111/imj.13561

15. Alvarado-Cardenas M, Marin-Sánchez A, Martínez MA, et al. Statin-associated autoimmune myopathy: A distinct new IFL pattern can increase the rate of HMGCR antibody detection by clinical laboratories. Autoimmun Rev. 2016;15(12):1161-1166. doi:10.1016/j.autrev.2016.09.005

16. Baucells A, Martínez MA, Alvarado-Cardenas M, et al. Anti-HMGCR Specificity of HALIP: A Confirmatory Study. J Immunol Res. 2020; 2020:6292631. Published 2020 Jul 16. doi:10.1155/2020/6292631

Publisher: IFCC Communications and Publications Division (IFCC-CPD)

The eJIFCC is a member of the **Committee on Publication Ethics (COPE).**

The eJIFCC (Journal of the International Federation of Clinical Chemistry) is an electronic journal with frequent updates on its home page. Our articles, debates, reviews and editorials are addressed to clinical laboratorians. Besides offering original scientific thought in our featured columns, we provide pointers to quality resources on the World Wide Web.

Produced by: Insoft Digital Web Solutions

Published by: IFCC International Federation of Clinical Chemistry and Laboratory Medicine

www.ifcc.org